Synthesis and Characterization of Styrene Butadiene Rubber Nano-Sized Particles via Differential Microemulsion Polymerization

by

Rifang Zou

A thesis
presented to the University of Waterloo
in fulfillment of the
thesis requirement for the degree of
Master of Applied Science
in
Chemical Engineering

Waterloo, Ontario, Canada, 2012

Author's Declaration

I hereby declare that I am the sole author of this thesis. This is a true copy of the thesis, including any required final revisions, as accepted by my examiners.

I understand that my thesis may be made electronically available to the public.

Abstract

Styrene-butadiene rubber (SBR) copolymer nanosized latex particles were synthesized via differential microemulsion polymerization (DMP) in a 300ml bench-scale semi-batch reactor, equipped with a thermocouple and a magnetic four-blade stirrer. This approach employed a continuous and slow addition of styrene and butadiene monomers drop-wise into a continuous aqueous phase comprising DI water, an initiator, a surfactant and a chain transfer agent. It was found that this approach offered an efficient heterogeneous phase path to synthesize styrene-butadiene copolymer latices with a high-butadiene-level of the resulting latex particles. The latex nanoparticles were formed as the SBR copolymer monomers undergo a self-assembly process in the continuous phase and were stabilized by their surrounding surfactant particles. The size of the latex particles could be easily adjusted by alternating the monomer addition speed, the reaction temperature, the amount of chain transfer agent applied and the type and the amount of surfactant introduced in the process. Not surprisingly, a small amount of chain transfer agent introduced into the DMP system might facilitate micellar nucleation and reduction of gel content in the polymer dramatically and may also aid increasing the size of the SBR latex particles. Owing to the small size of SBR latices prepared by the DMP method, the glass transition temperature (T_g) of the latices is much lower than the SBR latices generated by conventional technique. Furthermore, the increase of T_g was observed with an increase of the SBR particle size.

Acknowledgements

I gratefully acknowledge the Natural Science and Engineering Research Council of Canada (NSERC) and the Graduate Studies Office for the financial support.

I wish to express my gratitude to: Prof. Garry L. Rempel and Prof. Qinmin Pan, for their kind support and excellent guidance on my research direction and methods.

Many thanks also go to my colleagues: Yin Liu, Yan Liu, Minghui Liu, Ting Li, Lijuan Yang and Hui Wang, and Thai friends: Anong, Benz, Boong, Nikom and Sue for their help in the lab.

A special thank goes to Dr. Jialong Wu for his help on everything in the lab.

Table of Contents

Author's Declaration ii
Abstract iii
Acknowledgements iv
Table of Contents v
List of Figures vii
List of Tables ix
Nomenclature x
Chapter 1 Introduction 1
1.1 Background 1
1.2 Objective of the research 3
1.3 Outline of the thesis 3
Chapter 2 Literature Review 5
2.1 Introduction 5
2.2 Techniques for making polymeric nanoparticles 6
2.2.1 Miniemulsion polymerization 6
2.2.2 Microemulsion polymerization 14
2.3 Dispersion polymerization 21
2.4 Special properties and applications of polymeric nanoparticles 25
2.5 Conclusion 27
Chapter 3 Research Methodology and Approaches 28
3.1 Introduction 28
3.2 Experimental 28
3.2.1 Materials 28
3.2.2 Equipment and characterization 29
3.3 Approach Strategies 30
Chapter 4 Differential Microemulsion Polymerization Kinetics and Mechanisms 32
4.1 Introduction 32
4.2 Kinetics and mechanisms 32
4.3 Conclusion 35
Chapter 5 Factors Influencing SBR Particle Size 36
5.1 Introduction 36

5.2 Experimental 37
5.2.1 Analysis of SBR conversion 37
5.2.2 Analysis of SBR molecular weight and its distribution 37
5.2.3 Analysis of SBR particle size 37
5.3 Results and discussion 38
5.3.1 Influence of the addition rate of monomers 38
5.3.2 Influence of the reaction temperature 40
5.3.3 Influence of chain transfer agent 43
5.3.4 Influence of the type and the amount of surfactant 51
5.3.5 Influence of solvent (DI water) 57
5.3.6 Influence of initiator 58
5.3.7 Influence of monomer feed composition 60
5.4 Conclusion 63
Chapter 6 Recovery of SBR Rubber from Latex 64
6.1 Introduction 64
6.2 Experimental 64
6.3 Results and discussion 64
6.4 Conclusion 72
Chapter 7 Influence of Particle Size on Glass Transition Temperature 73
7.1 Introduction 73
7.2 Experimental 74
7.2.1 Synthesis of SBR nanoparticles 74
7.2.2 Determination of glass transition 75
7.2.3 Determination of styrene and butadiene composition in SBR samples 75
7.3 Results and discussion 77
7.4 Conclusion 81
Chapter 8 Conclusions and Recommendations 82
References 86
Appendix A: Raw Data 92
Appendix B: ^{1}H NMR Spectra 96

List of Figures

Figure 2.1: The principle of miniemulsion polymerization [15] 7
Figure 2.2: Calorimetric curve of a typical miniemulsion (styrene, SDS, KPS) [16] 9
Figure 2.3: The evolution of the average number of radicals per particle during a typical miniemulsion using styrene (KPS as initiator) [16] 9
Figure 2.4: Scheme for the formation of miniemulsion by ultrasonication [21] 11
Figure 2.5: Variation of the particle size by verifying the relative amount and type of surfactant employed in a styrene miniemulsion [21] 12
Figure 2.6: Calorimetric profiles for styrene emulsions with different amounts of initiators [3] 13
Figure 2.7: Profile of rate of polymerization (dX/dt) versus monomer conversion for the microemulsion polymerization of n-hexyl methacrylate stabilized by dodecyltrimethyl- ammonium bromide. The discrete points represent the experimental data, and the solid lines is the model predicting value according to Eq. (2.2) [Initiator/monomer = 0.045 wt% (top) and 0.015 wt% (bottom)] [49]. 18
Figure 2.8: A schematic representation of typical polymerization rate as a function of monomer conversion profiles for microemulsion polymerization [29] 19
Figure 2.9: A schematic representation of typical polymerization rate as a function of monomer conversion profiles for conventional emulsion polymerization [29] 20
Figure 2.10: Illustration of S-SBR polymeric nanoparticles [53] 22
Figure 2.11: Synthesis of spherical PBD/PS polymeric nanoparticles [53] 23
Figure 2.12: Phase diagram of PBD/PS diblock copolymer in hexane [53] 24
Figure 2.13: PBD/PS nanoparticles with different shapes prepared by Wang et al. [11] 24
Figure 2.14: Stress-strain performance comparison of two sulphur vulcanized polybutadiene rubber compound. Compound A reinforced with carbon black; compound B reinforced with spherical PBD/PS nanoparticles [53] 26
Figure 3.1: The schematic drawing of the DMP apparatus 31
Figure 5.1: Influence of the monomer addition rate on the SBR particle size in DMP systems 40
Figure 5.2: Influence of reaction temperature on SBR particle size 42
Figure 5.3: Variation of monomer conversion and particle size in the synthesis of styrene butadiene copolymer via DMP method at [n-DDM] = 0 48
Figure 5.4: Variation of conversion and particle size versus the [n-DDM] in the synthesis of styrene butadiene copolymer via DMP method at 50 °C 49

Figure 5.5: Variation of conversion and particle size versus the [n-DDM] in the synthesis of styrene butadiene copolymer via DMP method at 75 °C 49
Figure 5.6: TEM and GPC tests for a SBR copolymer sample synthesized with an n-DDM 50
Figure 5.7: TEM and GPC tests for a SBR copolymer sample synthesized without any n-DDM 51
Figure 5.8: Schematic structure of Gemini surfactant 52
Figure 5.9: Profile of SBR particle size with various [SDS] in a DMP approach 54
Figure 5.10: Profile of SBR particle size with various [Gemini surfactant] in a DMP approach 54
Figure 5.11: Profile of SBR particle size with various [SDS] and [Gemini surfactant] in DMP approach 55
Figure 5.12: Morphologies of SBR latex particles at different phases 56
Figure 5.13: Profile of SBR particle size at various amount of water added to the DMP system 58
Figure 5.14: Profile of SBR particle sizes and reaction conversions with various [KPS] 60
Figure 5.15: Profile of SBR particle size and conversion with various ratios of BD/ST 62
Figure 5.16: Profile of the size of SBR particles at various BD/ST mole ratios 63
Figure 6.1: Structure of sodium oleate ($C_{17}H_{33}COONa$) 65
Figure 6.2: Amount of surfactant is decreasing with increasing the time of washing. 1. SBR latex particle without washing by HCl solution. 2. SBR latex particle washed by HCl solution once. 3. SBR latex particle washed by HCl solution twice 67
Figure 6.3: The SBR latex has a better solubility with less surfactant covered 67
Figure 6.4: Physical properties change of a SBR latex 68
Figure 6.5: Morphologies of SBR particles. 1. SBR particles without covered by a surfactant 2. SBR particles with covered by a surfactant 68
Figure 6.6: DSC tests for the non-purified SBR rubber (sample 1 shown in Figure 6.4) 69
Figure 6.7: DSC tests for the purified SBR rubber (sample 2 shown in Figure 6.4) 70
Figure 6.8: DSC tests for the commercial SBR rubber 70
Figure 6.9: A DSC test for a SBR rubber synthesized with the DMP method at 75 °C 72
Figure 7.1: ^{1}H NMR spectrum of a commercial SBR (75% BD and 25% of ST) in CDCl3 [73] 76
Figure 7.2: Profile of glass transition temperature with various SBR particle sizes 80
Figure 7.3: Profile of BD concentration in SBR synthesized via DMP with various glass transition temperatures 81

List of Tables

Table 3.1: Summarization of the materials applied in the synthesis of styrene-butadiene copolymer nanoparticles via differential emulsion polymerization 29
Table 3.2: Summary of the equipment applied in characterization of styrene-butadiene copolymer samples synthesized via differential emulsion polymerization 30
Table 5.1: Summary of SBR particle sizes at various addition times for [SDS] = 4.0E-5 and 5.0E-5 mol/L 39
Table 5.2: Summary of SBR particle sizes at various reaction temperatures for differential microemulsion and conventional emulsion polymerization methods 42
Table 5.3: Summary of SBR particle size and reaction conversion at [n-DDM] = 0 47
Table 5.4: Summary of SBR particle size and reaction conversion at various [n-DDM] at 50 °C 48
Table 5.5: Summary of SBR particle size and reaction conversion at various [n-DDM] at 75 °C 50
Table 5.6: Summary of SBR particle size at various [SDS] 53
Table 5.7: Summary of SBR particle size at various [Gemini surfactant] 53
Table 5.8: Summary of SBR particle size at various amount of water added to the DMP system 57
Table 5.9: Summary of SBR particle sizes and reaction conversions at various [KPS] 60
Table 5.10: Summary of SBR particle size and reaction conversion at various ratios of BD/ST 62
Table 5.11: Summary of SBR particle size at various BD/ST mole ratios 62
Table 5.12: Some physical properties of styrene and butadiene monomers 63
Table 7.1: Values of hard sphere diameter σ_0 and T_g for non-polar various size organic molecules [70] 74
Table 7.2: Summary of particle size, reaction conversion and glass transition temperature with respect to synthesis methods 80
Table 7.3: Summary of BD and ST concentration in SBR samples with respect glass transition temperature 81

Nomenclature

δ: the ratio of mass transfer in water side to the overall mass transfer around that provides the radicals for a CTA, and the value of δ is: $0 < \delta \leq 1$

σ: the oil-water interfacial tension

ΔG°: Gibbs free-energy

ΔH°: Enthalpy

ΔS°: Entropy

ϕ_j: the volume fraction

γ: the surface or interface tension

ΔA: newly formed interface

A: the frequency factor

D_w:the diffusion coefficient of a CTA radical in the water phase

d_p: is the diameter of a particle

E: the activation energy

$k_{e,m}$: the rate constant of free radicals absorption rate by micelles

$k_{e,p}$: the rate constant of free radicals absorption rate by particle nuclei

k_d : the initiator decomposition rate constant

k_{des}: Desorption rate coefficient

k_p: is the propagation reaction rate constant

k_{Tf} :the CTA rate constant

k_{pi}: the re-initiation rate constant of a CTA radical

m: the number of monomer-swollen micelles

m_d: the partition coefficient of a CTA radical between the water and particle phases

$[M]_{eq}$: the equilibrium monomer concentration in particles

$[M_p]$: the concentration of monomer in the particles

$[M]_{d,0}$: the initial concentrations of monomer in the microemulsion droplets

$[M]_0$: the initial concentrations of monomer in the polymerization system

N: the number of monomer-swollen micelles containing free radicals

N_0: the number of particle nuclei containing no radicals (inactive) per unit volume of water

N_1: the number of particle nuclei containing one free radical (active)

n: the radical number per particle

$R^{\bullet}_{(eq)}$: the free radicals in the continuous aqueous phase

$[R^{\bullet}]_w$: the free radicals concentration in the continuous aqueous phase

T_g: the glass transition temperature

$[T_p]$: the concentration of CTA

W_d: the weight of dried SBR rubber

W_t: the total weight of SBR rubber monomers introduced to the polymerization process

$X_{ij}N_j$: the miscibility of the components, where X is the interaction parameter and N is the degree of polymerization

AIBN: 2,2′-azobisisobutyronitrile

BD: Butadiene

BPO: Benzoyl Peroxide

CMC: Critical micellar concentration

CSC: Critical stability concentration

CTA: Chain transfer agent

CTMA-Cl: Cetyltrimethylammonium chloride

DMP: Differential microemulsion polymerization

DI Water: Deionized water

DLS: Dynamic light scattering

DSC: Differential scanning calorimetry

DVB: Divinylbenzne

FT-IR: Fourier transform infrared spectroscopy

^{1}H NMR: Proton nuclear magnetic resonance

HSBR: Hydrogenated SBR

GPC: Gel permeation chromatography

GS: Gemini surfactant

KPS: Potassium persulfate

n-DDM: n-dodecyl mercaptan

NBR: Acrynitrile-butadiene rubber

OMC: Octyl methoxycinnamate

PDI: Polydispersity index

PTFE: Polytetrafluoroethylene

SBR: Styrene-butadiene rubber

S-SBR: Solution styrene-butadiene rubber

SDS: sodium dodecyl sulphate

ST: Styrene

TEM: Transmission electron microscopy

THF: tetrahydrofuran

Chapter 1 Introduction

1.1 Background

The copolymer of styrene butadiene rubber (SBR) is one of the most relevant technical rubbers, which accounts for about 40% of the total synthetic elastomer production, its major consumption being in tires and tire products [1]. SBR can be synthesized either by styrene and butadiene homogeneous phase solution polymerization or by heterogeneous phase emulsion polymerization. Indeed, in most cases, SBR latices are generated via typical radical emulsion polymerization processes. Pure SBR rubber is attained by coagulating the SBR copolymer from its emulsion solution, separation, washing and drying steps. Due to the existence of residual carbon-carbon double bonds in the polymer backbone, SBR rubbers are non-resistant to oxygen, ozone, ultraviolet light and high temperature. In order to alleviate this deficiency, selective hydrogenation of the unsaturated bonds in SBR copolymer is applied.

Prior to the hydrogenation step, the SBR rubber should be dissolved in a suitable solvent. Thus, by performing this step, the applied solvent breaks down the SBR rubber matrix to increase its exposed surface area to a catalyst, and in turn to make the hydrogenation step easily accessible. Once a homogeneous SBR rubber in solution is attained, the hydrogenation catalyzed by a noble metal under a high pressure of hydrogen gas is performed. In the final stage, the catalyst will be recovered from the solution and the dried hydrogenated SBR (HSBR) is obtained by evaporating its solvent completely [2-3]. This process for

hydrogenation of SBR rubber has been commercially carried out and provides various grades of HSBR rubbers. However, there are some apparent problems with this kind of hydrogenation process [4]. Besides the high cost of the catalyst, hydrogenation equipment, low efficiency often results from limited solubility and solvent-induced environmental concerns. Furthermore, this method is not applicable when hydrogenation of polydiene is required in the latex form.

In 1984, Wideman developed a breakthrough process to directly convert SBR and NBR latexes into their saturated forms without the application of noble metal catalysts, organic solvents, and high pressure hydrogenation equipment [5]. He described a procedure which involved a system containing hydrazine hydrate, an oxidant and a metal-ion catalyst. The NBR latex was directly hydrogenated up to 80% with hydrogen peroxide functioning as an oxidant, hydrazine acting as a reducing agent, and copper (II) salts functioning as a catalyst. Due to the low hydrogenation degree (80%) of this specified hydrogenation process; improvements have been made to increase the hydrogenation degree by: eliminating the cross-linking degree in polymeric materials, and reducing the polydiene particle size. Also, the replacement of copper (II) salts by boric acid helps to reduce the cross-linking and improves the hydrogenation degree dramatically, the study of the reduction of particle size on hydrogenation of polydiene materials such as SBR rubber has been a popular topic for investigation.

1.2 Objective of the research

Styrene-butadiene copolymer nanosized latex particles were prepared by differential microemulsion polymerization (DMP), which was initiated by a water soluble initiator potassium persulfate (KPS). The DMP approach is a very efficient way which requires a much less surfactant compared to microemulsion and miniemulsion polymerization to prepare nanosized polymeric particles. The nanosized polymeric particles generated by miniemulsion and microemulsion are about 50 to 200 nm and 20 to 50 nm, respectively. The objective of the research is to use much less amount of surfactant to prepare comparable size of SBR nanoparticles which were synthesized by miniemulsion and microemulsion. Furthermore, properties of SBR latex particles should also be characterized to study various factor influencing the particles properties prepared by the DMP approach.

1.3 Outline of the thesis

Chapter 1 provides the introduction, objective of the research and outline of the thesis.

Chapter 2 overviews the current most advanced heterogeneous emulsion polymerization techniques, which include miniemulsion and microemulsion polymerizations. In this chapter, the formation of an emulsion phase, kinetics and mechanisms, applications, surfactant and initiator influences related to the miniemulsion and microemulsion are reviewed. By summarizing the literature in this chapter, it becomes apparent that miniemulsion and microemulsion require a large amount of surfactant to produce small nanosized polymeric particles.

Chapter 3 reviews the differential microemulsion polymerization technique.

Chapter 4 gives a brief review of mechanisms and kinetics related to the differential microemulsion polymerization approach.

Chapter 5 investigates the major factors that can influence the size of SBR particles synthesized via differential microemulsion polymerization. These factors consist of the monomer addition rate, the reaction temperature, the type and the amount of surfactant applied, the amount of chain transfer agent, the amount of initiator, and the monomer feed composition.

Chapter 6 reviews the method of purifying the SBR latex particles by using an acidified ethanol solution. Purified SBR rubbers without any surfactant component show better results for the GPC, DSC, TEM and ^{1}H NMR characterization tests.

Chapter 7 provides the information on the influence of particle size on the glass transition temperature of SBR rubbers synthesized via differential microemulsion polymerization and conventional polymerization. Owing to the difference in the particle nucleation mechanisms of these two techniques, the resultant rubber may have different compositions and structures that influence the glass transition temperature. Indeed, the study shows that the glass transition temperature is particle size dependent.

Chapter 8 provides the conclusions for this thesis and provides the recommendations for the future work based on the results of the current research.

Chapter 2 Literature Review

2.1 Introduction

Methods that allow for the synthesis of polymeric nanosized particles with varied and complex structures and attractive functions have been receiving a great deal of attention during the past decade. This growing interest is due to the fact that optimally designed polymeric nanoparticles ranging in size from 10 nm to more than 100 nm have many potential benefits in technologies including medicine and health, information technology, material and manufacturing, aeronautics and space exploration, and environmental and energy applications [5-9].

In this chapter, three different techniques that are very popular in preparing nanosized polymeric particles are reviewed. The first and the second one are improved systems of the heterogeneous emulsion polymerization. Owning to the fact that initiators and surfactants have a great effect on a heterogeneous system, kinetics and mechanisms related to these two factors will be studied. Unlike the first two methods, the third one describes a dispersion polymerization process. As for the formation of polymeric nanoparticles, it has recently been found that block copolymers can undergo a self-assembly process to form nanoparticles in a selective solvent in which only one block is soluble; this method is a typical example to be reviewed for studying the formation of novel sized polymeric particles in a surfactant- free system.

2.2 Techniques for making polymeric nanoparticles

Conventional polymerization is extensively used for the preparation of small particles of polymer latex and coating materials. However, polymeric particles synthesized by this method are generally quite large (bigger than 10^3 nm), which is not applicable for nanoparticle preparation [10-11]. To improve this system, miniemulsion and microemulsion methods are invented to prepare particles in the range of 50 – 200 nm and 20 – 50 nm, respectively [12-13]. Miniemulsion and microemulsion polymerization techniques apply the self-assembly concepts to create a variety of stable polymeric nanoparticles with the requirement of a minimum amount of surfactant in a water based solvent. Given that the addition of surfactant in miniemulsion and microemulsion systems may limit the polymer solid content in the dispersion and also their applications, a method for the preparation of surfactant-free polymeric nanoparticles is also reviewed. The nanoparticles generated by this method have a mean average size that is most preferably less than 25 nm and the dispersity represented by the ratio of M_w to M_n less than about 1.1.

2.2.1 Miniemulsion polymerization

Miniemulsions are specially formulated heterogeneous phase systems. The small, homogeneous and stable nanodroplets of monomer or polymer precursors are evenly dispersed in their continuous phase, in which transportation of initiators, side products and heat is performed. Miniemulsion nanodroplets are transferred by polymer reactions to the final polymer latex without any kinetically controlled growth [14]. This means that each droplet is an independent unit that becomes the primary location of initiation, polymerization

or polyaddition of reactant monomers. The term “nanoreactor” is often used to describe miniemulsion droplets that behave like an independent reaction vessel keeping their particular identity without serious kinetic events involved. Figure 2.1 schematically illustrates the principle of miniemulsion polymerization.

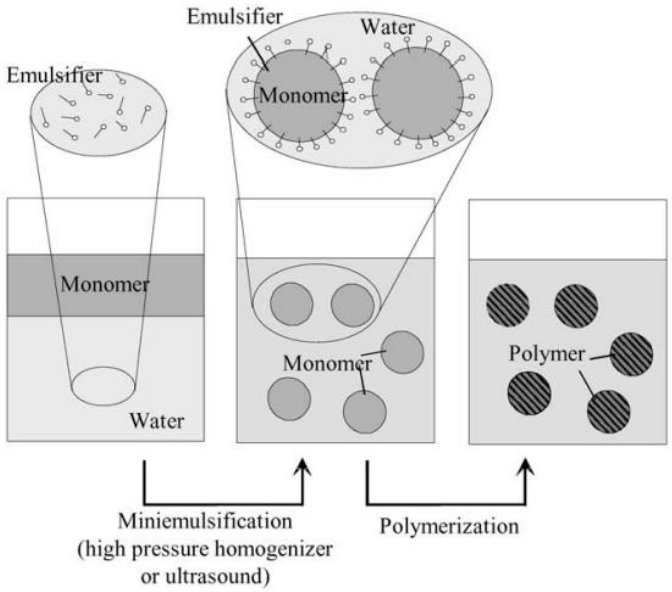

Figure 2.1: The principle of miniemulsion polymerization [15]

Miniemulsion polymerization shows a promise to produce nanosized SBR particles between 30 nm and 500 nm when appropriate combination of saturated high shear treatment, surfactants, and the presence of an osmotic pressure agent insoluble in the continuous phase is employed. Due to the nanoreactor situation, even at high conversions, still a lower gel fraction of polymer produced compared to the polymers synthesized via conventional emulsion polymerization is possible. The reduction of gel fraction is attributed to the high ratio of monomer-to-polymer above a critical point in the miniemulsion droplet that reduces the branching and delays the crosslinking possibilities [16]. This is the reason for

investigating miniemulsion polymerization as a means of preparing poly styrene-butadiene (PSB) lattices.

2.2.1.1 Mechanisms and kinetics of miniemulsions

Nucleation mechanisms of miniemulsion polymerization are generally considered to differ from a conventional emulsion polymerization, and hence the properties of the resulting latexes will be different. In principle, for heterogeneous phase polymerization, three particle nucleation mechanisms are currently discussed in the literature [15]: micellar nucleation, homogeneous nucleation and droplet nucleation. The micellar particle nucleation mechanism also called heterogeneous nucleation occurs when radicals from the aqueous phase enter the micelle. Micellar nucleation is the predominant nucleation process when the surfactant concentration is above the critical micelle concentration (CMC). Homogeneous nucleation is also called surfactant-free emulsion polymerization and occurs in the continuous aqueous phase, in which nuclei locus formed by oligomer aggregation, and the polymer chain grows when monomers in the aqueous phase react with the oligomeric radicals [16-17]. This mechanism relies on the solubility of the employed monomer and the initiator concentration. The droplet nucleation mechanism takes place when monomer droplets are polymerized by the radicals that enter the nucleation sites. In a miniemulsion polymerization, nucleation typically takes place in the small and relatively stable monomer droplet; therefore, the droplet nucleation is expected to be the dominant mechanism [15]. As a result, the particle size is independent of the initiator concentration and the overall reaction rate is only influenced by the number of droplets [16]. Conductance measurements during the miniemulsion

polymerization were performed to support the droplet nucleation as the predominant mechanism of particle formation [19]. Figure 2.2 indicates the calorimetric curve of a typical miniemulsion polymerization of styrene.

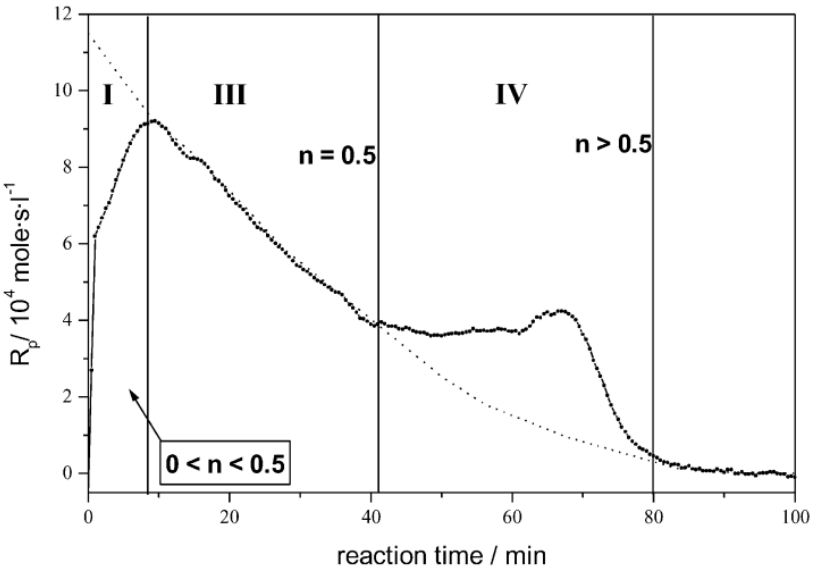

Figure 2.2: Calorimetric curve of a typical miniemulsion (styrene, SDS, KPS) [16]

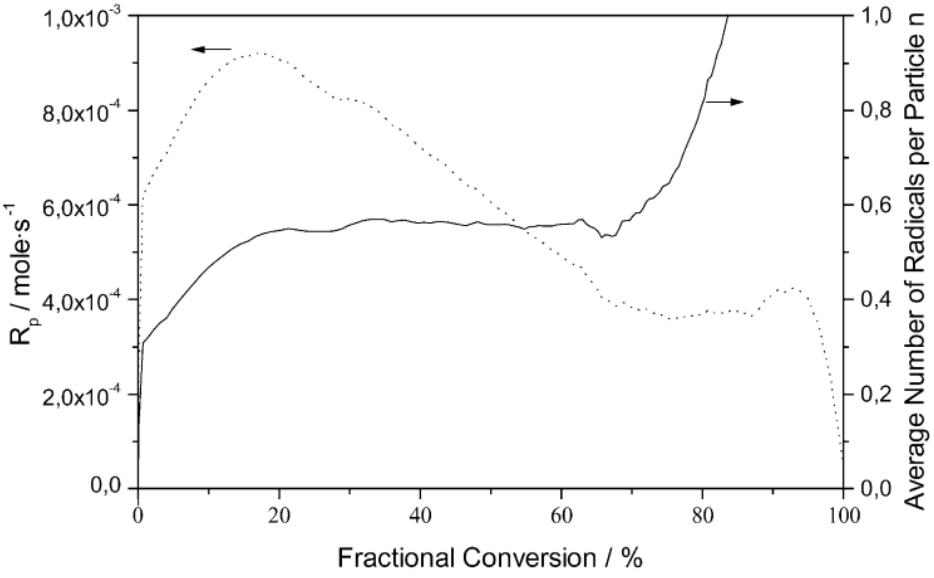

Figure 2.3: The evolution of the average number of radicals per particle during a typical miniemulsion using styrene (KPS as initiator) [16]

As shown in Figure 2.2, three distinct intervals are recognized during the miniemulsion polymerization. The first interval (interval I) is the process of particle nucleation. This interval describes the process to reach a steady state radical concentration in the droplets formed by emulsification. As seen from Figure 2.3, this process ends at low conversion, maximum 20%, which shows that every droplet nucleates before unbalanced mass transfer can play a crucial role. Moreover, as indicated from Figure 2.2, the reaction time for this process is about 8 minutes which is expected. Due to the low styrene concentration in water, it will take some time to dissolve in the aqueous phase in order to take up highly hydrophilic sulphate radicals from KPS into the droplets for nucleation. Interval III begins after the average radical number per particle ($n \cong 0.5$) is reached during interval I. Thus, by following the droplet nucleation mechanism, only the monomer in the droplet is available for polymerization, and this is exponentially depleted from the reaction site as indicated by the dotted line in Figure 2.2. Additionally, the peak found in interval IV is the typical gel-peak that is caused by the viscosity increase inside the particle and the coupled kinetic hindrance of radical recombination. Similarly to some microemulsion polymerization processes, there is no interval II of constant reaction rate. This explains that the diffusion of monomer is in no phase of the rate determining step [20].

2.2.1.2 Miniemulsion preparation for styrene-butadiene copolymer nanoparticles

Miniemulsion preparation of SBR nanoparticles starts with mechanical emulsification of the premix of the fluid phases containing surfactants and further surface-active additives. In general, the emulsification includes two steps: firstly, deformation of droplets to increase the

total surface area of the emulsions; and secondly, stabilization of newly formed areas by surfactants.

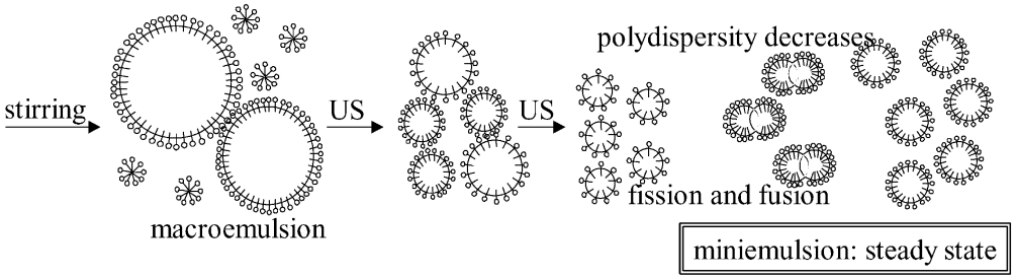

Figure 2.4: Scheme for the formation of miniemulsion by ultrasonication [21]

Miniemulsion can be obtained by different methods. However, the most commonly used technique is ultrasonication [22]. As a high force dispersion device, ultrasonication creates enough energy to disrupt large monomer droplets into smaller ones. The energy is much higher than the difference in surface energy $\gamma\Delta A$, where γ is the surface or interface tension and ΔA is the newly formed interface [23, 24]. During the deformation of a single droplet, there are nearly no surfactant molecules absorbing at the newly formed surface. This indicates that the absorption time of a surfactant molecule is longer than the disruption step. Therefore, the elongation of residual times is necessary to ensure surfactant adsorption at the newly formed droplets. In miniemulsion of styrene and butadiene monomers, the droplet size is determined by the amount of monomer and water, the monomer solubility and the amount of surfactant. However, at the beginning of emulsification, it was found that the initial droplet size is a function of the mechanical agitation [22, 26]. The monomer droplets size changes quite rapidly during sonication until it reaches a steady state. The polydispersity of the droplets decreases once this state is reached, and the size of the monomer droplet is no

longer a function of the amount of applied mechanical energy. The scheme displayed in Figure 2.4 shows a progress of the formation of miniemulsion by ultrasonication.

2.2.1.3 Influence of surfactant

In miniemulsions, the size of the droplet and the fusion-fission rate equilibrium during sonication directly depend on the amount of surfactant employed. By variation of the relative amount of surfactant to monomer, the particle size can be varied over a wide range [26]. Figure 2.5 indicates variation of the particle size by verifying the relative amount and type of surfactant employed in a styrene miniemulsion [21].

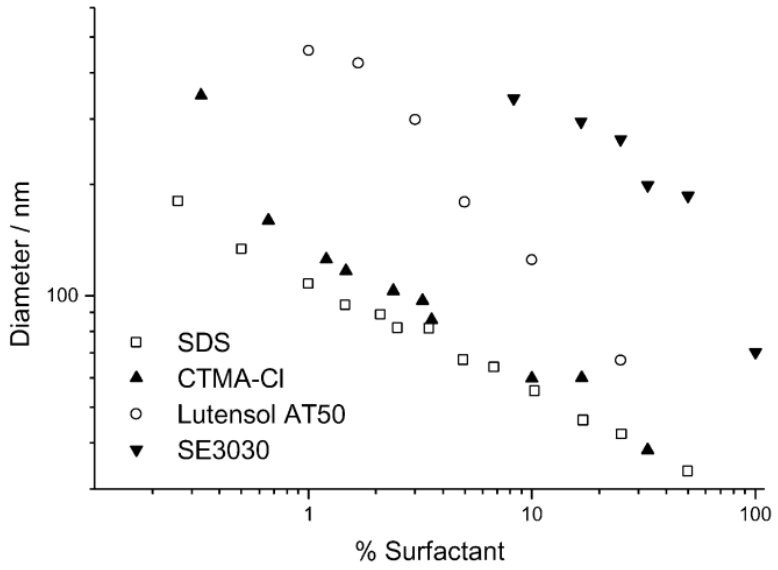

Figure 2.5: Variation of the particle size by verifying the relative amount and type of surfactant employed in a styrene miniemulsion [21]

Among the four types of surfactant as indicated in Figure 2.5, SDS is an anionic surfactant, cetyltrimethylammonium chloride (CTMA-Cl) is a cationic surfactant, and Lutensol AT50 and SE3030 are non-ionic surfactants. Latices synthesized with SDS and CTMA-Cl show

almost the same curve. Thus, it concluded that the efficiency of the surfactant and the size dependent surface coverage are independent of the sign of charge. However, the efficiency of the two non-ionic surfactants is lower and the polydispersity of the latex is broader compared to ionic ones. This is due to the lower efficiency of the steric stabilization of non-ionic surfactants as compared to electrostatic stabilization of ionic ones. In order to overcome this obstacle, a much denser packing of non-ionic surfactant is necessary for synthesizing smaller and more uniform sized nanoparticles.

2.2.1.4 Influence of initiators – Water soluble initiators

The formation of free radicals by decomposition of water soluble initiators occurs in the water phase. As revealed by calorimetry, varying the concentrations of initiators gives surprising similar calorimetric profiles (Figure 2.6).

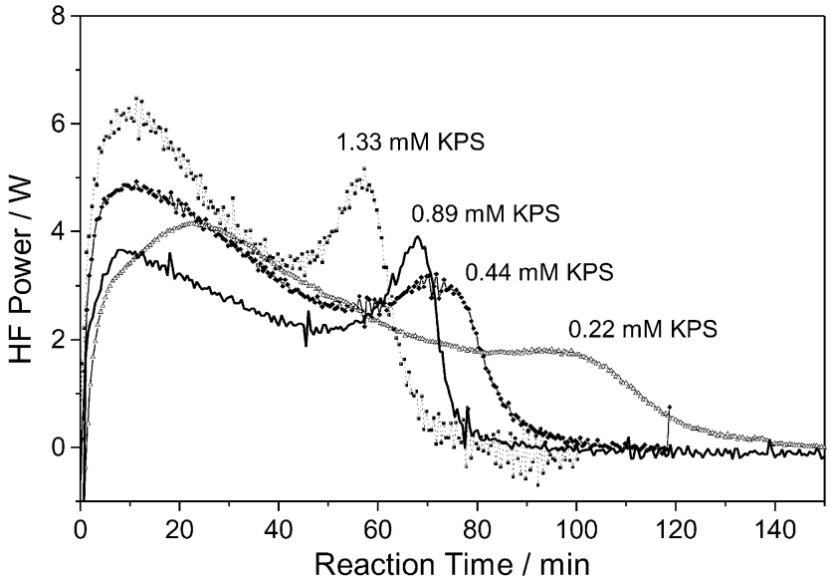

Figure 2.6: Calorimetric profiles for styrene emulsions with different amounts of initiators [3]

Similarly to Figure 2.2, Figure 2.6 indicates that after passing the particle nucleation phase, interval I, the polymerization process in interval III is independent of the amount of initiator. Thus, the increase in the concentration of initiator cannot accelerate the rate of polymerization. However, the interval IV depends on the amount of initiator. The earlier and the more pronounced the gel-peak is the more dependent the initiator concentration is.

2.2.1.5 Influence of initiators – Oil soluble initiators

Oil soluble initiators can also be used for miniemulsion polymerization of monomers owning to their extremely low water solubility. Initiators with different water solubilities, namely LPO, BPO and AIBN have been investigated [27]. The investigation focused on the ability of the initiators in stabilizing monomer droplets against degradation by molecular diffusion and their efficiency for polymerization. As radicals in the droplets can be formed either by desorption of the radicals from initiator decomposition or by entry of radicals from the continuous phase, the way to make oil soluble initiators effective only when one or both of the formed radicals are sufficiently hydrophilic is to undergo desorption. Compared to different oil soluble initiators, AIBN is more efficient than LPO and BPO based on reported studies of styrene miniemulsions.

2.2.2 Microemulsion polymerization

Microemulsion polymerization provides a unique micro-environment existing with its: extremely large internal interfacial area (~$10^5 m^2 dm^{-3}$), optical transparency and thermodynamic stability, which can be advantageous to produce novel materials with interesting morphologies and a polymer with specific properties. Therefore, the field of

developing nanosized SBR particles by microemulsion polymerization is receiving a great deal of attention. The concept of free radical polymerization in microemulsion droplets was established by the work of Schauber in 1979 [28]. Microemulsion polymerization involves the free radical polymerization inside very fine monomer droplets. The polymer colloid products generally exhibit small latex particles and very-high-polymer molecular weight (in the range 10^6 – 10^7 $gmol^{-1}$) that cannot be achieved readily by conventional emulsion or miniemulsion polymerization [29-31]. In addition, the particle nucleation and growth kinetics and mechanism in microemulsion systems are also quite different from those of emulsion and miniemulsion polymerization systems. Research interests in polymerization techniques of microemulsions have grown rapidly since the 1980s due to a wide range of potential applications in the preparation of fine latex particles, novel porous materials, polymeric supports for binding metal ions, conducting polymers and transparent colloidal systems for photochemical and other chemical reactions [32-36].

2.2.2.1 Formation of microemulsion

In a colloidal system at a constant temperature, volume and composition, the change of Helmholtz free energy (dF) with respect to the development of the oil-water interfacial area ($dA > 0$) can be written as:

$$dF/dA = \sigma - W_{des} \qquad (2.1)$$

where σ is the oil-water interfacial tension and W_{des} is the sum of various factors, such as: the work of desorption of the surfactant per unit interfacial area, changes of entropy, surface charge density and molecular interactions between constituents of the interfacial film. When

σ is really small (10^{-3}mNm^{-1} or smaller) and W_{des} is sufficiently large, the value of dF/dA becomes negative. Since the development of the oil-water interfacial area is increasing ($dA > 0$) when the amount of particles is growing, the value of dF is smaller than zero ($dF < 0$) in the process of development of microemulsion. Under this circumstance, the spontaneous formation of small particles (10^0-10^1 nm) is achieved in a thermodynamically stable microemulsion system [29].

2.2.2.2 Influence of surfactants

Surfactants are key formulation variable that determine the size and the size distribution of the particles formed during microemulsion polymerization. Radicals generated in the aqueous phase enter the monomer emulsion droplets as single radicals or oligomeric radicals and propagate to form particles. The colloidal stability is due to the adsorption of surfactant molecules on the surfaces of the monomer droplets and growing polymer particles.

The choice of surfactant is critical since it controls the stability of the emulsions prior to and after polymerization. The anionic surfactant sodium dodecyl sulphate in combination with a short-chain alcohol (e.g., n-pentanol) as the cosurfactant is the most popular stabilization package used in common microemulsion polymerization systems. In the preparation of oil in water microemulsions, incorporation of amphipathic cosurfactant into the adsorbed layer of anionic surfactant around the oil droplet greatly reduces the electrostatic repulsion force between two adjacent molecules, which lowers the oil-water interfacial tension to close to zero and enhances the flexibility of the interfacial layer. All these synergistic factors promote the spontaneous formation of transparent one phase microemulsions that allows satisfactory

control of the reaction temperature and the product is an ultrahigh-molecular-weight polymer dispersion that exhibits excellent fluidity. When dodecyltrimethylammonium bromide, a cationic surfactant, is applied alone, no cosurfactant is required to form satisfactory microemulsion products in a microemulsion system. However, it should be noted that spontaneous formation of thermodynamically stable microemulsions generally requires a small amount (only a few percent) of monomers along with a very large amount (>10%) of surfactant due to the extremely large oil-water interfacial area that needs to be stabilized.

2.2.2.3 Mechanisms and kinetics of microemulsions

Significant efforts have been devoted to microemulsion polymerization mechanisms and kinetics since the 1980s. Studies of oil-in-water (or water-in-oil) microemulsion systems simplify the investigation of the interactions among monomer, polymer, surfactant, and water; and therefore, provide a fundamental understanding of the complex polymerization mechanisms and kinetics in self-organized reaction media [37-47]. These studies showed that the monomer solubility in water has a significant influence on the polymerization kinetics and mechanisms. It was postulated that, for monomers that have a very limited water solubility, nucleation in the microemulsion droplets predominates the polymerization process due to the effective capture of free radicals generated in the aqueous phase by the very large amount of microemulsion droplets. On the other hand, polymerization of the relative hydrophilic monomers initiated by the water soluble initiator may lead to a homogenous and microemulsion droplet nucleation mix mode of particle nucleation.

A model used for predicting the kinetics of microemulsion polymerization was developed by Morgan et al. [49] as shown below.

$$\ln(1 - X) = -f k_d [I]_0 k_p [M]_{d,0} t^2 / [M]_0 \qquad (2.2)$$

where, X is the monomer conversion, f is the initiator efficiency factor, k_d is the initiator decomposition rate constant, k_p is the propagation reaction rate constant, t is the reaction time, and $[M]_{d,0}$ and $[M]_0$ are the initial concentrations of monomer in the microemulsion droplets and in the polymerization system, respectively.

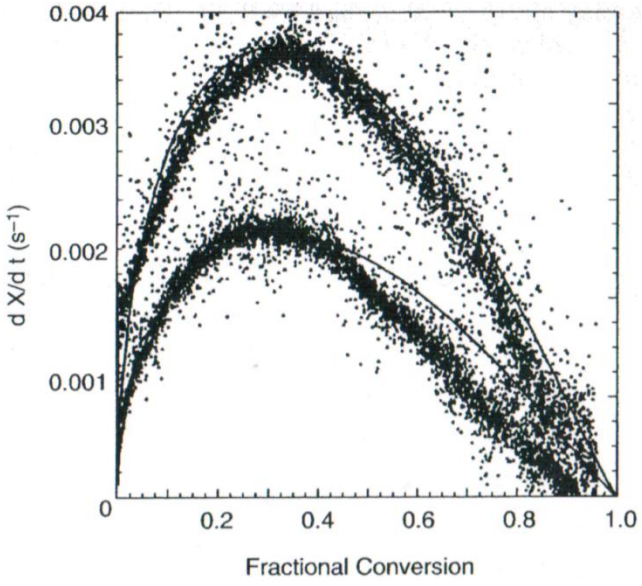

Figure 2.7: Profile of rate of polymerization (dX/dt) versus monomer conversion for the microemulsion polymerization of n-hexyl methacrylate stabilized by dodecyltrimethyl- ammonium bromide. The discrete points represent the experimental data, and the solid lines is the model predicting value according to Eq. (2.2) [Initiator/monomer = 0.045 wt% (top) and 0.015 wt% (bottom)] [49].

This kinetic equation was derived based on the assumption that: (a) all the free radicals generated in the aqueous phase can enter the microemulsion droplet and initiate the

polymerization; (b) any bimolecular termination reaction is negligible in the aqueous phase; (c) the adsorption of free radicals by the latex particles is insignificant; (d) the growing polymeric radicals terminated primarily by a monomer chain transfer action. This model predicts well at lower conversion; poor performance obtained at high monomer conversion was often observed (Figure 2.7). The deviation between the predicted value and experimental value shows that homogeneous nucleation and flocculation of particle nuclei cannot be completely prohibited in microemulsions.

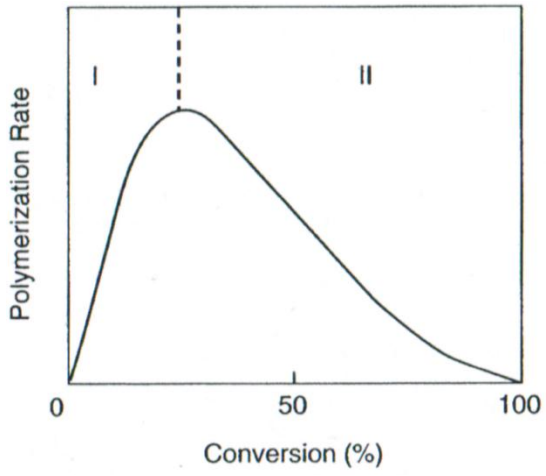

Figure 2.8: A schematic representation of typical polymerization rate as a function of monomer conversion profiles for microemulsion polymerization [29]

In fact, this model is the only one that can predict the course of microemulsion polymerization. Figure 2.8 displays a schematic representation of typical polymerization rate as a function of the monomer conversion profile for the oil-in-water microemulsion polymerization, which shares a similar polymerization rate profile as found in Figure 2.7. The rate of polymerization increases to a maximum with the progression of the reaction (Interval I), and decreases toward the end of the reaction (Interval II). Furthermore, the

period of constant polymerization rate that is often detected in conventional emulsion polymerization (Figure 2.9) disappears in the microemulsion polymerization. This is attributed to the fact that the resultant latex particles (20 – 30 nm in diameter) are so small that they cannot accommodate more than one free radical, and thus the rapidly increased monomer conversion with time due to greatly retarded bimolecular termination reaction is suppressed to successfully reduce the gel effect.

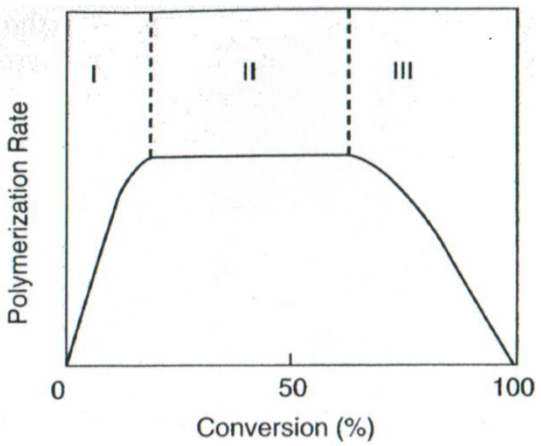

Figure 2.9: A schematic representation of typical polymerization rate as a function of monomer conversion profiles for conventional emulsion polymerization [29]

The water-insoluble dye technique was also adopted to study microemulsion polymerization mechanisms and kinetics [50]. The rationale behind this approach is that: most of the dye molecules can be incorporated into the microemulsion droplets prior to initiation, and will be integrated into the resultant latex particles after their accommodated droplets are initiated by free radicals originating from a water soluble initiator and undergo free radical polymerization. Ultimately, the weight percentage of the dye integrated into the final latex particles serves as the indicator for the extent of nucleation in the microemulsion

polymerization process [50]. Based on the experimental data, it was suggested that the increase of water soluble initiator (sodium persulfate) concentration not only increases the chance of the capture of free radicals by the microemulsion droplets but also promotes the precipitation of oligomeric radicals out of the aqueous phase to form the particle nuclei [51]. The latter cause may override the former as the reduction of dye content in the resultant latex particles was found with the increase of the water soluble initiator concentration.

Oil-soluble initiator, 2,2′-azobisisobutyronitrile (AIBN), was also studied in reference 35 with respect to the particle nucleation and growth mechanisms involved in the microemulsion polymerization. Considering the limited solubility of AIBN in the aqueous phase, the formation of particle nuclei in the aqueous phase can be suppressed to some extent. However, this was not the case. As the microemulsion droplet is too small to accommodate two AIBN radicals produced as pairs, the particle nucleation process may involve the desorption of one free radial out of the microemulsion droplet, and the entry of one free radical into the droplet containing no free radicals. Under these circumstances, the particle nucleation process undergoes a very low efficiency initiation reaction. Therefore, to overcome this situation, a much higher AIBN concentration is required to attain comparable dye content in the resultant latex that is synthesized in microemulsion polymerization initiated by water soluble initiators.

2.3 Dispersion polymerization

Dispersion polymerization can also be applied to synthesize nanosized polymeric particles. Since there is no surfactant used in this approach, it is also called surfactant-free

polymerization. In U.S. Patent Application 20100004398 [52], Wang et al. from Bridgestone America unveiled a new method for preparation of polymeric SBR nanoparticles with varied complex structures and functions via dispersion polymerization. The SBR nanoparticles with a core/shell configuration consisting of more than one layer with an average size range from 20 to 50 nm. Figure 2.10 illustrates several spherical shaped nanoparticles interacting with each other at their interphase regions.

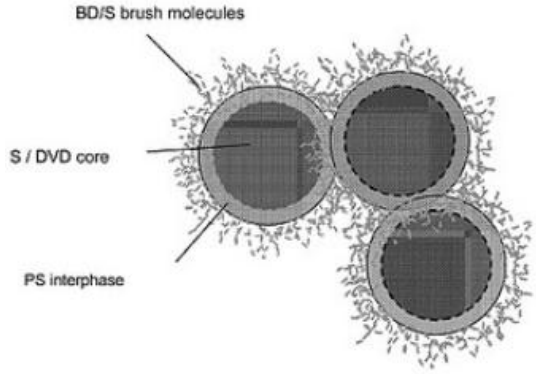

Figure 2.10: Illustration of S-SBR polymeric nanoparticles [53]

2.3.1.1 Preparation of SBR nanoparticles via dispersion polymerization

SBR polymeric particles were prepared in a hexane solution. Because the solubility of polystyrene blocks in hexane is much lower than polybutadiene, this living diblock aggregate forms spherical micelles, with the styrene blocks directed toward the center of micelles and the butadiene block as tails extending therefrom. After forming the micelles, 8 wt% of divinylbenzne (DVB) was added. DVB reacts with the living anions on the polystyrene chain ends to form the nanoparticle with a highly cross linked region in core (Figure 2.11 Option A). Alternatively, instead of adding styrene and DVB in a sequential manner, they can be

added at the same time, as shown in Figure 2.11 Option B. This option provides an opportunity to obtain the nanoparticle with a more uniform cross linked core region.

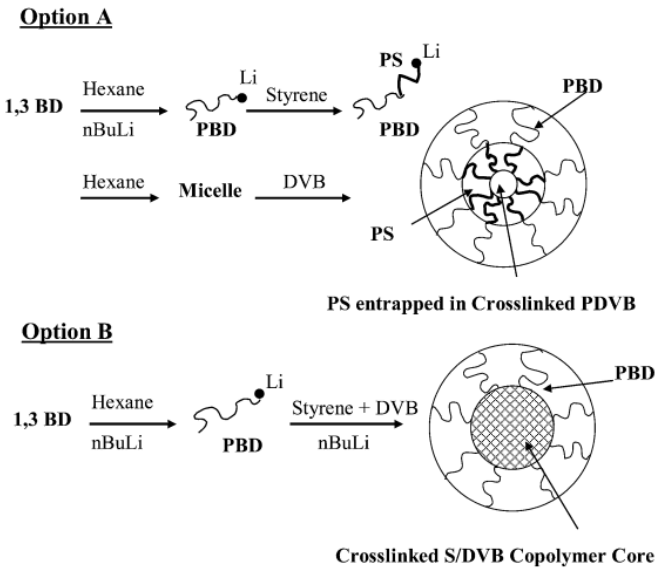

Figure 2.11: Synthesis of spherical PBD/PS polymeric nanoparticles [53]

2.3.1.2 Kinetics and Mechanisms

The micellization of styrene-butadiene diblock copolymers is an enthalpy driven process with the negative Gibbs free energy in Eq. (2.3) dominated by a negative ΔH°.

$$\Delta G^\circ = \Delta H^\circ - T\Delta S^\circ \qquad (2.3)$$

The change in entropy is also negative. However, due to the stronger polymer/polymer interaction in the micelle cores compared to polymer/solvent and solvent/solvent interaction in the absence of micelles, $T\Delta S^\circ$ is much smaller than ΔH°, which results a negative value of Gibbs free energy [53]. By alternating the thermodynamic conditions of the self-assembly of BD/ST block copolymers, micelles of different structures are expected to be generated. Various micelle shapes that can be prepared in a given solvent governed by the shell to core

volume fractions of the components (ϕ_j, i=1, 2), the miscibility of the components ($X_{ij}N_j$, where X is the interaction parameter and N is the degree of polymerization), and on the shell

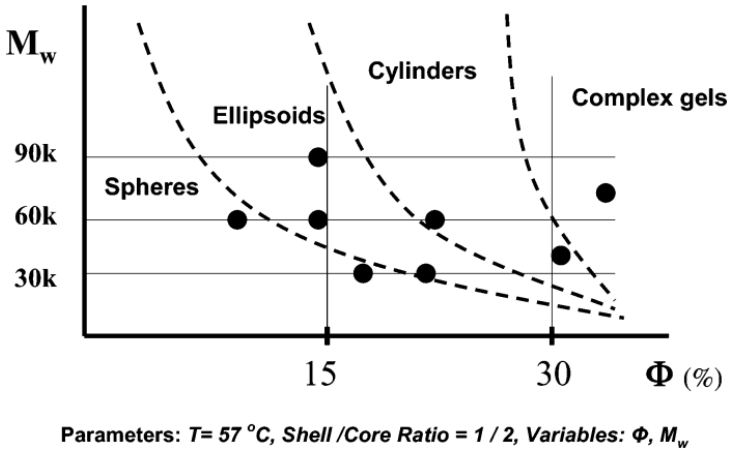

Figure 2.12: Phase diagram of PBD/PS diblock copolymer in hexane [53]

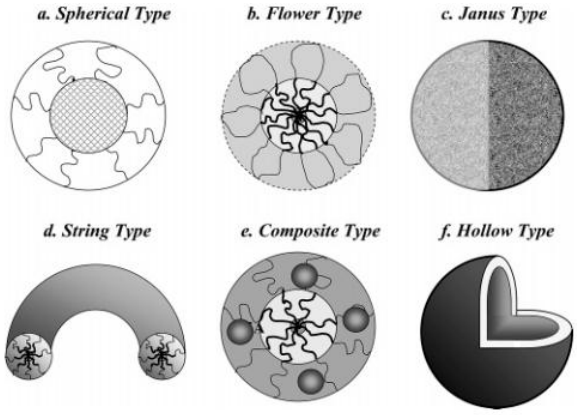

Figure 2.13: PBD/PS nanoparticles with different shapes prepared by Wang et al. [11]

to core volume fraction [54, 55]. Figure 2.12 shows a phase diagram of PBD/PS diblock copolymer in hexane. From the diagram, it can be seen that increasing the block copolymer concentration in hexane favors the formation of a cylinder shape, while decreasing the molecular weight of the block copolymer favors the formation of a sphere shape. On the

basis of this information, Wang et al also prepared a variety of spherical and non-spherical nanoparticles as shown in Figure 2.13.

2.4 Special properties and applications of polymeric nanoparticles

Since its first industrial scale appearance in 1937, considerable research has been aimed at synthesizing a rubber with specific properties that may offer enhanced physical, chemical or biological properties in different applications. Over the past decade, there has been considerable research interest in the area of developing nanoscaled SBR polymeric particles. The most important reason for this is that nanoscaled SBR polymeric materials functioning as reinforcing agents will provide a better reinforcement than the conventional solid powders fillers such as carbon black and silica. Due to the size in the nanoscale, SBR reinforcing agents are dispersed well in the rubber matrix to reinforce the filler network by providing certain chemical interaction between the filler and the matrix.

Wang et al. [56] from *Bridgestone Americas* has synthesized various SBR nanoparticles with different shapes and sizes, cross-linked polystyrene cores and polybutadiene brushes. Polymeric nanoparticle shells act as “load holding chains” that connect to the hard reinforcing core of the particle at one end, and covalently entangles with the host polymer network in the other end during the vulcanization step. As a result, greater reinforcement and superior failure properties are found for the compound (compound A) containing polymeric nanoparticles. In contrast, rubber compounds (compound B) reinforced with carbon black having a filler/network linkage in the form of van der Waals bonding are weaker than the covalent bonding leading to a weaker performance of the compound. Figure 2.14 shows the

difference of the stress-strain performance between compound A and compound B enforced by polymeric nanoparticles and carbon black, respectively.

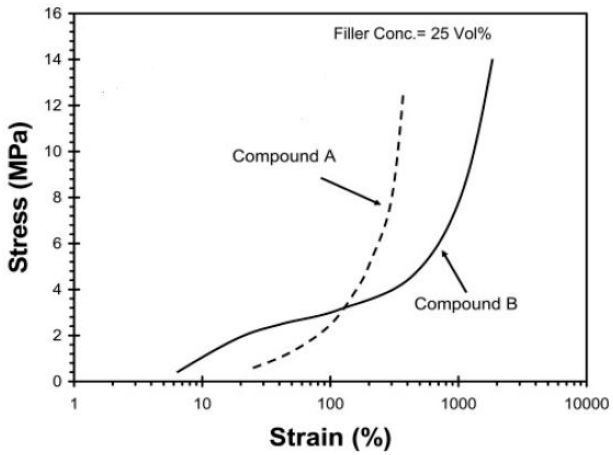

Figure 2.14: Stress-strain performance comparison of two sulphur vulcanized polybutadiene rubber compound. Compound A reinforced with carbon black; compound B reinforced with spherical PBD/PS nanoparticles [53]

In addition, polymeric nanoparticles have significant importance in the biomedical field. The polymeric nanoparticles prepared by the most commonly used nanopecipitation method are intended for cutaneous applications. This is due to the fact that high surface area of polymeric nanoparticles can facilitate the contact of the encapsulated molecules with the stratum corneum, and the incorporation of drugs with nanocapsules is able to modify the activity of drugs by changing their formulated physico-chemical properties and control the drug release and increase the drug adhesivity in the skin. The nanoencapsulation of a sunscreen, the octyl methoxycinnamate (OMC), to improve a remanence and a limited penetration in the skin is a typical example of the application of polymeric nanoparticles. Results have shown that the incorporation of OMC in nanocapsules decrease its release compared to the free OMC emulsions. This is attributed to the significant reduction of UV-

inducted erythema by the gel containing nanocapsules. Thus, the sunscreen can remain longer on the surface of skin. Furthermore, the encapsulation of OMC in nanocapsules has shown a decreased diffusion rate, as well as OMC has shown a slower penetration rate of the sunscreen in the skin when nanoencapsulated.

2.5 Conclusion

Miniemulsion, microemulsion and dispersion polymerization in preparing the polymeric nanoparticles have been examined. The mechanism in miniemulsion dominated by droplet nucleation produces nanoparticles in the range 50 to 200 nm, while the mechanism in microemulsion dominated by micellar nucleation generates nanoparticles in the range 20 to 50 nm. The smaller particle size from microemulsion determined by a thermodynamic stable and a spontaneously formed state relies on the high concentration of surfactant (7 – 15%). The requirement of a large amount of surfactant raises concerns with respect to the additional cost of the surfactant and post-treatment of microemulsion polymerization, which may severely limit the potential applications of microemulsion polymerization. Dispersion polymerization utilizing the differences in solubility between one and another organic solutions produce SBR nanoparticles in the range 20 to 50 nm in a hexane solution. This approach is an enthalpy driven process, in which the self-assembly technique directs the formation of polymeric nanoparticles. In addition, the application of polymeric nanoparticles was also reviewed. It has been shown that the application of nanoscaled polymeric materials can be found not only in the area of tire industry but also in the field of biomedical applications.

Chapter 3 Research Methodology and Approaches

3.1 Introduction

This chapter summarizes the major materials and equipment employed in synthesizing styrene-butadiene copolymer nanoparticles via differential microemulsion polymerization. In addition, characterization tests are also briefly described, but the detailed description related to specific characterization can be found in the experimental section of the following chapters. Last but not least, the last section "Approach Strategies" shows a typical procedure of synthesizing SBR polymeric particles via the DMP approach.

3.2 Experimental

3.2.1 Materials

Potassium persulfate (KPS, 98%), sodium dodecyl sulphate (SDS, 95%), sodium oleate (95%), n-dodecyl mercaptan (98%), were used as received from Sigma-Aldrich. Butadiene was purchased from Air Liquid Inc. (95%); styrene purchased from Sigma-Aldrich (98%) was washed with 10% sodium hydroxide solution to remove the inhibitator before used for the polymerization experiments. Gemini surfactant trimethylene-1,3-bis (dodecyldimethyl-ammonium bromide) (denoted as 12-3-12) was synthesized by the procedure provided in the appendix [57], methanol, ethanol and tetrahydrofuran (THF) were purchased from Aldrich and used as received. Deionized water is used as the continuous phase during polymerization. Table 3.1 summaries the materials with their formula and corresponding molecular weight.

Table 3.1: Summarization of the materials applied in the synthesis of styrene-butadiene copolymer nanoparticles via differential emulsion polymerization

Chemicals	M.W. (g/mol)	Molecular Formula
Butadiene (BD)	54.09	C_4H_6
Styrene (ST)	104.15	C_8H_8
Potassium persulfate (KPS)	270.32	$K_2S_2O_8$
n-Dodecyl mercaptan (n-DDM)	202.4	$C_{12}H_{26}S$
Sodium dodecyl sulfate (SDS)	288.38	$NaC_{12}H_{25}SO_4$
Sodium oleate	304.45	$C_{18}H_{33}NaO_2$
Gemini surfactant (GS)	627.8	$C_{31}H_{68}Br_2N_2$
Deionized (DI) water	18	H_2O

3.2.2 Equipment and characterization

Equipment applied and its application for characterization is given below:

(1) Parr series 5100 Low Pressure Reactors (300 ml) with Parr 4842 temperature controllers were used to prepare SBR nanoparticles; (2) Bio-Rad Excalibur 300 MXPC System (FT-IR) operated with Merlin software was used to collect spectral data for the SBR samples; (3) the average size of the polymer particles of the synthesized latex was determined by dynamic light scattering (DLS) at 25 C using a Nanotrac 150 particle size analyzer (BETATEK Inc., Toronto, CA); (4) LEO 912 AB 100 kV Energy Filtered Transmission Electron Microscopy (EFTEM) (Carl Zeiss Inc., Germany) was applied to confirm the size and to observe the morphology of the SBR nanoparticles; (5) Differential scanning calorimetry (DSC) （TA Instruments Inc., model: Q2000） is carried out to investigate the thermal properties of SBR nanoparticles; (6) NMR (Bruker Avance – III 300) was used to determine the level% of butadiene and styrene in a SBR sample; (7) Gel permeation chromatography (GPC) was applied to calculate the SBR particle molecular weight distribution; (8) Ohaus

Analytical Plus Balance AP250D was applied to measure the weight of initiator, surfactant, chain transfer agent, DI water and stoppers.

Table 3.2: Summary of the equipment applied in characterization of styrene-butadiene copolymer samples synthesized via differential emulsion polymerization

Instrument	Manufacture	Function
Gel permeation chromatography (GPC)	Bio-Rad, U.S.A.	Macromolecule molecular weight determination
Nuclear magnetic resonance (NMR)	Bruker Inc., U.S.A.	Macromolecule structure determination
Microtrac - Dynamic Light Scattering (DLS)	BETATEK Inc., Canada	Nanoparticle size measurement
Differential scanning calorimetry (DSC)	TA Instruments Inc., U.S.A.	Glass transition temperature measurement
Transmission Electron Microscopy (TEM)	LEO Electron Optics GmbH, Germany	Nanoparticle morphology observation

3.3 Approach Strategies

Styrene-butadiene rubber (SBR) nanoparticles were synthesized through differential microemulsion polymerization. As shown in Figure 3.1, in the first step, the continuous aqueous phase (labeled as B) was prepared by dissolving SDS or Gemini surfactant and KPS in DI water in a Parr reactor vessel (300ml) equipped with stirrer, thermometer and a steam heating channel. KPS was used as the initiator, and SDS or Gemini surfactant was used as the surfactant. Then, the reactor was sealed and was purged by nitrogen for 3 minutes. Butadiene was condensed into a 30 ml PTFE tube that was cooled by ice. Styrene and butadiene mixtures (labeled as A) were obtained by mixing the added styrene and butadiene well in the tube. The mixture was combined with the continuous phase in a differential manner over about 1 hour at a stirring of 1000 rpm when the reaction temperature was reached. The appearance of solution in the reactor transformed from transparent into translucent, opaque

and then milky white with the progress of polymerization. Pure SBR was obtained by precipitation with excess 10% sodium chloride, separating with vacuum filtration, and drying at room temperature in a vacuum oven for 12 hours.

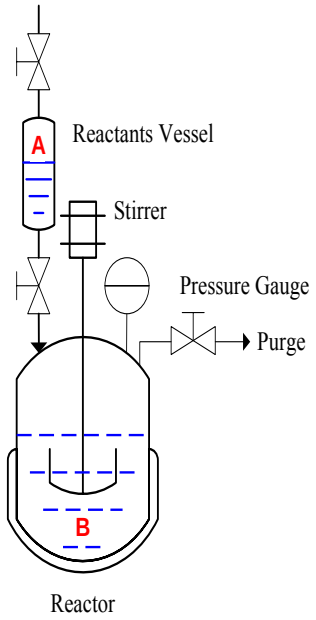

Figure 3.1: The schematic drawing of the DMP apparatus

Chapter 4 Differential Microemulsion Polymerization Kinetics and Mechanisms

4.1 Introduction

In a semi-batch differential microemulsion polymerization system, the reactor was initially charged with water, surfactants, and a potassium persulfate initiator. After the reaction temperature (50 °C) was reached, a continuous addition of a mixture of styrene and butadiene monomers over a period of time (normally a few hours) was followed. The appearance of solution in the reactor transformed from transparent into translucent, opaque and then milky white with the progress of polymerization. The reaction system is characterized by monomer-swollen micelles dispersed in the continuous aqueous phase. These micelles are so well stabilized by surfactant molecules that only a small portion of monomer molecules were dissolved in the continuous aqueous phase with the progress of polymerization. Therefore, the DMP approach is proposed as a micellar nucleation dominated process due to the effective capture of free radicals by the extremely large oil-water interface area generated by monomer-swollen micelles. This chapter primary deals with the mechanisms and kinetics of differential emulsion polymerization, and is followed by the determination of the factors that could influence the size of polymeric particles from the given mechanistic equations.

4.2 Kinetics and mechanisms

The general features of a differential microemulsion polymerization comprise hydrophobic monomers (styrene and butadiene), water, surfactant and water soluble potassium persulfate.

Waterborne free radicals initiate the polymerization of the monomer molecules dissolved in the continuous aqueous phase initially to form oligomeric radicals that eventually successfully transformed into particle nuclei. When the critical length is reached, those oligomeric radicals become so hydrophobic that they have a great tendency to continue to attack monomer molecules in the aqueous phase, and stop after the depletion of monomer [58]. Since only a small fraction of monomers are dissolved in the continuous phase, the particle nucleation is insignificant in the DMP synthesis of the SBR latex. In addition, particle nucleation is not effective in competing with micelles in capturing free radicals owing to their relative small droplet surface area. This suggests that the micellar nucleation process dominates in the process of synthesizing styrene butadiene copolymers via the DMP approach.

According to the theory described above, the particle nucleation process is simulated by a mechanical model comprising a series of elementary reactions as given below [59].

Adsorption of radicals by micelles

$$m + R^{\bullet}_{(eq)} \rightarrow N, \qquad dN/dt = k_{e,m} m [R^{\bullet}]_w \tag{4.1}$$

Adsorption of radicals by active particles

$$N_1 + R^{\bullet}_{(eq)} \rightarrow N_0, \qquad dN_0/dt = k_{e,p}\, N_1 [R^{\bullet}]_w \tag{4.2}$$

Adsorption of radicals by inactive particles

$$N_0 + R^{\bullet}_{(eq)} \rightarrow N_1, \qquad dN_1/dt = k_{e,p} N_0 [R^{\bullet}]_w \tag{4.3}$$

where m represents the number of monomer-swollen micelles, N represents the number of monomer-swollen micelles containing free radicals, N_0 stands for the number of particle

nuclei containing no radicals (inactive) per unit volume of water and N_1 represents the number of particle nuclei containing one free radical (active),. $R^{\bullet}_{(eq)}$ stands for the free radicals in the continuous aqueous phase, and $[R^{\bullet}]_w$ is the free radicals concentration in the continuous aqueous phase. $k_{e,m}$ and $k_{e,p}$ represent the rate constant for the free radicals absorption rate by micelles and particle nuclei, respectively. Thus, the total rate of particle nucleation can be written in the form of the following equations by computing a mole balance of free radicals.

$$d[R^{\bullet}]_w/dt = 2fk_d[\mathrm{I}] - k_{e,m}m[R^{\bullet}]_w - k_{e,p}N_1[R^{\bullet}]_w - k_{e,p}N_0[R^{\bullet}]_w$$

$$= 2fk_d[\mathrm{I}] - k_{e,m}m[R^{\bullet}]_w - k_{e,p}(N_1+N_0)[R^{\bullet}]_w \quad (4.4)$$

$$= 2fk_d[\mathrm{I}] - k_{e,m}m[R^{\bullet}]_w - k_{e,p}N_p[R^{\bullet}]_w$$

$$dN/dt = k_{e,m}m[R^{\bullet}]_w \quad (4.5)$$

Because of the extremely reactive free radicals, at the pseudo-steady-state, $d[R^{\bullet}]_w/dt = 0$. Thus,

$$k_{e,m}m[R^{\bullet}]_w = 2fk_d[\mathrm{I}] - k_{e,p}N_p[R^{\bullet}]_w \quad (4.6)$$

Substituting Eq. (4.6) into Eq. (4.5), the rate of particle nucleation becomes

$$dN/dt = 2fk_d[\mathrm{I}]/\{1+[k_{e,p}N_p/(k_{e,m}m)]\} \quad (4.7)$$

If the desorption of radicals out of the particle nuclei is taken into consideration, the following equation can predict the rate of particle nucleation in the realm of polymerizing relative hydrophobic monomers via the emulsion polymerization approach.

$$dN/dt = (2fk_d[\mathrm{I}]+ k_{des}nN_p/N_A)/\{1+[k_{e,p}N_p/(k_{e,m}m)]\} \quad (4.8)$$

In the polymerization of styrene butadiene copolymers via the DMP approach, micellar nucleation dominates the process, and hence $k_{e,m}m >> k_{e,p}N_p$, $k_{e,m}m >> k_{des}nN_p/N_A$ and $k_{e,p}N_p/(k_{e,m}m) << 1$. Therefore, Eq. (4.8) can be written as:

$$dN/dt = (2fk_d[\mathrm{I}] + k_{des}nN_p/N_A)\, k_{e,m}m/(k_{e,p}N_p) \qquad (4.9)$$

According to Eq. (4.9) the rate of micelles (dN/dt) to capture free monomer is proportional to the concentration of initiator ([I]), the initiator decomposition rate constant (k_d), and the rate for desorption of free radicals out of the particle nuclei ($k_{des}nN_p/N_A$). The terms k_d and $k_{des}nN_p/N_A$ can be controlled by reaction temperature and chain transfer agent, respectively, and will be discussed in the following chapter.

4.3 Conclusion

The kinetics and mechanisms for the micellar nucleation dominated DMP approach was studied. It concluded that an increase of the concentration of initiator and a rise of the reaction temperature can improve the rate of micelles (dN/dt) to capture free monomers. In addition, as a chain transfer agent can influence the rate of radical desorption (k_{des}) out of the particle nuclei, a rise of chain transfer agent concentration may also help to increase the rate of micelles (dN/dt) to capture free monomers. Detailed discussion for the influence on the particle size and dN/dt by these three factors will be addressed in Chapter 5.

Chapter 5 Factors Influencing SBR Particle Size

5.1 Introduction

Several factors influence SBR nanoparticle size. Besides initiator concentration, reaction temperature and chain transfer agent discussed in the last chapter, the addition rate of monomers, the type and the amount of surfactant, and the monomer feed composition also have an effect on the nucleation mechanisms and thus influence the particle size accordingly. In an oil in water microemulsion polymerization, the surfactant plays a crucial rule not only in lowering the interfacial tension between oil and water to facilitate the formation of micelles but also in stabilizing the newly formed latex particles in the continuous aqueous phase. Within the process of synthesizing the SBR nanoparticles via differential microemulsion polymerization, an initiator was introduced to the system at the start to maintain a monomer starvation condition. Thus, the addition rate of monomers to the system may control the free radical competition between homogeneous and micellar nucleation. Moreover, solubility of monomer in water can also influence the nucleation mechanisms. A monomer with a hydrophilic property facilitates homogeneous nucleation whereas a hydrophobic monomer promotes the formation of micelles in the continuous aqueous phase and undergoes a heterogeneous nucleation process. Since the solubility in water between butadiene and styrene is different, the feed composition is another factor which should be considered.

5.2 Experimental

5.2.1 Analysis of SBR conversion

Conversion (X%) of styrene-butadiene copolymer is determined by a gravimetric method, utilizing Eq. (5.1):

$$X\% = \frac{Wd}{Wt} \times 100 \quad (5.1)$$

where W_d and W_t stand for the weight of dried SBR rubber and total weight of SBR rubber monomers respectively introduced into the polymerization process.

5.2.2 Analysis of SBR molecular weight and its distribution

The molecular weight and polydispersity index (PDI) were determined using a gel permeation chromatograph (GPC), which was calibrated with a polystyrene standard (PS 99 K, M_w = 98251 and M_n = 96722). Dried SBR rubber samples were dissolved in the solvent THF and filtered through a filter with a 0.5 μm GHP membrane. 100 μL filtered THF containing a SBR sample was injected into the GPC analysis column at a flow rate of 1.0 mL/min at room temperature.

5.2.3 Analysis of SBR particle size

The average particle size of the polymeric nanoparticles was measured using a dynamic light scattering technique (DLS) using Microtrac-Nanotrack 150 (Betatek Inc.). For the measurement, two to three drops of the sample was diluted to 1 ml with DI water and measured in standard progression with the particles reflective index equal to 1.535.

TEM was used to observe the morphology of the SBR nanoparticles and was also applied to confirm the particle size. The DI water diluted SBR latex solution was incubated on a 400-mesh copper grid at room temperature. Excess solution was taken away by a piece of tissue paper from the edge of the grid. Latex particles on the grid were stained with 2% (w/v) uranyl acetate for several minutes before the grid was delivered into the TEM chamber for imaging.

5.3 Results and discussion

5.3.1 Influence of the addition rate of monomers

The addition rate of monomers is a major factor that can affect the particle size in the DMP approach. As indicated in the Table 5.1 & Figure 5.1, the influence of monomer addition rate on the polymeric nanoparticle size has been studied in a KPS initiated semi-batch differential emulsion polymerization system. As the addition rate is slowing down, the addition time is extended dramatically from 30 minutes to 60 minutes. Accordingly, the nanoparticle size diminishes from approximately 48 nm to 33 nm. This is ascribed to the fact that the lower addition rate promotes the dispersion of monomers into the aqueous continuous phase, which contains higher concentration of surfactant molecules [59, 60]. A monomer droplet encapsulated or stabilized by surfactant molecules in the form of micelles will be uniformly distributed in the aqueous phase. As a result, the mass transfer of monomers between the oil phase and aqueous phase will be suppressed to the largest extent that leads to a microemulsion dominated continuous phase and consecutively produces smaller nanoparticles.

In contrast, when the addition rate is faster, the time interval between each addition unit is less than the time required for the micelle formation from the monomer droplets. Thus, monomer droplets without full coverage by surfactant will aggregate with each other to form monomer reservoirs, which will undergo a coarse (macro) emulsion polymerization process that produces larger polymeric particles. Therefore, the study of the addition rate of the monomers shows that a transition between microemulsion and coarse emulsion polymerization in a DMP system and the polymeric particle size can be managed by the manipulation of the monomer addition speed into the system.

Table 5.1: Summary of SBR particle sizes at various addition times for [SDS] = 4.0E-5 and 5.0E-5 mol/L

[SDS] (mol/L)	SBR sample	addition time (min)	particle size (nm)
4.0E-05	107	34	51.1
	108	40	43.4
	109	45	34.3
	111	49	35.9
	113	63	34.2
5.0E-05	114	35	48.3
	115	37	44.4
	116	42	35.1
	119	48	32.0
	120	62	32.7

Reaction conditions: Reaction temperature = 50 °C, reaction hour = 8 hr, [BD] = 4.6E-3 mol/L, [ST] = 7.4E-4 mol/L, [KPS] = 4.0E-6 mol/L, [n-DDM] = 3.1E-6 mol/L

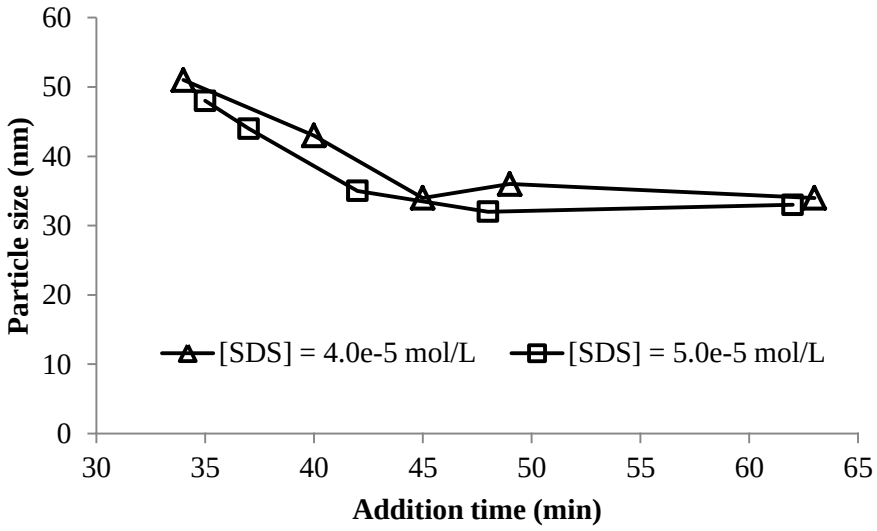

Figure 5.1: Influence of the monomer addition rate on the SBR particle size in DMP systems

5.3.2 Influence of the reaction temperature

Unlike conventional emulsion and miniemulsion polymerization systems, the initial state of a differential microemulsion highly relies on the reaction temperature immediately before the initiation of polymerization. In a DMP system, an initiator is introduced into the system to decompose into free radicals prior to the addition of monomers. The initiation takes place once the monomers reach the aqueous continuous phase. As the initiator decomposition rate constant k_d and propagation rate constant k_p are temperature dependent, the reaction temperature will have a great influence on the DMP system.

According to emulsion polymerization theories [61], the relation between the rate of polymerization and the polymer particle number can be expressed according to the following equations:

$$R_p = k_p [\mathrm{M}]_{\mathrm{eq}} \, n \, N / N_A \tag{5.2}$$

$$k_p = A \, e^{-E/RT} \tag{5.3}$$

where, R_p is the rates of polymerization, $[\mathrm{M}]_{\mathrm{eq}}$ is the equilibrium monomer concentration in the particles and N_A is Avogadro's constant, N is the particles number, A is the frequency factor, E is the activation energy and n is the average radical number per particle. Based on Eq. (5.2), a linear relation can be found between rates of polymerization (R_p) and the average radical number per particle (n) if R_p is divided by the polymer particles number (N) and appropriate constants, and herein the average radical number per particle (n) can be estimated. In addition, a connection between the number of radicals per particle (n) and the reaction temperature can also be derived by the combination of Eq. (5.2) and (5.3). It has been found that the number of radicals per particle (n) is estimated to increase with increasing temperature (T). Since the number of micelles are much larger than the number of polymer particles ($N_{micelles} >> N_{particles}$), and the microemulsion particles from the DMP system are too small to accommodate more than one radical in each particle at a given time, the rate of the entry of a second radical into the polymeric particle is negligible and hence the micelle nucleation dominates the polymerization process. During the micellar nucleation, the monomer initiation and polymerization occur within a micelle and hence the particle size will be thermodynamically stable and will be minimized. At a higher reaction temperature, the entry into micelles by free radicals increases accordingly with the increasing amount of free radicals, and herein a smaller average particle size can be achieved. Table 5.2 & Figure 5.2 shows that the particle size decreases with increasing reaction temperature and the decrease is more apparent in the conventional emulsion runs.

Table 5.2: Summary of SBR particle sizes at various reaction temperatures for differential microemulsion and conventional emulsion polymerization methods

polymerization method	SBR sample	temp (℃)	particle size (nm)
differential microemulsion polymerization	91	45	65.4
	92	50	56.4
	93	55	47.6
	94	60	43.3
	95	65	44.2
	96	70	36.0
	97	45	82.1
	98	50	48.4
	99	55	45.0
	100	60	44.6
	101	65	49.1
	102	70	49.9
conventional emulsion polymerization	103	50	168
	104	50	155
	105	60	123
	106	75	91.5

Reaction conditions: Reaction hour = 8 hr, reaction temperature = 50 °C, [SDS] = 3.3E-5 mol/L, [BD] = 4.6E-3 mol/L, [ST] = 7.4E-4 mol/L, [KPS] = 4.0E-6 mol/L, [n-DDM] = 3.1E-6 mol/L

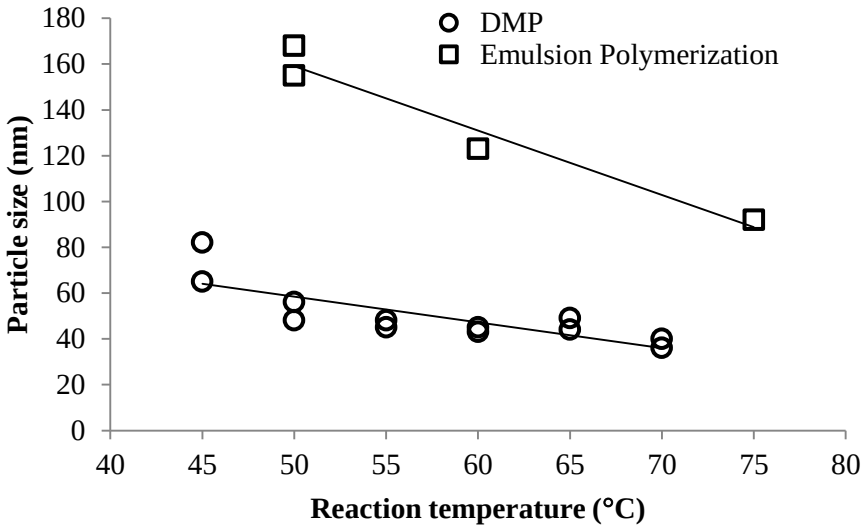

Figure 5.2: Influence of reaction temperature on SBR particle size

5.3.3 Influence of chain transfer agent

Chain transfer agents (CTA) are extensively used in styrene-butadiene emulsion copolymerization to help reduce the molecular weight and regulate the molar mass distribution. Mercaptans are the most efficient and the most common type of CTAs utilized in emulsion polymerization. A CTA has almost no effect on the number of polymeric particles produced but can enhance the influence on the rate of polymerization. For example, a CTA with higher values of the chain transfer constant and solubility in water will decrease the rate of emulsion polymerization per particle by increasing the radical desorption from the polymer particles [62, 63]. The desorption rate coefficient k_{des} has been proposed by M. Nomura et al. [64] as given by Eq. (5.4) when transfer reaction to chain transfer agents dominates:

$$k_{des} = \frac{12 D_w \delta}{m_d d_p^2} \left(\frac{k_{Tf}[T_p]}{k_{pi}[M_p]} \right) \tag{5.4}$$

where D_w is the diffusion coefficient of a CTA radical in the water phase, m_d is the partition coefficient of a CTA radical between the water and particle phases, d_p is the diameter of a particle, k_{Tf} is the CTA rate constant, k_{pi} is the re-initiation rate constant of a CTA radical, $[T_p]$ is the concentration of CTA, $[M_p]$ is the concentration of monomer in the particles, and δ is the ratio of mass transfer in water side to the overall mass transfer around the particle that provides the radicals for a CTA, and the value of δ is: $0 < \delta \leq 1$. As described in Eq. (5.2), the rate of polymerization in a conventional emulsion system is expressed in terms of the number of radicals per particle (n), the number of polymer particles (N), propagation rate constant (k_p) and the equilibrium monomer concentration in the particles ($[M]_{eq}$). Therefore,

in order to represent the significance of radical desorption by a CTA, the number of radicals per particle (n) can be written in the following form:

$$n = \frac{1}{2}\left[-C + \sqrt{C^2 + 2C}\right], \qquad C = \frac{r_i}{k_{des}N} \tag{5.5}$$

where r_i is the rate of radical production in the water phase.

Based on Eq. (5.2) and (5.5), it can easily be seen that a decrease in k_{des} will cause the propagation rate R_p to increase. This is due to the fact that a decrease in k_{des} leads to an increase in the value of n and in turn results in an increase of R_p as the rate of propagation (R_p) is proportional to the number of radicals per particle (n) as long as the number of particles (N) is constant. According to Eq. (5.4), a reduction in the value of k_{des} can be achieved by diminishing the CTA rate constant (k_{Tf}), the concentration of a CTA ([T_p]) and the solubility of a CTA in water. Based on this theory, it shows that at the same CTA concentration and CTA rate constant, n-dodecyl mercaptan (n-DDM) may perform the best on increasing the rate of emulsion polymerization of styrene-butadiene copolymer because of its very low solubility in water. The extremely low solubility of n-DDM in water leads to a large value of m_d, and therefore will cause the value of k_{des} to be very small. A small value of k_{des} will result in an increase in the propagation rate R_p. Herein, the reaction rate will be faster in a reaction with n-DDM than the reaction without any n-DDM.

As indicated in Table 5.3 & Figure 5.3, four experiments were carried out without the addition of any chain transfer agent n-DDM. These four experiments applied the same amount of surfactants (sodium oleate), monomers, solvents and initiators. Not surprisingly, reactions undergoing the DMP process without any chain transfer agent have a very low

reaction rate and consequently result a very low reaction conversion and result in a small particle size. This type of result is expected as the lower conversion of the reaction, the less amount of monomers participate in the reaction and the smaller particle size produced.

Another aspect of the influence of n-DDM on the reaction conversion was also studied. As shown in Table 5.4 & Figure 5.4, the concentration of n-DDM is increased from 0 to about 6E-5 mol/L. Consequently, the reaction conversion rise from 10% to 75% and the particle size rise from 14 nm to 52 nm along with the increasing amount of CTA applied. According to the theory, in emulsion polymerization, as the concentration of a CTA ($[T_p]$) increases, the value of k_{des} will increase and lead to the decrease of the propagation rate R_p. and therefore under the same reaction condition the reaction rate will be slower and the reaction conversion lower than those when using a lower concentration. Nevertheless, this prediction is only works for conventional emulsion polymerization. In a DMP system, the increasing amount of a CTA promotes the reaction rate, and thus the reaction conversion is higher than those when using a smaller concentration of the CTA.

The reason of why the application of n-DDM in a DMP system has a reverse outcome compared to the result observed for a conventional emulsion polymerization is attributed to a change in the polymerization mechanism. Unlike the conventional emulsion polymerization, in a DMP system, nucleation in the microemulsion droplets predominates the polymerization process due to the effective capture of free radicals generated in the aqueous phase by the very large amount of microemulsion droplets. When the depletion of emulsifier droplets takes place, their molecules will be absorbed on the surfaces of the growing particles in the

aqueous phase, and the reduction in the rate of polymerization per particle in the presence of n-DDM decreases the growth rate of the surface areas of the particles, and therefore decreases the consumption rate of micelles in the system because of adsorption. Hence, the rising concentration of n-DDM will result in an increase rate of particle formation as long as polymer particles are prepared from micelles. As displayed in Figure 5.6 and 5.7, SBR nanoparticles generated with given amount of n-DDM as visually observed from the TEM images have a more uniform size in comparison with those SBR nanoparticles prepared without any n-DDM. GPC tests were also performed on these two groups of nanoparticles. Similarly to the result of visual observation, nanoparticles synthesized with n-DDM result in a lower value of PDI (= 4.668), while those without n-DDM result in a much higher value of PDI (= 9.915). Based on these test results, it concluded that in the synthesis of SBR nanoparticles in a DMP system, the addition of n-DDM facilitates the micellar nucleation process as the particle shape is regular and smaller. However, a DMP system without any n-DDM undergoes a combined homogeneous and micellar nucleation process. Particles generated in micellar nucleation are smaller than those produced by a homogeneous nucleation process, and thus the apparent irregular shape of SBR nanoparticles are observed under a TEM. In addition, due to the extremely low solubility of styrene and butadiene in water, it will take a longer time for them to dissolve in water to undergo a homogeneous nucleation, and thus most of monomers will stay in the aqueous phase in the form of micelles. However, owning to the absence of a CTA, the amount of free radicals attacking the monomers in the aqueous phase are more than the radicals initiating the monomers in the

micelles. Therefore, by considering these scenarios, the conversion from a DMP reaction is low without any addition of CTAs.

Furthermore, the influence of n-DDM on the reaction conversion was also examined at a higher reaction temperature (75 °C) as shown in Table 5.5 & Figure 5.5. At a higher reaction temperature, it was expected that the reaction rate would be faster, and therefore, the reaction conversion will be higher than the conversion at the lower temperature. Based on the results presented in Table 5.4 & Figure 5.4, and Table 5.5 & Figure 5.5, it can be seen that the reaction conversion at higher temperature (75 °C) is higher than at the lower one (50 °C). However, the difference is not apparent. Thus, it is concluded that the reaction temperature does not influence the reaction conversion very much at the same level of CTA applied. Even though the reaction rate is faster at a higher reaction temperature (Eq.5.2 & Eq.5.3), the influence of temperature on reaction rate is weaker than the influence of a CTA, which reduces the value of k_{des} and increases the reaction rate R_p (Eq.5.2, Eq.5.4 & Eq.5.5).

Table 5.3: Summary of SBR particle size and reaction conversion at [n-DDM] = 0

SBR sample	rename sample	conversion (%)	particle size (nm)
124	1	14.4	15.5
137	2	14.5	17.2
138	3	14.9	16.5
139	4	10.3	14.3

Reaction conditions: Temperature = 50 °C, reaction hour = 8 hr, [Na Oleate] = 3.3E-5 mol/L, [BD] = 4.6E-3 mol/L, [ST] = 8.9E-4 mol/L, [KPS] = 4.0E-6 mol/L

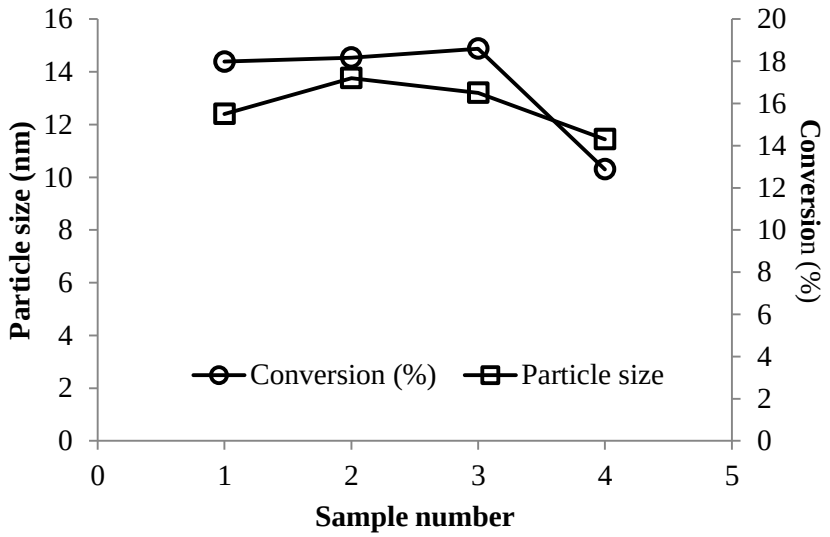

Figure 5.3: Variation of monomer conversion and particle size in the synthesis of styrene butadiene copolymer via DMP method at [n-DDM] = 0

Table 5.4: Summary of SBR particle size and reaction conversion at various [n-DDM] at 50 °C

SBR sample	[n-DDM] (mol/L)	conversion (%)	particle size (nm)
139	0	10.3	14.3
124	0	14.4	15.5
137	0	14.5	17.2
138	0	14.9	16.5
131	3.1E-06	39.3	32.3
128	3.1E-06	56.2	33.5
132	1.4E-05	54.6	28.6
133	1.4E-05	93.8	38.9
129	2.9E-05	44.5	64.4
130	2.9E-05	42.8	54.2
135	5.7E-05	76.3	47.2
136	5.7E-05	75.2	52.1

Reaction conditions: Temperature = 50 °C, reaction hour = 8 hr, [Na Oleate] = 3.3E-5 mol/L, [BD] = 4.6E-3 mol/L, [ST] = 8.9E-4 mol/L, [KPS] = 4.0E-6 mol/L

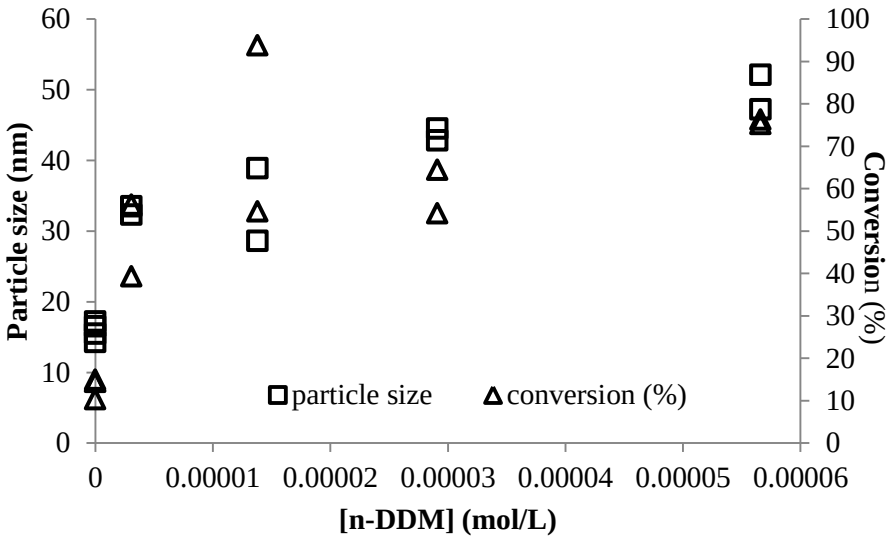

Figure 5.4: Variation of conversion and particle size versus the [n-DDM] in the synthesis of styrene butadiene copolymer via DMP method at 50 °C

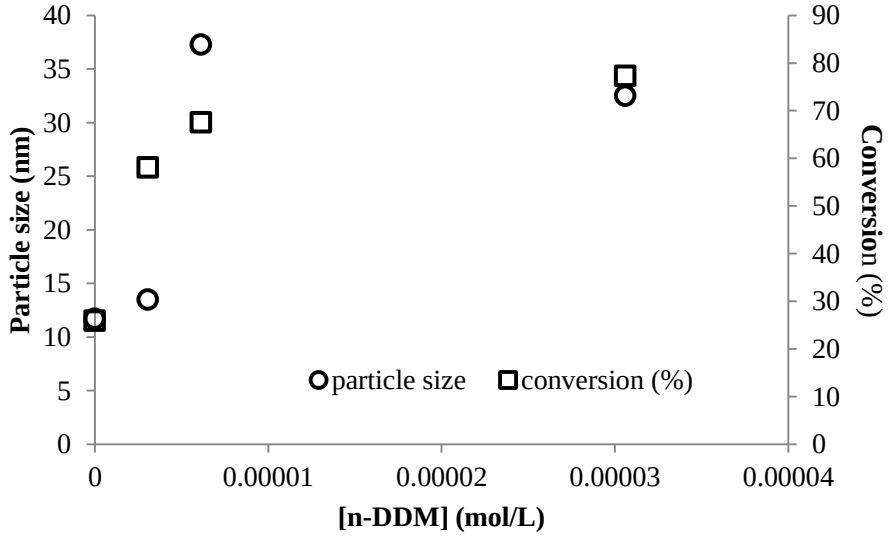

Figure 5.5: Variation of conversion and particle size versus the [n-DDM] in the synthesis of styrene butadiene copolymer via DMP method at 75 °C

Table 5.5: Summary of SBR particle size and reaction conversion at various [n-DDM] at 75 °C

SBR sample	[n-DDM] (mol/L)	conversion (%)	particle size (nm)
67	0	25.9	11.7
68	3.1E-06	58.1	13.5
70	6.1E-06	67.6	37.3
69	3.1E-05	77.3	32.5

Reaction conditions: Temperature = 75 °C, reaction hour = 8 hr, [Na Oleate] = 3.3E-5 mol/L, [BD] = 4.6E-3 mol/L, [ST] = 8.9E-4 mol/L, [KPS] = 4.0E-6 mol/L

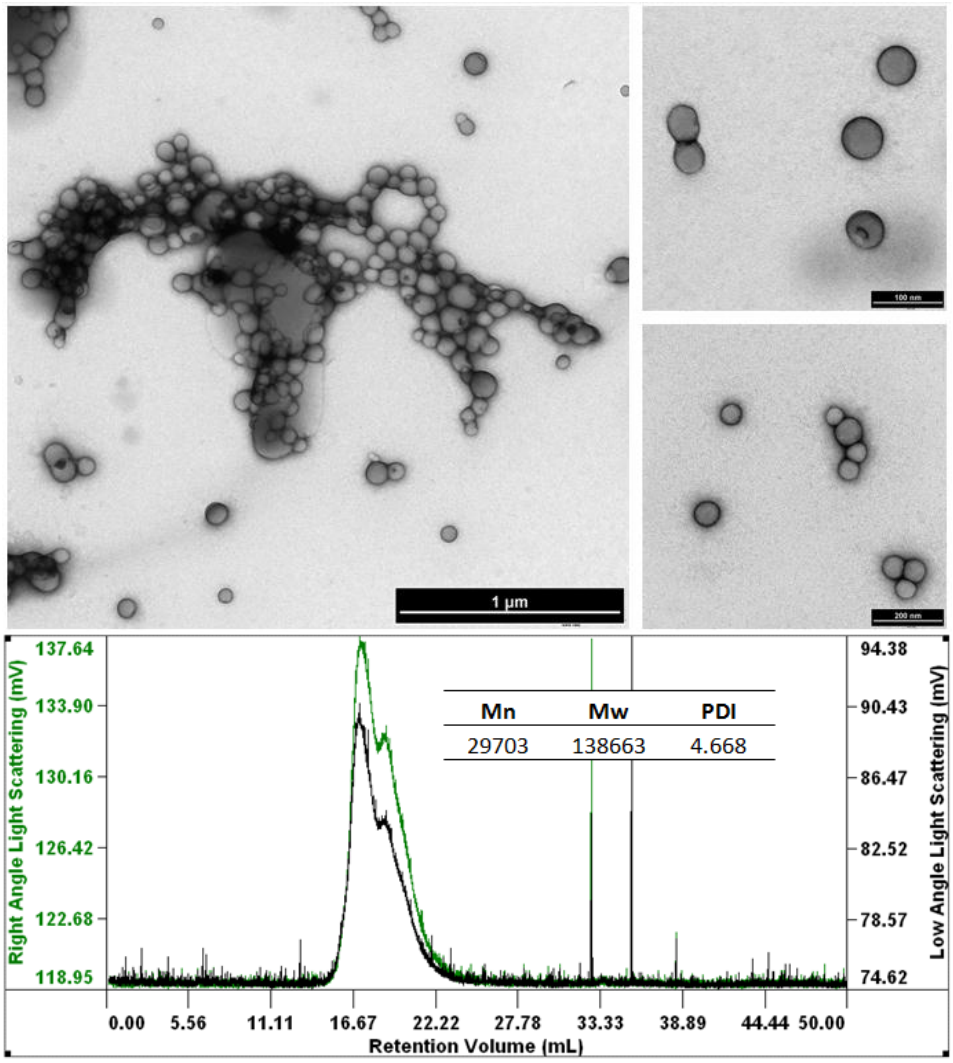

Figure 5.6: TEM and GPC tests for a SBR copolymer sample synthesized with an n-DDM

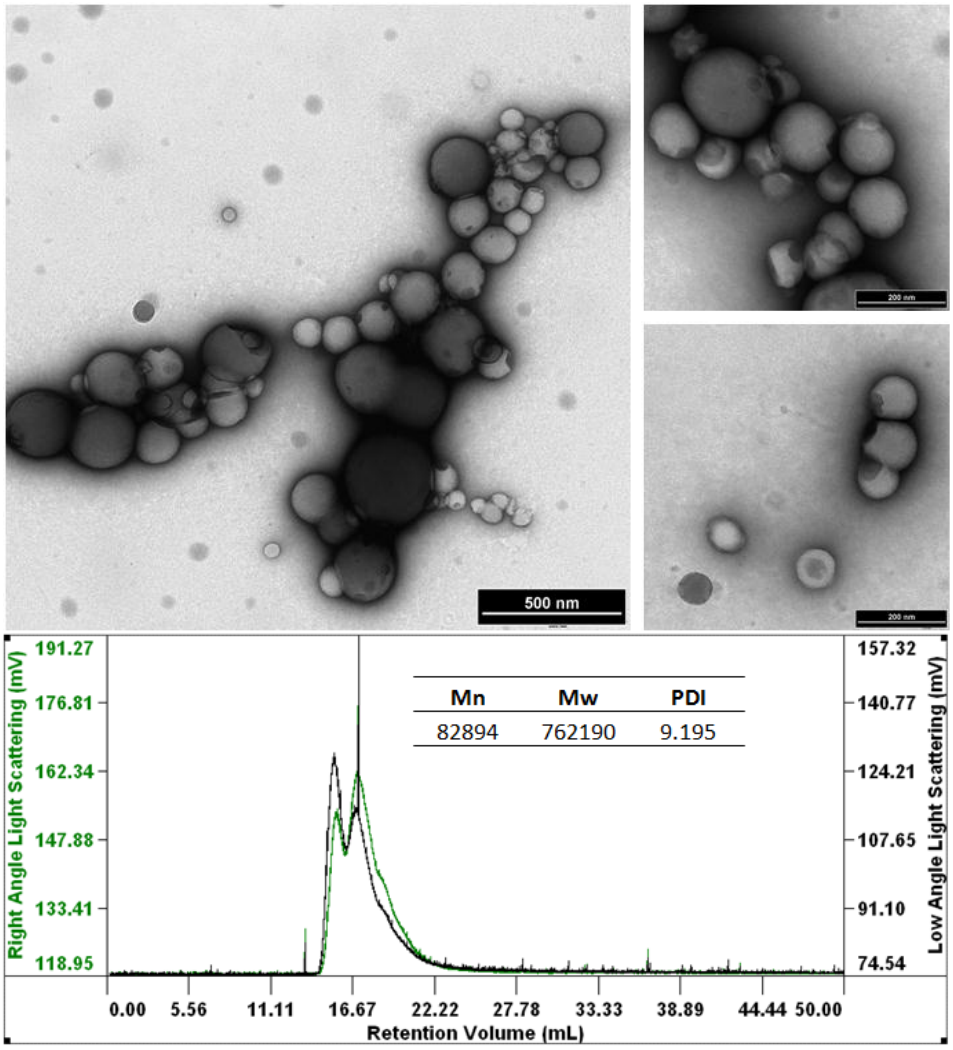

Figure 5.7: TEM and GPC tests for a SBR copolymer sample synthesized without any n-DDM

5.3.4 Influence of the type and the amount of surfactant

Surfactant is a key factor that primarily determines the size and size distribution of the particles generated in an emulsion polymerization system. In synthesizing styrene-butadiene rubber copolymer latices via differential microemulsion polymerization, sodium dodecyl sulfate (SDS) and Gemini surfactant trimethylene-1,3-bis(dodecyldimethylammonium bromide) are applied. SDS, one of the most widely used emulsion polymerization surfactants,

has a negatively charged hydrophilic sulphate group that attaches to an extended hydrophobic backbone. The hydrophilic group influences the degree of hydrolysis, the degree of latex stability with time and the behavior of the surfactant as a function of pH, while the hydrophobic backbone controls the surfactant critical micelle concentration (CMC) value, the interfacial tension and the adsorption behavior of the surfactant onto the latex particle surface. Gemini surfactants that were first reported in the literature in the 1970s have been receiving a great deal of attention during the last decade [65, 66]. A Gemini surfactant with two C_m (m is the number of alkyl carbon atoms) tails and a C_s (s is the number of alkyl carbon atoms) spacer separating the quaternary nitrogen atoms can be referred as *m-s-m* (Figure 5.8) [67]. Gemini surfactants possess more than one hydrophobic tail and hydrophilic head groups have remarkably low CMC values compared to conventional monomeric surfactants.

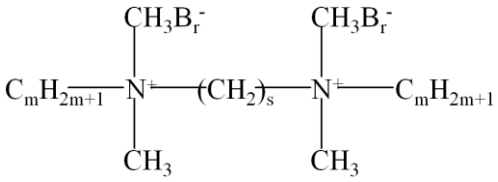

Figure 5.8: Schematic structure of Gemini surfactant [57]

Present contributions on studying the influence of surfactant have shown that an increase in the surfactants concentration will cause the SBR latex particles size to decrease in three phases that are defined by the surfactant critical micelle concentration (CMC) and critical stability concentration (CSC). CMC is the micelle formation concentration, while the CSC is the smallest particle formation concentration. These two factors are essential characteristics

of a surfactant and vary with the surfactant status. Before the emulsion system reaches its CMC, it is called the first phase. During this phase, a slight increase of surfactant concentration will lead to a great reduction in the particle size. In the second phase, which is after the CMC but before the CSC, particle size drops slowly with the increasing concentration of surfactant. At last, the emulsion system enters the third phase once the CSC is reached. During this phase, latex particles stabilize at a minimum size, and resist changing with increasing concentration of surfactant.

Table 5.6: Summary of SBR particle size at various [SDS]

SBR sample	[SDS] (mol/L)	particle size (nm)
8	2.6E-05	172
11	3.3E-05	51.2
12	4.5E-05	64.0
13	5.2E-05	59.4
9	1.3E-04	22.8

Reaction conditions: Temperature = 75 °C, reaction hour = 8 hr, [BD] = 9.8E-4 mol/L, [ST] = 6.5E-4 mol/L, [KPS] = 2.8E-6 mol/L

Table 5.7: Summary of SBR particle size at various [Gemini surfactant]

SBR sample	[Gemini surfactant] (mol/L)	particle size (nm)
38	3.3E-05	24.3
47	3.8E-05	25.0
48	4.3E-05	28.1
49	4.8E-05	27.4
50	5.3E-05	32.3

Reaction conditions: Temperature = 75 °C, reaction hour = 8 hr, [BD] = 4.6E-3 mol/L, [ST] = 7.4E-4 mol/L, [KPS] = 4.0E-6 mol/L, [n-DDM] =3.1E-6 mol/L

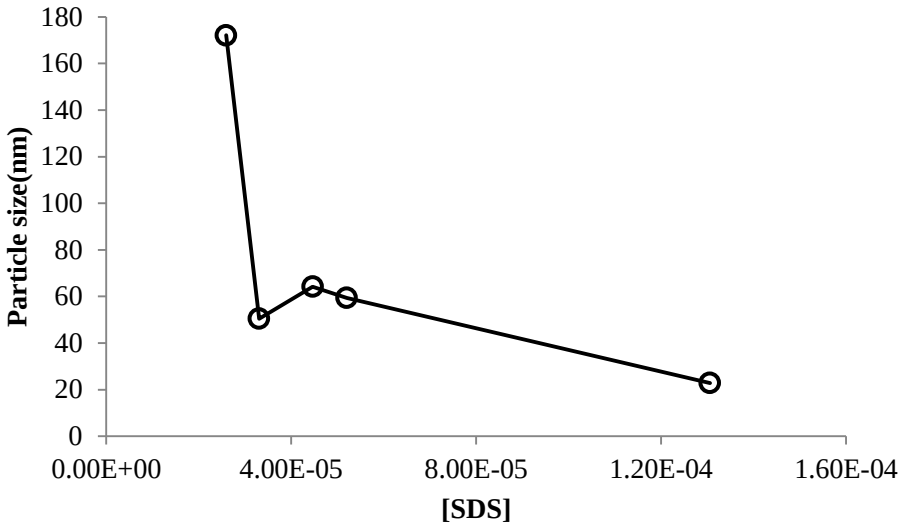

Figure 5.9: Profile of SBR particle size with various [SDS] in a DMP approach

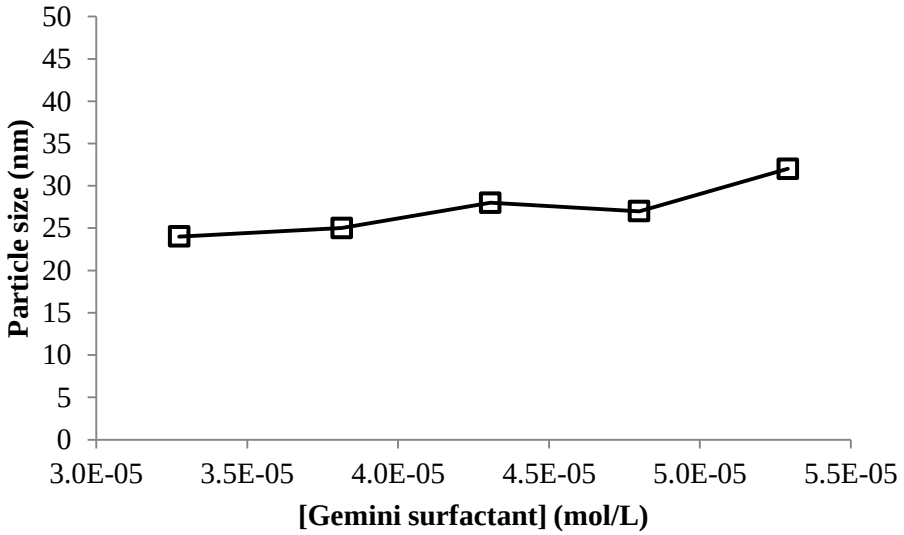

Figure 5.10: Profile of SBR particle size with various [Gemini surfactant] in a DMP approach

This agreement that holds for the trend in three dynamic phases of particle size reduction can be found in the SDS system as shown in Table 5.6 & Figure 5.9. In contrast, the Gemini surfactant system shows very a different result from the trend predicted by theory. In Table 5.7 & Figure 5.10 it shows that the particle size has a trend of slightly increasing along with

the increasing concentration of the Gemini surfactant. The reason of getting this type of result in a Gemini surfactant based system is attributed to the property of Gemini surfactant. Owning to the multi hydrophobic and hydrophilic group characteristics, a Gemini surfactant has a remarkably low CMC value compared to conventional monomeric surfactants. Therefore, based on this theory, it was proposed that if a monomeric surfactant such as SDS reached its CMC value, a Gemini surfactant with the same concentration must reach its own CMC or CSC value, as well. This prediction has been proven to be valid by plotting the size of particles synthesized with a SDS and a Gemini system in the same profile. Figure 5.11 shows that when the SDS concentration reaches its CMC value, the Gemini surfactant with the same concentration reaches its CSC value. In this case, the particle size is kept unchanged with the increasing concentration of the surfactant (Figure 5.10).

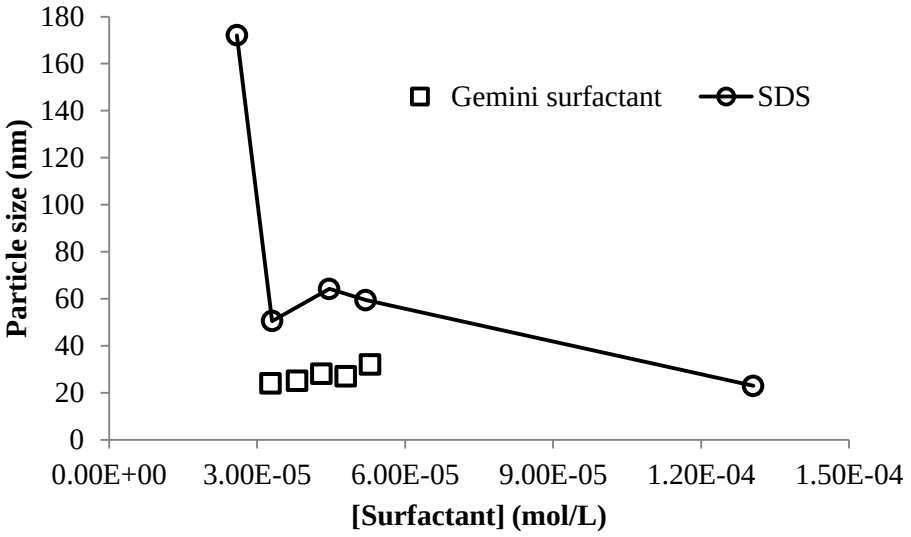

Figure 5.11: Profile of SBR particle size with various [SDS] and [Gemini surfactant] in DMP approach

Morphologies of particles synthesized at various degrees of emulsion polymerization were observed under a TEM. It has also found that SBR latex nanoparticles generated above the CSC value (the third phase) are still very stable after they were stored at room temperature for three months. On the contrary, particles prepared above the CMC but below the CSC (the second phase) have a tendency to aggregate with each other. Figure 5.12 shows the morphologies of SBR particles prepared during the second and the third phases respectively in a Gemini surfactant based emulsion system. The unstable SBR latex particles from the second phase is attributed to the lower value of surfactant concentration. A low concentration of surfactant is not sufficient to cover the surface area of all latex particles in the aqueous phase, and thus aggregation will take place among latex particles after a certain time period.

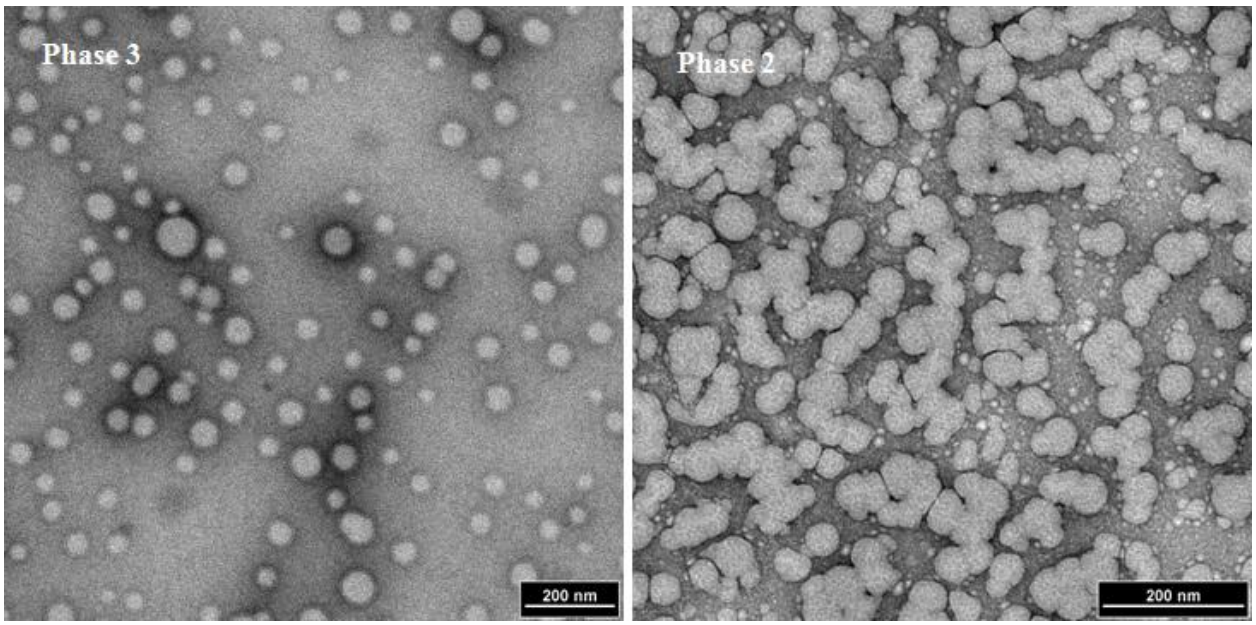

Figure 5.12: Morphologies of SBR latex particles at different phases

5.3.5 Influence of solvent (DI water)

The influence of solvent, which is DI water, was also investigated. When the amount of DI water added to the DMP system increases, the concentrations of surfactant, chain transfer agent, initiator, and monomers decreases. Nevertheless, the molar ratio between each factor is constant. For example, the molar ratio of monomers to surfactant, the molar ratio of initiator to monomers, the molar ratio of chain transfer agent to monomers are constant along with an increase in the amount of DI water. In general, the particle size does not change with an increase in the amount of water in a microemulsion system if the surfactant concentration is beyond its CMC or CSC value. In a microemulsion polymerization system, the size of monomer micelles determines the resultant particle size if the micelles are stabilized by a sufficient amount of surfactant. The only factor that will be influenced is the reaction rate because of a decrease of initiator concentration. However, if the concentration of surfactant is diluted to lower its CMC value, the particle size will be influenced, too. Table 5.8 & Figure 5.13 shows an increase in particle size with an increasing amount of DI water introduced into the system. The amount of water in the system increases from 32.2 g to 72.3g. As a result,

Table 5.8: Summary of SBR particle size at various amount of water added to the DMP system

SBR Sample	[Gemini] (mol/L)	DI water (g)	particle size (nm)
35	3.3E-05	32.2	17.9
37	3.3E-05	32.2	19.5
38	3.3E-05	32.2	24.0
43	2.5E-05	42.3	49.1
44	2.0E-05	52.3	31.8
45	1.7E-05	62.3	40.3
46	1.5E-05	72.3	41.9

Reaction conditions: Temperature = 75 °C, reaction hour = 8 hr

the Gemini surfactant concentration decreases from 3.3E-5 to 1.5E-5 mol/L. An increase in the particle size is observed in this case, and it can be concluded that the CMC value of the Gemini surfactant is about 3.0E-5 mol/L in preparation of the SBR nanoparticles by using the DMP approach.

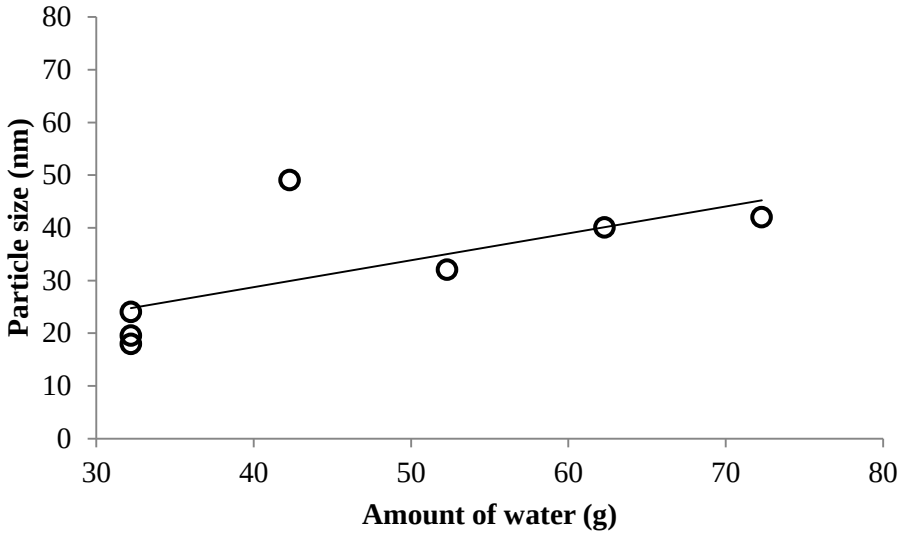

Figure 5.13: Profile of SBR particle size at various amount of water added to the DMP system

5.3.6 Influence of initiator

Potassium persulfate (KPS) was used as the initiator to synthesize SBR latex nanoparticles via the DMP method. Table 5.9 & Figure 5.14 show the initiator effect on SBR nanoparticles generated in a Gemini surfactant based DMP system. The amount of initiator introduced to the system increased from 0.03 g by a factor of 0.005 g to 0.05 g; accordingly, the concentration of KPS increased from about 3.4e-6 mol/L to 5.7e-6 mol/L, and its weight% to monomers increased from 0.28% to 0.47%. Based on the results provided in Figure 5.14, it is seen that the particle size has a slight tendency to decrease or is not influenced, and its

reaction conversion increases with the increasing amount of KPS. It is expected that the conversion of the reactions increases accordingly with a rising KPS concentration as the higher concentration of KPS promotes the reaction rate and leads to a higher reaction conversion at a given time period. However, the particle size shows a result that is the reverse of the trend predicted based on microemulsion theory, which predicts that the particle size should increase with an increase in the KPS concentration [68].

In a microemulsion system, it was suggested that the increase of the water soluble initiator concentration not only increases the chance for the capture of free radicals by the microemulsion droplets but also promotes the precipitation of oligomeric radicals out of the aqueous phase to form the particle nuclei. The latter cause may override the former as a reduction of oil soluble dye content in the resultant latex particles was found with an increase of the water soluble initiator concentration. For a homogeneous nucleation dominated process, free radicals generated in the aqueous phase will propagate with the joining of the monomers until the oligomeric radicals exceeded their solubility and precipitate. Precipitated oligomeric radicals will be accommodated by micelles to form polymer precursors to produce larger size polymer particles than the particles prepared by a micellar nucleation process. Since the homogeneous nucleation process becomes dominate as the concentration of KPS increases, it is predicted the particle size will increase with an increasing amount of KPS. The reason for the particle size to decrease in a DMP system is attributed to its unique mechanism. Given that the principle of a DMP system is to create and maintain a monomer starved situation, in which empty micelles are formed before the initiation; the droplet manner of addition of monomers will be encapsulated by the empty micelles immediately in

the aqueous phase, and thus the micelle size will determine the particle size that is independent of the KPS concentration.

Table 5.9: Summary of SBR particle sizes and reaction conversions at various [KPS]

SBR sample	[KPS] (mol/L)	particle size (nm)	conversion (%)
59	3.4E-06	42.3	68.3
60	4.0E-06	42.2	82.2
61	4.6E-06	44.1	77.1
62	5.2E-06	40.3	86.6
63	5.7E-06	41.5	78.1

Reaction conditions: Temperature = 50 °C, reaction hour = 8 hr, [BD] = 4.6E-3 mol/L, [ST] = 7.4E-4 mol/L, [SDS] = 3.3E-5 mol/L, [n-DDM] =3.1E-6

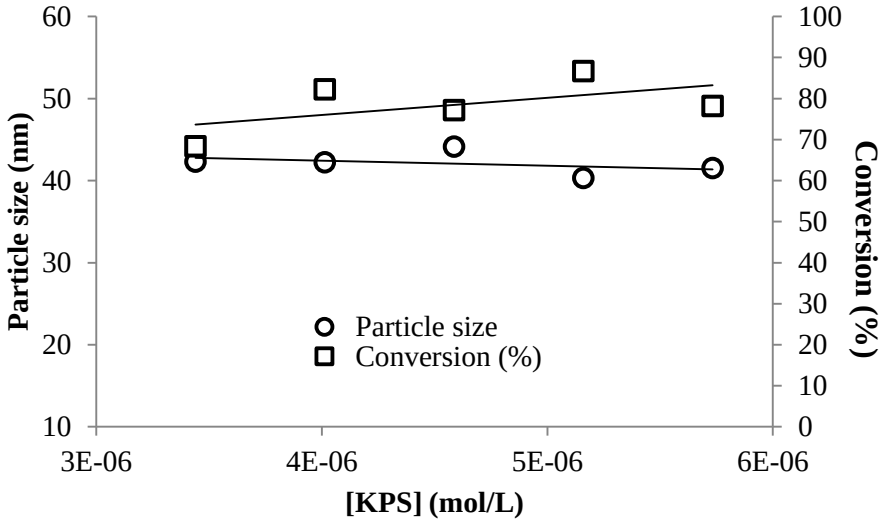

Figure 5.14: Profile of SBR particle sizes and reaction conversions with various [KPS]

5.3.7 Influence of monomer feed composition

The influence of monomer feed composition on SBR nanoparticle size was examined at 50 °C by applying the water soluble initiator KPS. The results are shown in Table 5.10 & Figure

5.15. A decrease in particle size was observed with increasing the butadiene (BD) concentration. These results can be attributed to the presence of an increasing amount of micellar nucleation when the BD concentration in the monomer feed is increased.

The solubility of BD in the aqueous phase is very low (Table 5.12); even though its solubility is slight higher than ST, due to its extremely low boiling point (Table 5.12), it will only be present in the gaseous phase at 50 °C which reduces its surface area with the aqueous phase and promotes the micellar nucleation in the O/W microemulsion medium. The solubility of ST in the aqueous phase is lower than BD, and therefore the major polymerization mechanism of ST should also be via micellar nucleation. Indeed, with an increase of BD content in the monomer feed, the chance of micellar nucleation can apparently increase, and thus produce smaller SBR nano latex particles. However, the reaction conversion decreases with increasing BD content as shown in Figure 5.15. This is due to the low solubility and relatively low boiling point of BD. When the BD content increases in the monomer feed to the reactor, the rate of reaction will become slower as the BD monomer takes some time to "dissolve" in the aqueous phase to form micelles and then undergo polymerization. Therefore, the conversion decreases over the same reaction period with increasing content of BD in the feed stream. In addition, more experiments were carried out to study the BD/ST molar ratio influence on the particle size. As indicated in Table 5.11 & Figure 5.16, two groups of experiments were performed. Group one was carried out at a ratio of 1.5, while group two was performed at a ratio of 6.2. Based on the results delivered by these two groups of experiments, it confirms the results Figure 5.15, which shows that the particle size decreases with an increase in the concentration of butadiene in the feed composition.

Table 5.10: Summary of SBR particle size and reaction conversion at various ratios of BD/ST

SBR sample	mole ratio of BD/ST	particle size (nm)	conversion (%)
38	6	24.0	48.8
39	12	23.0	22.1
41	22	14.4	13.7
40	39	12.2	5.10

Reaction conditions: Temperature = 75 °C, Reaction hour = 8 hr, [Gemini surfactant] = 3.3E-5 mol/L, [KPS] = 4.0E-6 mol/L, [n-DDM] =3.1E-6 mol/L

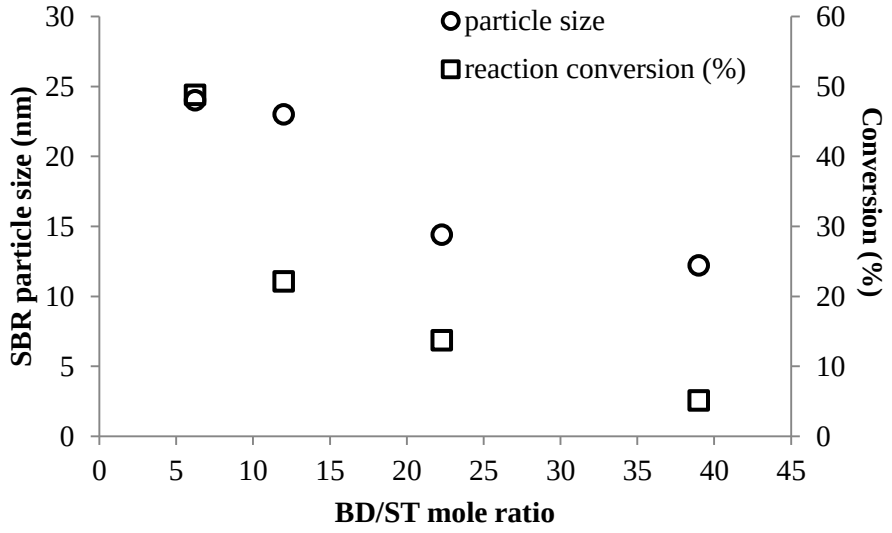

Figure 5.15: Profile of SBR particle size and conversion with various ratios of BD/ST

Table 5.11: Summary of SBR particle size at various BD/ST mole ratios

mole ratio of BD/ST	SBR sample	particle size (nm)
1.5	19	34.0
	20	35.0
	21	28.1
	22	28.3
6.2	32	20.1
	35	17.9
	37	19.5
	38	24.0

Reaction conditions: Temperature = 75 °C, Reaction hour = 8 hr, [Gemini surfactant] = 3.3E-5 mol/L, [KPS] = 4.0E-6 mol/L, [n-DDM] =3.1E-6 mol/L

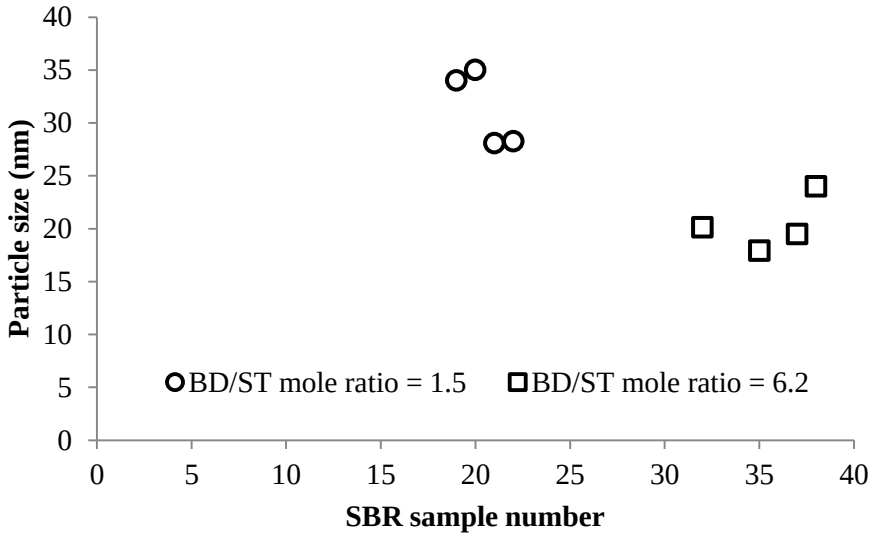

Figure 5.16: Profile of the size of SBR particles at various BD/ST mole ratios

Table 5.12: Some physical properties of styrene and butadiene monomers

monomers	water solubility (g/100 g water)	boiling point (℃)
Styrene	0.03 at 40 ℃	145.2
Butadiene	0.19 at 50 ℃	-4.4

5.4 Conclusion

In conclusion, smaller SBR nanoparticles could be generated with a slower addition rate of monomers, a higher reaction temperature, a higher concentration of surfactant or a surfactant with a multiple hydrophobic and hydrophilic groups, such as Gemini surfactant, and a higher BD/ST ratio in the monomer feed stream. An addition of CTA facilitates the micellar nucleation process as the particle shape is regular and smaller. In a DMP system, the increasing amount of a CTA promotes the reaction rate, and thus the reaction conversion is higher than those when using a smaller concentration of the CTA.

Chapter 6 Recovery of SBR Rubber from Latex

6.1 Introduction

One of the key stages in the synthesis of SBR latex nanoparticles is to recover the SBR rubber from the aqueous latex solution. This stage involves removing the surfactant molecules surrounding the outer layer of a SBR nanoparticle in order to obtain purified SBR rubber for characterization tests such as TEM, DSC, ^{1}H NMR and GPC. In this study, we analyzed coagulated of styrene-butadiene latex at room temperature with acidified ethanol as a coagulating agent.

6.2 Experimental

Experiments on the SBR rubber recovery from its latex solution were carried out in a 500 ml glass vessel placed on a hotplate equipped with a thermocouple and a magnetic stirrer. The vessel was firstly charged with 250 ml of 8.6% HCl acidified ethanol solution. Then SBR particles were isolated by drop-wise addition of latex into ethanol with constant stirring. The precipitated particles were vacuum-filtrated, washed with a 1:1 mixture of ethanol and DI water and dried in a vacuum oven for 12 h at 65 °C in order to obtain the purified SBR rubber that can be dissolved in a THF solution for GPC tests and a chloroform (CCl_4) solution for ^{1}H NMR characterization.

6.3 Results and discussion

Precipitating and washing the SBR latex is a crucial step in the post experiment treatment. Choosing an appropriate precipitating agent is a key factor to generate an accurate

experimental result. The way to pick an appropriate agent is based on the chemical properties of the surfactant used. For instance, sodium oleate is used as the surfactant in the reaction for polymerizing ST and BD. As shown in Figure 6.1, a sodium carboxylate (-COONa) acts as a functional group in this molecule. Therefore, in order to wash off this compound from a SBR latex particle outer shell, an acid solution should be applied. Since sulfuric acid and nitric acid are strong enough to oxide the C=O double bond in the sodium carboxylate group, and in turn will impact the precipitating results, a hydrochloric acid (HCl) solution would be the best choice for the precipitating and washing agent. The HCl solution is a specified diluted solution. In our case, the HCl diluted solution contains 1N hydrochloric acid and ethanol solution.

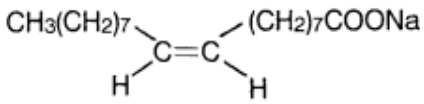

Figure 6.1: Structure of sodium oleate ($C_{17}H_{33}COONa$)

$$C_{17}H_{33}COONa + HCl \rightarrow C_{17}H_{33}COOH + NaCl \quad (6.1)$$

$$C_{17}H_{33}COOH + C_2H_5OH \rightarrow C_{17}H_{33}COOC_2H_5 + H_20 \quad (6.2)$$

Reactions take place once the SBR latex solution is added to the HCl acidified ethanol solution. As displayed in the Eq. 6.1, sodium oleate reacts with HCl and produces oleic acid and sodium chloride. This reaction is preferred as it produces a weaker acid from a stronger acid. Nevertheless, the reaction does not terminate at this step. The product oleic acid from Eq. 6.1 will continue to react with ethanol to yield an ester and a water molecule, which is shown in Eq. 6.2. Consequently, the sodium oleate will be washed away from the outer shell

of the SBR latex particle in the form of sodium chloride (NaCl), the ester ($C_{17}H_{33}COOC_2H_5$) and water in the filtration step. To get more purified SBR latex, a multiple washing process is required. Thus, sodium oleate that was trapped inside the SBR rubber during the precipitating process can be removed by repetitive washings using the HCl acidified ethanol solution. For each time of washing, following steps are required:

1. Dissolve the dried SBR latex in an organic solvent solution. Depending on the SBR latex solubility in a THF solution, the organic solvent can be either a THF or a toluene solution.
2. Precipitate and wash the SBR latex with the HCl/C_2H_5OH solution and filtrate it to get a purer product.
3. Dry the purified SBR latex in a vacuum oven at 65 °C for 12 hours.

Figure 6.2 illustrates the washing process with adequate HCl/C_2H_5OH solution. The blue circle in the center represents the SBR latex, while the green curling lines surrounded the circle stands for the surfactant. As shown in following pictures, the amount of surfactant is eliminated with increasing the time of washing. Figure 6.2 and Figure 6.3 provide a scenario, which describes that SBR particles with lower amount of surfactant having a better solubility in an organic solvent. For instance, SBR latex particles washed with HCl/C_2H_5OH solution will have more surface exposed to their neighbor particles. As a result, due to the inter-molecular forces, SBR latex particles will conjugate with each other when a balance force among them is broken by acid introduction. However, the conjugated SBR particles will separate after dissolving in an organic solvent. This solution can be used for characterizing tests, such as: GPC and ^1H NMR.

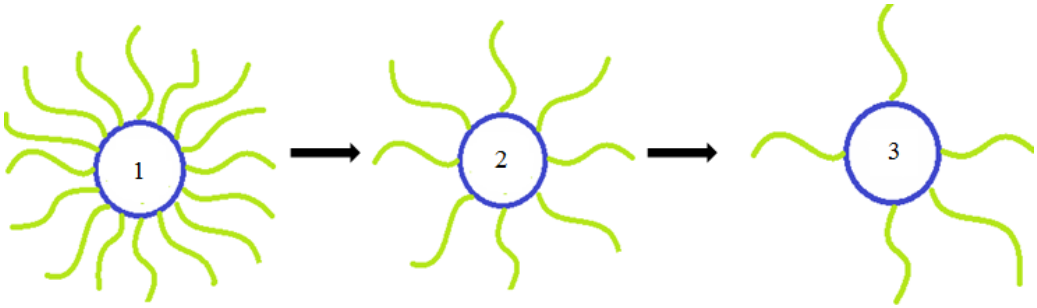

Figure 6.2: Amount of surfactant is decreasing with increasing the time of washing. 1. SBR latex particle without washing by HCl solution. 2. SBR latex particle washed by HCl solution once. 3. SBR latex particle washed by HCl solution twice

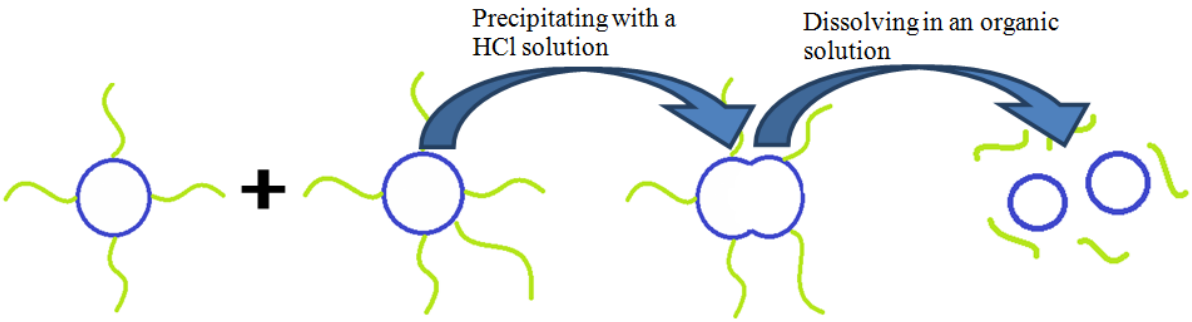

Figure 6.3: The SBR latex has a better solubility with less surfactant covered

To give a better understanding on the theory discussed above, Figure 6.4 gives an example showing the latex physical properties changes. Sample 1 displays a piece of non-purified SBR latex; while sample 2 shows a purified one. The weight of the sample 1 is 1.352g. However, after washed three times, the weight of the sample 2 decreased to 0.938g. The weight difference between sample 1 and sample 2 is believed to be the surfactant loss plus some of weight loss of SBR latex. Sample 3 shows the SBR rubber from sample 2 have a better solubility in a THF solution.

Figure 6.4: Physical properties change of a SBR latex

Furthermore, the morphologies of purified and non-purified SBR latex particles were also investigated under a TEM. Figure 6.5 shows the difference between SBR particles without surfactant and SBR particles with surfactant. Sample 1 without surfactant out-layer has a soft gel looking, while sample 2 with a surfactant layer has a more rigid and solid appearance.

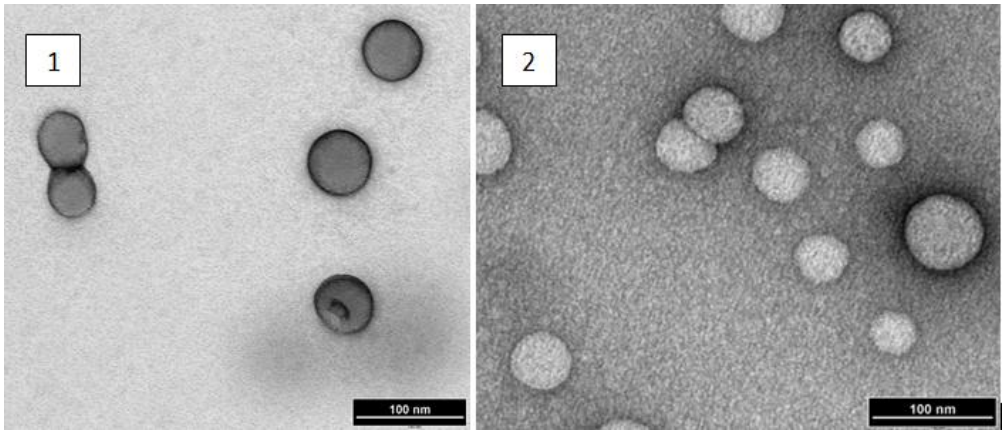

Figure 6.5: Morphologies of SBR particles. 1. SBR particles without covered by a surfactant 2. SBR particles with covered by a surfactant

Moreover, DSC tests were also carried out to confirm the latex purification results. Figure 6.6 and Figure 6.7 are DSC plots for the latex shown in sample 1 and sample 2 of Figure 6.4.

As mentioned abover, sample 1 is the unpurified latex which was directly precipitated from an emulsion solution. Sample 2 is the purified sample that was washed three times from sample 1 by the HCl/C_2H_5OH solution. Based on the test results, it has been shown that the non-purified SBR latex gives more noisy signals than the purified one. Furthermore, the DSC plot trend of the purified SBR latex is very similar to the one produced in industry except it has a lower T_g. The T_g for the SBR product synthesized in the lab is -43 °C, while for commercial SBR it is -22 °C. The reason that the SBR synthesized in the lab has a lower T_g is because it has a much smaller particle size (~30nm on average) than the particle size (~ 1um) of the commercial rubber, which is synthesized via conventional emulsion polymerization. The influence of the polymeric particle size on its T_g will be discussed in the next chapter.

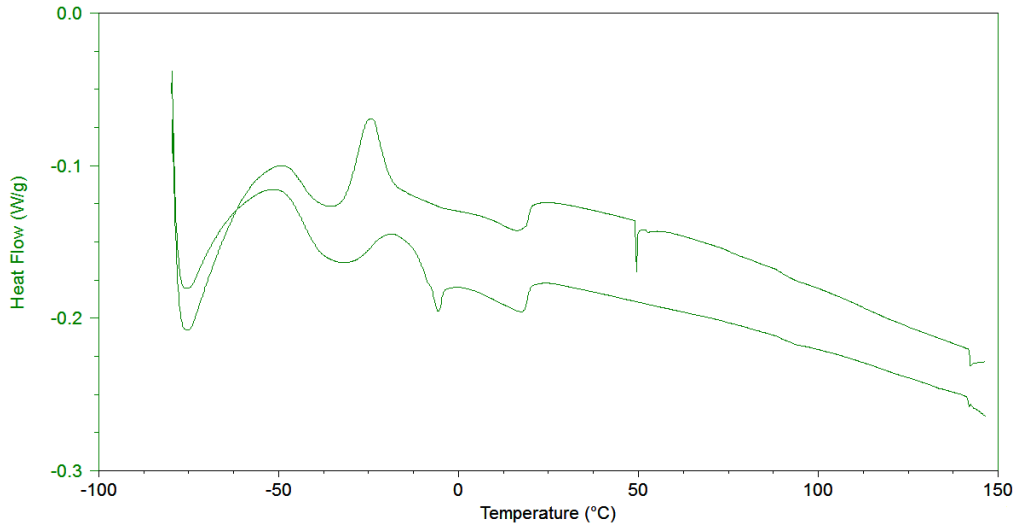

Figure 6.6: DSC tests for the non-purified SBR rubber (sample 1 shown in Figure 6.4)

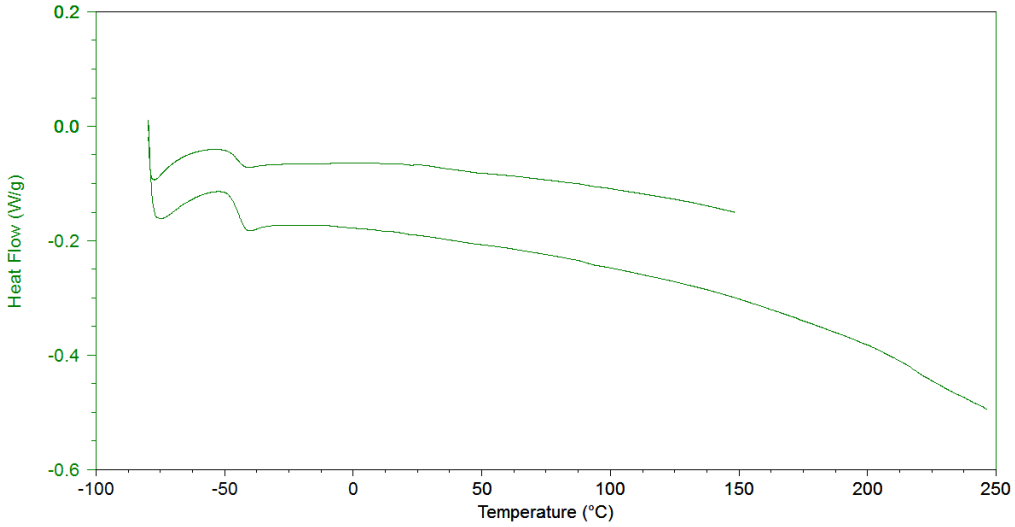

Figure 6.7: DSC tests for the purified SBR rubber (sample 2 shown in Figure 6.4)

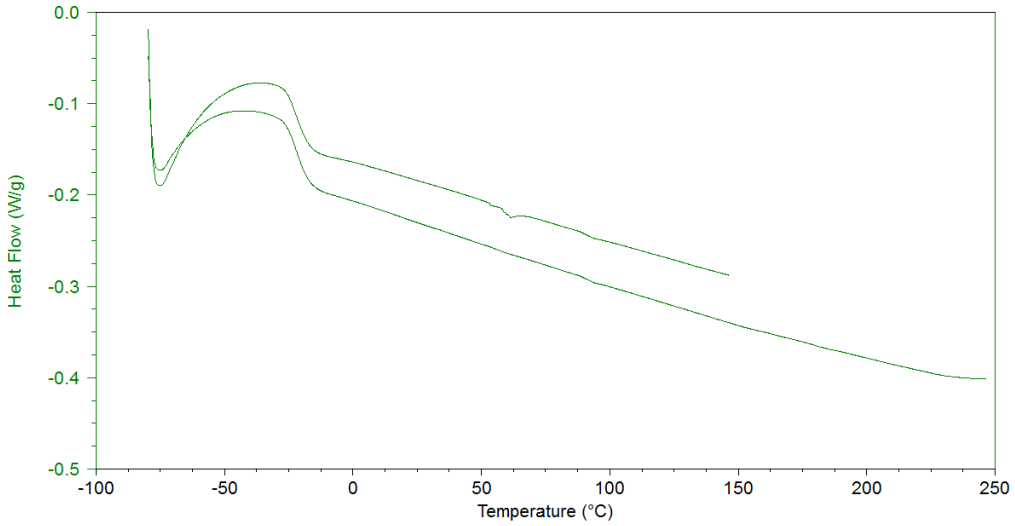

Figure 6.8: DSC tests for the commercial SBR rubber

SBR latex synthesis was also carried out at a higher temperature (75 °C). It has been confirmed that SBR rubbers prepared at this temperature by the DMP method could not be dissolved by an organic solvent even if it was treated using a HCl/C_2H_5OH solution. This

result could be explained in that a high reaction temperature leads to high gel content in the SBR latex, which affects the solubility of SBR in an organic solvent. In the micellar nucleation dominated DMP system, the principle locus of particle nucleation is the monomer swollen micelles, and the entry of each radical to a micelle initiates the nucleation event. At a higher reaction temperature, the transfer of monomer to polymer in micelles may influence the stability of micelles and change the interactions between micelles. The unstable micelles agglomerate with each other or with the premature polymer particles to form highly cross-linked polymeric particles.

A DSC test was performed on the SBR latices synthesized at 75 °C to characterize its purity. As displayed in Figure 6.9, the glass transmission temperature (T_g) for the SBR latex synthesized with DMP method at a 75 °C reaction temperature is -42.66 °C, which is close to the T_g of the SBR latex synthesized at 50 °C, as shown in Figure 6.7. Moreover, this curve does not have any noisy signals, which confirms that the surfactant is washed away by an HCl/C_2H_5OH solution. This DSC tests were carried out to confirm that the latex is SBR even though it cannot dissolve in an organic solvent. Based on these observations it is concluded that SBR nanoparticles prepared at a higher reaction temperature are highly cross-linked.

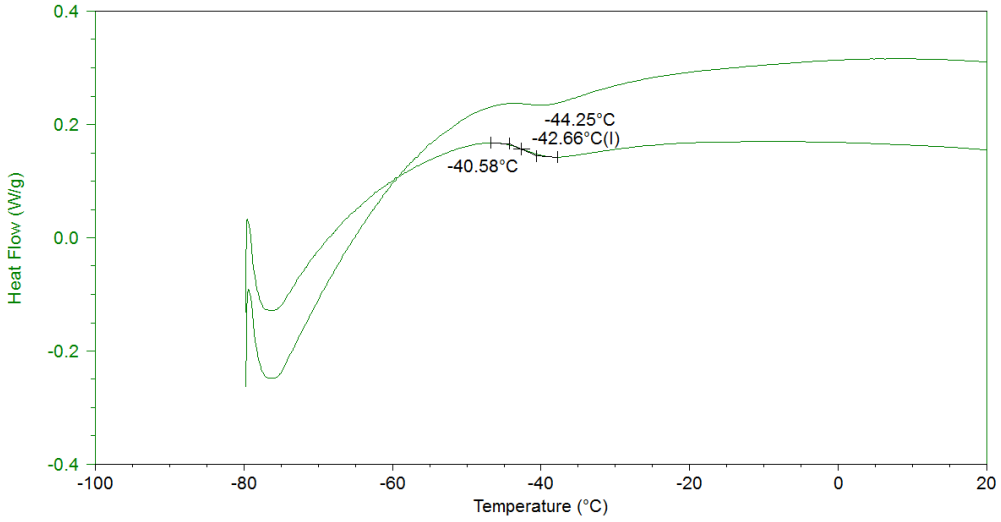

Figure 6.9: A DSC test for a SBR rubber synthesized with the DMP method at 75 °C

6.4 Conclusion

A hydrochloric acid (HCl) diluted solution containing 1N hydrochloric acid and ethanol solution was used as the washing or conjugating agent for the SBR latex solutions. The surfactant, sodium oleate, was washed away from the out layer of SBR latex particles in forms of sodium chloride, ester and water molecules. Purified SBR rubbers were able to dissolve in an organic solution for characterization tests.

Chapter 7 Influence of Particle Size on Glass Transition Temperature

7.1 Introduction

The glass transition temperature regarded as an intrinsic characteristic of thermal particles that has been observed in both molecular and colloidal systems [70-72]. In general, particles with a diameter of less than 1 nm are defined as molecules, whereas the others with a diameter in the range of nanometers to microns are defined as colloidal. Factors that influence the glass transition of a thermal particle can be various; irrespective of the particle structure, particle polarity and intermolecular forces between particles. Particle size is another important factor that could affect its glass transition temperature. Larsen R. J. et al. [69] have investigated the relation between particle size and glass transition temperature (T_g) of non-polar gradual organic molecules. Based on their studies it has been found that, T_g increases with the molecule size. Table 7.1 displays a list of organic molecules which shows that when the molecular size is enlarged, their corresponding T_g is going to increase.

During the studies of synthesis of nanosized polymeric SBR particles, SBR rubbers synthesized via the DMP method had lower T_g than the commercial ones. It proposed that the size of particles was the essential factor behind these findings. Therefore, investigation of the connection between SBR particles size and T_g was also performed in our research, and this chapter will focus on discussing these findings on the influence of SBR particle size on their glass transition temperature.

Table 7.1: Values of hard sphere diameter σ_0 and T_g for non-polar various size organic molecules [70]

	σ_0	T_g
1. Cyclohexene	0.55	81
2. Toluene	0.57	113
3. Ethylbenzene	0.60	111
4. Isopropylbenzene	0.63	127
5. 4 tert-butyl pyridine (4-TBP)	0.65	166
6. Phenolphthalein-dimethylether (CGE)	0.66	204
7. Dimethylphthalate (DMP)	0.69	195
8. O-terphenyl	0.76	244
9. Triepoxide N-N-diglycidyl-4-glycidyloxyaniline (DGGOA)	0.78	244
10. Phenolphthalein-dimethylether (PDE)	0.84	294
11. Diglycyl ether of bisphenol A (DEGBA)	0.85	257
12. Kresolphtalein-dimethylether (KDE)	0.88	311
13. 1,3, 5-tri-α-naphthyl benzene	0.96	342

7.2 Experimental

7.2.1 Synthesis of SBR nanoparticles

Styrene-butadiene copolymer particles were synthesized by DMP and conventional emulsion polymerization methods. For the DMP approach, an initiator (KPS), a chain transfer agent and a surfactant were mixed with DI water to form a continuous phase initially. After the reaction temperature was stabilized at 50 °C, a mixture of styrene and butadiene was introduced to the system into a drop-wise manner. In contrast, to the conventional emulsion process, the styrene and butadiene monomers were mixed with a surfactant, a chain transfer agent and water in the formation of a continuous phase, and the addition of initiator was introduced subsequently once a homogenous emulsion with a constant temperature of 50 °C was reached. SBR rubbers were isolated by an acidified ethanol solution from the latex

solution produced by the DMP and conventional emulsion polymerization methods, respectively. Isolated SBR rubbers were dried at 65 °C in a vacuum oven for 12 hours.

7.2.2 Determination of glass transition

Resulting SBR rubber was tested by DSC to measure the polymer glass transition temperature (T_g), at which the inflection point of heat capacity occurs as a measure of T_g. The temperature and heat flow signals were calibrated with indium. The temperature scan rate was set as 10 °C/min. In addition, ^{1}H NMR experiments were also performed to analyze the butadiene and styrene components in the SBR rubber synthesized by the DMP approach. The interpretation of the NMR spectrum is discussed in the following paragraph.

7.2.3 Determination of styrene and butadiene composition in SBR samples

The level% of SBR copolymer monomer was calculated based on the integrated area of proton atoms. As indicated in Figure 7.1, Scheme 1 and Scheme 2, the peaks at 7.11, 7.16 and 7.24 are related to the phenyl protons in styrene; the broad peak at 2.53 ppm corresponds to the styrenic CH proton and its integral area relative to phenyl protons area is 1:5, which confirms the above assignments. The peaks at 5.36 and 5.40 ppm are related to two trans hydrogen of butadiene resulting from 1,4-addition; while peaks at 4.91, 4.95, 5.03 ppm and 5.51pm show the presence of two geminal hydrogen of pendant vinylic groups from 1,2-addition. A singlet peak at 2.02 ppm is related to the CH_2 protons in 1, 4-trans butadiene segments. The peaks appearing at 1.69 and 1.96 ppm are related to CH_2 protons from styrene and trans-1,4-butadiene units (Scheme 2). If the CH_2 group of trans 1,4-butadiene neighbors to the 1,2-addition, it shift to 1.23 ppm (Scheme 1). However, they are desheilded to 2.24

ppm if the CH_2 group of trans 1,4-butadiene is adjacent to the styrenic CH proton because of the anisotropic effect of the phenyl ring relative to the other methylene ones (Scheme 2).

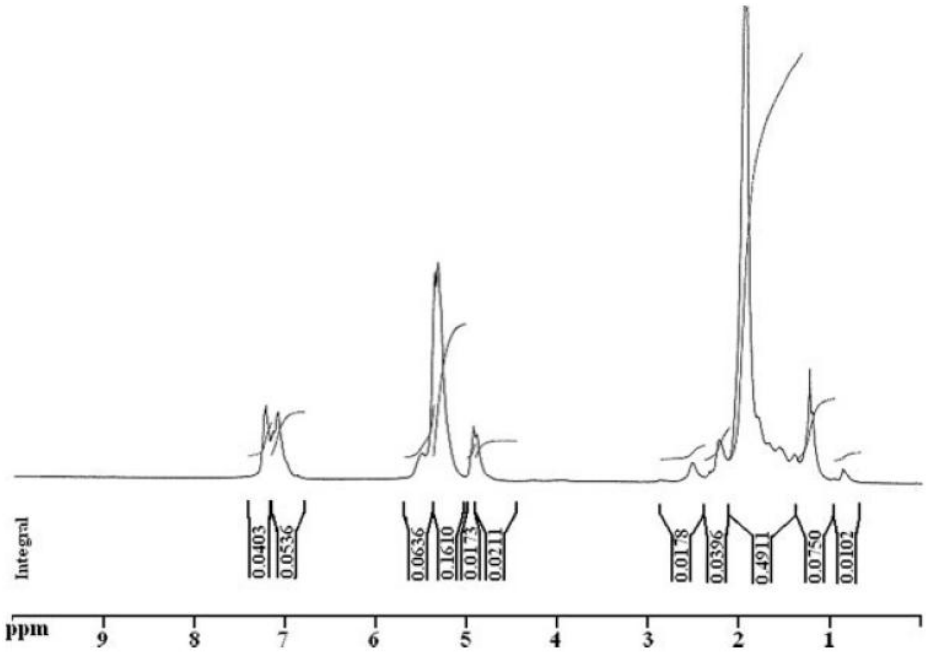

Figure 7.1: ^{1}H NMR spectrum of a commercial SBR (75% BD and 25% of ST) in CDCl3 [73]

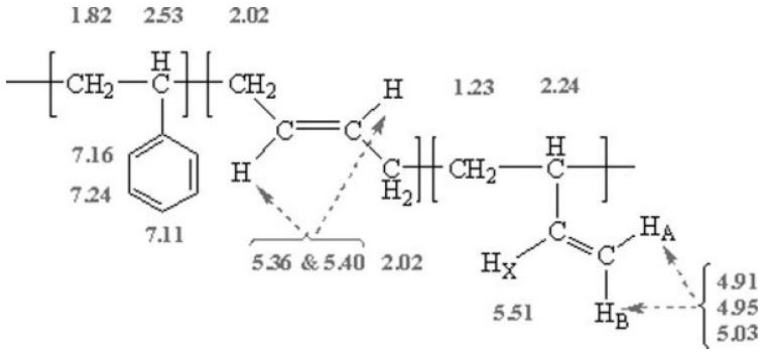

Scheme 1: Chemical shifts of the butadiene styrene hydrogens structure at SBR [73]

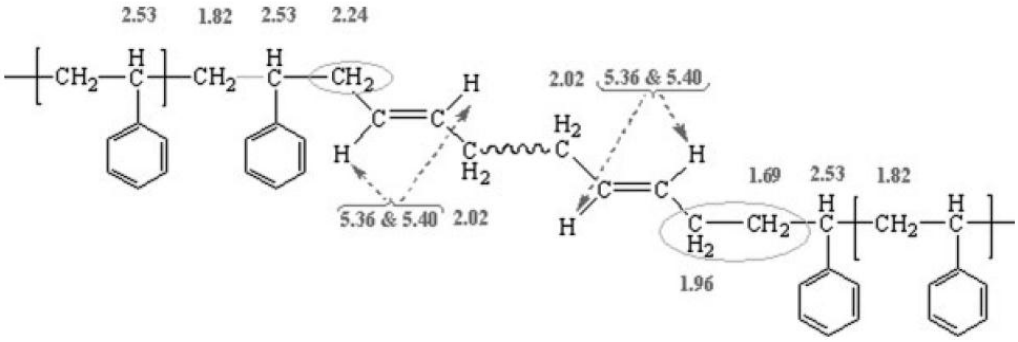

Scheme 2: Chemical shifts of butadiene when trans 1,4-butadienes are beside the styrenic groups [73]

Therefore, based on the proton interval area describe above, the level% of butadiene (1,2-addition and 1,4-addition) and styrene in a SBR copolymer can be calculated as given below:

$$\text{ST \%} = \frac{A_{7.24+7.16+7.11+2.53+1.82+1.69}}{A_{7.24+7.16+7.11+2.53+1.82+1.69} + A_{5.51+5.4+5.36+5.03+4.95+4.91+2.24+2.02+1.96+1.23}}$$

$$\text{BD \%} = \frac{A_{5.51+5.4+5.36+5.03+4.95+4.91+2.24+2.02+1.96+1.23}}{A_{7.24+7.16+7.11+2.53+1.82+1.69} + A_{5.51+5.4+5.36+5.03+4.95+4.91+2.24+2.02+1.96+1.23}}$$

$$\text{BD (1,2 addition) \%} = \frac{A_{5.51+5.03+4.95+4.91+2.24+1.23}}{A_{7.24+7.16+7.11+2.53+1.82+1.69} + A_{5.51+5.4+5.36+5.03+4.95+4.91+2.24+2.02+1.96+1.23}}$$

$$\text{BD (1,4 addition) \%} = \frac{A_{5.4+5.36+2.24+2.02+1.96}}{A_{7.24+7.16+7.11+2.53+1.82+1.69} + A_{5.51+5.4+5.36+5.03+4.95+4.91+2.24+2.02+1.96+1.23}}$$

Accordingly, the level% of butadiene and styrene in the SBR copolymers synthesized via the DMP method can also be determined by the methods showing above.

7.3 Results and discussion

SBR samples were prepared by DMP and conventional emulsion polymerization techniques. Their particle size and glass transition temperature (T_g) were determined by DLS and DSC,

respectively. Table 7.2 summarizes the test results generated for these samples. Based on the experimental data, a connection between the particle size and T_g were also plotted. It shows that T_g is dependent on the particle size since a linear relation between these two factors was found as shown in Figure 7.2; plus, the T_g of the SBR rubber synthesized via the DMP approach is lower than those rubbers prepared when using a conventional emulsion polymerization method. SBR particles synthesized when using the DMP approach have a lower T_g which may be attributed to the particles containing a higher concentration of butadiene. The T_g for butadiene and styrene are -75 °C and 100 °C, respectively. Therefore, a SBR rubber with higher concentration of butadiene will have a lower T_g. Figure 7.3 and Table 7.3 show that the T_g decreases with an increasing concentration of butadiene in the resultant SBR rubber. It was proposed that the difference in the nucleation mechanism between DMP and conventional emulsion polymerization resulted in the difference of butadiene composition in the SBR synthesized.

As discussed in Chapter 6, due to the drop-wise addition of monomers during the polymerization process in DMP, the micellar nucleation dominated the polymerization mechanism as the homogeneous nucleation was suppressed to a large extent under this scenario, and hence particles with a smaller size were generated. Nevertheless, conventional emulsion polymerization, which involves introducing all of the monomers at one time, resulted in homogeneous and micellar nucleation mixed mechanism, and particles with a larger size were produced. Owning to the extremely low solubility in water, butadiene and styrene will form micelles rather than dissolve in the continuous aqueous phase. Therefore, micellar nucleation is preferred for them over homogeneous nucleation. Since DMP is a

micellar nucleation dominated process, the reaction conversion is expected higher than for conventional emulsion polymerization. Table 7.2 shows that the reaction conversions in DMP are higher than conventional emulsion polymerization over the same reaction period. Therefore, based on this observation, it is concluded that DMP is a micellar nucleation dominated process. In a micellar nucleation process, a higher portion of butadiene will take part in the reaction. As a result, smaller particles with a higher concentration of butadiene were generated by DMP. On the other hand, in conventional emulsion polymerization, fractional parts of the monomers undergo homogeneous nucleation. However, due to the extremely low solubility of butadiene in the continuous aqueous phase, and extremely low boiling point, the continuous aqueous phase contains more styrene monomers than butadiene monomers. As mentioned in Chapter 6, for a homogeneous nucleation, the oligomeric radicals react with monomers in the aqueous phase to maintain the growth of their polymer chain, and stop growing once all monomers are consumed. Thus, in this process, larger particles are produced. As the monomer concentration in the continuous aqueous phase is low, the larger size of the particle, the lower concentration of the butadiene in the resultant SBR particle, and therefore, the relation between T_g and SBR particles size is observed, with larger particles having a lower T_g.

Table 7.2: Summary of particle size, reaction conversion and glass transition temperature with respect to synthesis methods

SBR sample	synthesis method	particle size (nm)	conversion(%)	T_g (℃)
123	Conventional Emulsion	129	52.4	-38.9
126	Conventional Emulsion	167	56.7	-34.4
134	Conventional Emulsion	189	60.1	-17.8
127	Conventional Emulsion	223	49.0	-35.3
140	DMP	41.1	56.2	-45.1
141	DMP	45.8	78.9	-43.3
142	DMP	56.3	76.3	-46.6
143	DMP	65.5	70.4	-44.4

Reaction conditions: Reaction temperature = 50 °C, Reaction time = 8 hr, [BD] = 4.6E-3, [ST] = 8.9E-4, [KPS] = 4.0E-6, [n-DDM] = 3.1E-6, [Na Oleate] = 3.3E-5

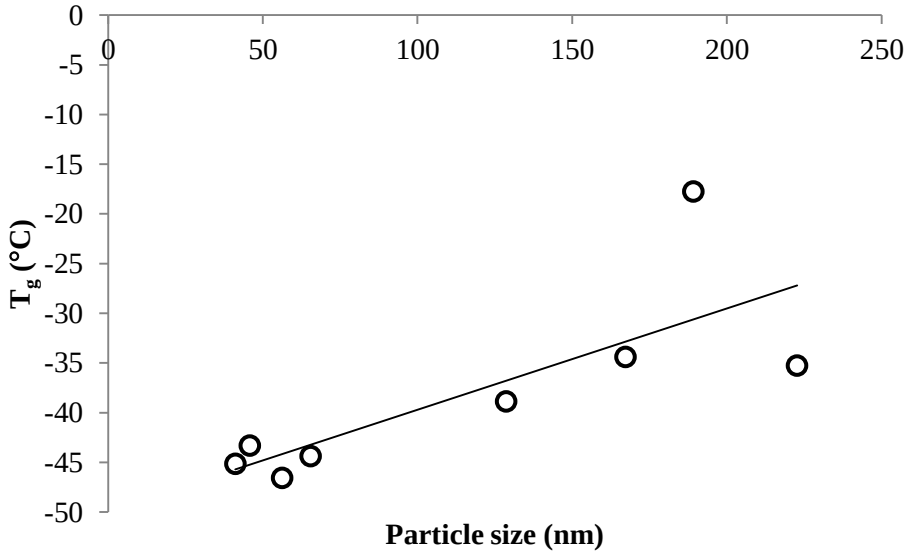

Figure 7.2: Profile of glass transition temperature with various SBR particle sizes

Table 7.3: Summary of BD and ST concentration in SBR samples with respect glass transition temperature

SBR Sample	T_g (℃)	^{1}H NMR			
		ST	BD-(1,2)-Addition	BD-(1,4)-Addition	BD (Total)
127	-35.28	28.74%	22.27%	40.55%	62.81%
123	-38.87	23.55%	37.46%	38.98%	76.45%
141	-43.32	22.14%	19.28%	58.58%	77.86%
140	-45.14	23.87%	47.18%	39.35%	86.53%

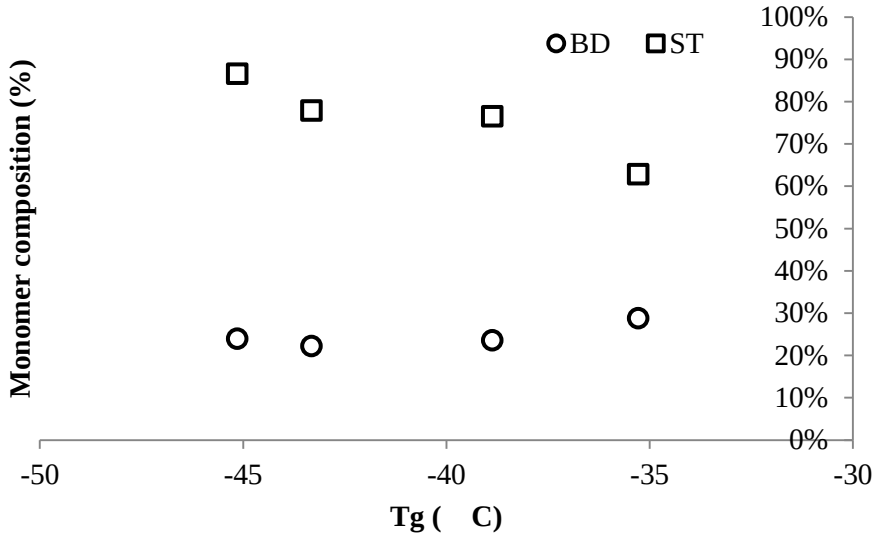

Figure 7.3: Profile of BD concentration in SBR synthesized via DMP with various glass transition temperatures

7.4 Conclusion

In conclusion, the DMP approach promoted the micellar nucleation process, and thus generated smaller size SBR nanoparticles with a higher concentration of butadiene. Therefore, SBR particles prepared by the DMP method had a lower glass transition temperature than those from conventional emulsion polymerization.

Chapter 8 Conclusions and Recommendations

Synthesis of styrene-butadiene nanoparticles via differential microemulsion polymerization was performed in a 300 ml bench scaled reactor. The general features of this DMP system comprised hydrophobic monomers (styrene and butadiene), water, surfactant and a water soluble potassium persulfate. Due to the extremely low solubility in water, butadiene and styrene formed micelles rather than dissolving in the continuous aqueous phase. Therefore, the mechanism of this process was dominated by micellar nucleation.

Factors influencing the size of SBR particles generated by the DMP approach were also investigated. Results of the studies are concluded in the following paragraphs.

1. *Addition rate of monomers:* A decrease in the size of particles prepared with the slower addition rate of monomers was observed. Slower addition rate promoted the dispersion of monomer micelles in the continuous aqueous phase, and thus facilitated the micellar nucleation and smaller SBR particles can be generated.
2. *Reaction temperature:* Reaction temperature could influence the initiator decomposition rate constant k_d and propagation rate constant k_p, and the number of radicals per particle, as well. A decrease in the size of particles with the increase of reaction temperature was also observed in this case. The number of radicals determined the number of monomer micelles, and increased with the reaction temperature. Therefore, an increase of reaction temperature promoted the micellar nucleation and smaller SBR particles were generated.
3. *Chain transfer agent:* An increase in particle size with an increase on the amount of CTA added to the system was observed. The CTA could reduce the rate of emulsion polymerization by increasing the radical desorption from the polymer particles. For a

micellar nucleation dominated DMP system, an increase in the CTA concentration facilitated the radical desorption rate from the oligomeric radicals and thus suppressed the homogeneous nucleation in the continuous aqueous phase. Alternatively, it promoted the micellar nucleation. For butadiene and styrene with an extremely low solubility in water, nucleation in micelles was faster than in the aqueous phase, and thus a higher reaction conversion was achieved when a CTA promoted the micellar nucleation in the DMP system. A larger size of SBR particles was resulted with an increase of the reaction conversion.

4. *The type and the amount of surfactant:* A decrease in particle size with an increasing amount of surfactant was also noticed. The smallest particle size was achieved after the concentration of the SDS surfactant reached its CSC value. In addition, a lower CSC value of the Gemini surfactant was also found compared with SDS. This is attributed to the multi hydrophobic and hydrophilic groups present in a Gemini surfactant, which can lower its CSC value.
5. *Solvent:* An increase in particle size with an increasing in the amount of water present was found in this investigation. It was proposed that the increasing amount of water diluted the Gemini surfactant concentration to be below its CMC value, and thus a larger particle size resulted. Normally, the size of SBR particles is not influenced by the amount of water as long as its CMC value is maintained.
6. *Initiator:* A water-soluble initiator potassium persulfate (KPS) was used as the initiator to synthesize SBR latex nanoparticles via the DMP method. It was found that the particle size was not influenced by the concentration of KPS, but the reaction conversion rose along with an increase of KPS concentration. This result was expected. For a micellar nucleation dominated process, the particle size is controlled by the size of micelles, not the reaction rate.

Nevertheless, an increase of KPS concentration accelerated the reaction rate, and hence the reaction conversion rose.

7. *Monomer feed composition:* The monomer feed composition was determined from the BD/ST ratio. An increase of the BD/ST ratio slowed down the reaction rate. This was due to the low solubility and boiling point of butadiene. When the composition of butadiene was increased in the feed stream, the monomer composition in the gas phase in the reactor rose. Since gas phase monomers take a longer time than the monomers in the aqueous phase to participate in the polymerization reaction, a increase in the BD/ST ratio will result in a lower reaction conversion compared to a lower ratio under the same reaction time. Moreover, at a lower reaction conversion, less amount of monomers took part in the polymerization, and an smaller average particle size was generated.

Recovery of SBR rubber from the latices was also investigated. It was found that the HCl acidified ethanol solution could effectively remove the sodium oleate surfactant from the out-layer of SBR particles. Purified SBR rubber showed a light yellow color and could be dissolved by THF solution and CCl_4 solution for GPC and ^1H NMR tests.

The relation between particle size and glass transition temperature is the last topic discussed in this thesis. It is concluded that the glass transition temperature was particle size dependent. For a micellar nucleation dominated DMP system, butadiene could easily access the polymerization. Therefore, the butadiene content in the particles prepared by the DMP approach was higher than particles generated by the conventional emulsion polymerization. Higher butadiene content resulted in a lower glass transition for a SBR rubber. As the size of

the particles generated with the conventional emulsion polymerization were larger than the DMP approach. The relation between the particle size and the glass transition temperature was found to be linear.

The recommendation for the future work lies in the field of applying oil-soluble initiators for developing SBR nanoparticles via the DMP method. Given that the DMP approach is a micellar nucleation dominated process, radicals from an oil-soluble initiator could easily access the oil phase comprising styrene and butadiene. Therefore, the time for a micelle to accommodate a radical is reduced. As a result, the initiation in a micelle can take place earlier, and the depletion of micelles and coalescence between micelles can be avoided to a large extent. Hence, a smaller particle size will be achieved. In addition, it is also recommended to do the direct hydrogenation on the SBR latex particles by applying Wideman's approach. Giving that the size of SBR nanoparticles generated by the DMP method is small enough (~30 nm), it would be helpful on improving the degree of hydrogenation of SBR particles in the latex form.

References

1. Lovell P. A. and El-Aasser M. S., Emulsion Polymerization and Emulsion Polymers, John Wiley and Sons: Chichester, 1997.
2. Mohammadi N. A., Rempel G. L., Homogeneous selective catalytic hydrogenation of C=C in acrylonitrile-butadiene copolymer, *Macromolecules*, 20, 2362 (1987).
3. Weinstein A. H., Elastomeric Tetramethylene-Ethylethylene-Acrylonitrile Copolymers, *Rubb. Chem. Technol.*, 57, 203 (1984).
4. He et al., *J. Appl. Polym. Sci.*, 64, 2047–2056 (1997).
5. Wideman L. G., U.S. Pat. 4,452,950 (1984) (The Goodyear Tire & Rubber Co.).
6. Langer R., Biomaterials in drug delivery and tissue engineering: one laboratory's experience, *Acc. Chem. Res.*, 33, 94-101(2000).
7. Bhadra D., Bhadra S., Jain P., Jain N. K., Pegnology: a review of PEG-ylated systems, *Pharmazie*, 57, 5-29 (2002).
8. Kommareddy S., Tiwari S. B., Amiji M. M., Long-circulating polymeric nanovectors for tumor-selective gene delivery, *Technol Cancer Res Treat*, 4, 615-25 (2005).
9. Lee M., Kim S. W., Polyethylene Glycol-Conjugated Copolymers for Plasmid DNA Delivery, *Pharm Res*, 22, 1-10 (2005).
10. Vanderhoff, J. W., El-Aasser M. S., Tseng, C. M., Interfacial aspects of miniemulsions and miniemulsion polymers, *J. Dispers. Sci. Technol.*, 5, 231 (1984).
11. Ugelstad J., Mork P. C., Kaggerud K. H., Ellingsen T., Berge A., Swelling of oligomer-polymer particles: New methods of preparation of emulsion and polymer dispersions, *Adv. Colloid Interface Sci.* 13, 101 (1980).
12. Miller C. M., El-Aasser M. S., Recent Advances in Polymeric Dispersions; NATO ASI Series E: Applied Science, 335; Kluwer Academic Publishers: Dordrecht, 1997.
13. Candau F., Polymerization in Organized Media; Gordon & Breach: Philadelphia, 1992; Chapter 4.
14. Chou Y. J., El-Aasser M. S., Vanderhoff J. W., Mechanism of emulsification of styrene using hexadecyltrimethylammonium bromide-cetyl alcohol mixtures, *J. Dispersion Sci. Technol.*, 1, 29-50 (1981).

15. Antonietti M., Landfester K., Polyreactions in miniemulsions, *Prog. Polym. Sci.*, 27, 689 – 757 (2002).
16. Bechthold N., Landester K., Miniemulsion polymerization: applications and new materials, *Macromolecules*, 33, 4682-9 9 (2000).
17. Tauer K., Kuhn I., Nucleation in Emulsion Polymerization: A New Experimental Study. 1. Surfactant-Free Emulsion Polymerization of Styrene, *Macromolecules*, 28, 2236-9 (1995).
18. Blackley D. C., Polymer latices. 2nd ed. London: Chapman & Hall, 1997.
19. Fontenot K., Schork F. J., Batch polymerization of methyl methacrylate in mini/macroemulsions, *J. Appl. Polym. Sci.*, 49: 633-55 (1993).
20. Gilbert R. Emulsion polymerization. San Diego: Academic Press, 1995.
21. Markus A*, Katharina L. Polyreactions in miniemulsions, *Prog. Polym. Sci.*, 27, 689 – 757 (2002).
22. Fontenot K., Schork F. J., Synthesis of colloidal particles in miniemulsions, *Ind. Eng. Chem. Res.*, 32, 373-85 (1993).
23. Sorokin V.I., The effect of fountain formation at the surface of a vertically oscillating liquid, *Sov Phys/Acoust*, 3, 281-91 (1957).
24. Li M. K., Fogler H. S., Acoustic emulsification. Part 1. The instability of the oil-water interface to form the initial droplets, *J. Fluid Mech.*, 88, 499-511(1978).
25. Fontenot K. J. J., Schork F. J., Miniemulsion polymerization. Reichert KH, Moritz H, editors. Fourth International Workshop on Polymer Reaction Engineering, vol.127. Weinheim, Germany: Dechema Monographs, 1992. P. 429-39.
26. Bechthold N., Tiarks F., Willert M., Landfester K., Antonietti M., Miniemulsion polymerization: applications and new materials, *Macromol Symp*, 151, 549-55 (2000).
27. Alduncin J. A , Forcada J., Asua J. M., Miniemulsion Polymerization Using Oil-Soluble Initiators, *Macromolecules*, 27, 2256-61 (1994).
28. Schauber C., These Docteur-Ingenieur, Universite de Mulhouse, France, 1979.
29. Chern C. S., in *Principles and applications of emulsion polymerization*, Hoboken, New Jersey: John Wiley & Sons, Inc.; 2008. p. 154–6.

30. Capek I., Radical polymerization of polar unsaturated monomers in direct microemulsion systems, *Adv. Colloid Interface Sci.* 80, 85 (1999).
31. Capek I., Microemulsion polymerization of styrene in the presence of anionic emulsifier, *Adv. Colloid Interface Sci.* 82, 253 (1999).
32. Xu H. J. and Gan L. M., Recent advances in the synthesis of nanoparticles of polymer latexes with high polymer-to-surfactant ratios by microemulsion polymerization, *Curr. Opin. Colloid Interface Sci.* 10, 239 (2005)
33. Hentze H. P. and Kaler E. W., Polymerization of and within self-organized media, *Curr. Opin. Colloid Interface Sci.* 8, 164 (2003)
34. Chern C. S., in *Encyclopedia of Polymer Science and Technology*, Kroschwitz J. I. (Ed.), John Wiley & Sons, New York, 2002.
35. Candau F., in *Polymerization in Organized Media*, *Paleos C. M. (Ed.)*, Gordan & Breach, Philadelphia, 1992, Chapter 4, pp. 215-282.
36. Candau F., in *Handbook of Microemulsion Science and Technology*, Kumar P. and Mittal K. L. (Eds.), Marcel Dekker, New York, 1999, pp. 679-712.
37. Perez-Puna V. H. et al., *Langmuir*, 6, 1040 (1990).
38. Guo J. S. et al., Particle nucleation and monomer partitioning in styrene O/W microemulsion polymerization, *J. Polym. Sci., Poly. Chem. Ed.*, 30, 691 (1992).
39. Feng L. and Ng K.Y.S., In situ kinetic studies of microemulsion polymerizations of styrene and methyl methacrylate by Raman spectroscopy, *Macromolecules*, 23, 1048 (1990).
40. Feng L. and Ng K.Y.S., Characterization of styrene polymerization in microemulsions by Raman spectroscopy, *Colloids Surf.*, 53, 349 (1991).
41. Puig J. E., Perez-Luna V. H., Perez-Gonzales M., Macias E.R., Rodriguez B.E., and Kaler E.W., *Colloid Polym. Sci.* 271,114 (1993).
42. Gan L. M., Chew C. H., Lee K. C. and Ng S. C., *Polymer*, 34, 3064 (1993).
43. Gan L. M., Chew C. H., Ng S. C., and Loh S. E., Polymerization of methyl methacrylate in ternary oil-in-water microemulsions, *Langmuir*, 9, 2799–2803 (1993).
44. Gan L. M., Chew C. H., Lee K. C. and Ng S. C., *Polymer*, 35, 2659 (1994).

45. Gan L. M., Chew C. H., Lim J. H., Lee K. C., Copolymerization of Styrene and Methyl Methacrylate in Ternary Oil-in-Water Microemulsions: Monomer Reactivity Ratios and Microstructures by ^{1}H NMR and 13C NMR, *Macromolecules*, 6335–6340 (1994).
46. Rodriguez-Guadarrama L. A., Mendizabal E., Puig J. E. and Kaler E. W., Polymerization of methyl methacrylate in 3-component cationic microemulsion, *J. Appl. Polym. Sci.*, 48, 775 (1993).
47. Bleger F., Murthy A.K., Pla F. and Kaler E.W., Particle Nucleation during Microemulsion Polymerization of Methyl Methacrylate, *Macromolecules*, 27, 2559 (1994).
48. Morgan J. D., Lusvardi K. M., and Kaler E. W., Kinetics and Mechanism of Microemulsion Polymerization of Hexyl Methacrylate, *Macromolecules*, 30, 1897 (1997).
49. Vries R. de, Co C. C. and Kaler E. W., Microemulsion Polymerization. 3. Molecular Weight and Particle Size Distributions, *Macromolecules*, 34, 3233 (2001).
50. Guo J. S., El-Aasser M. S., and Vanderhoff J. W., Microemulsion polymerization of styrene, *J. Polym. Sci., Polym. Chem. Ed.* 27, 691 (1989).
51. Chern C. S. and Wu L. J., Kinetics of the microemulsion polymerization of styrene with short-chain alcohols as the cosurfactant, *J. Polym. Sci., Polym. Chem. Ed.*39, 3199 (2001)
52. Wang et al., US Patent 0185273 A1Application Publication (2007).
53. Wang et al., Synthesis, Characterization, and Application of Novel Polymeric Nanoparticles, *Macromolecules,* 2007, 40, 499-508.
54. Tuzar Z; Kratochvil P. Micelles of block and graft copolymers in solution. In Matjevic, E., Ed.; Surface and Colloid Science; Plenum Press: New York, 1993; Vol. 15, Chapter 1, pp 1-83.
55. Hamley I. W. In Hamley, I. W., Ed.; The Physics of Blockcopolymers, 4; Oxford Science Publication: Oxford, 1998; Chapters 3 and 4, pp 131-265.
56. Fontenot K. J. J., Schork F. J., Miniemulsion polymerization. In: Reichert KH, Moritz H, editors. Fourth International Workshop on Polymer Reaction Engineering, vol.127. Weinheim, Germany: Dechema Monographs, 1992. P. 429-39.

57. Zana R., Benrraou M., Rueff R., Alkanediyl-.alpha., omega.-bis(dimethylalkylammonium bromide) surfactants. 1. Effect of the spacer chain length on the critical micelle concentration and micelle ionization degree, *Langmuir,* 7, 1072-1075 (1991).
58. Chern, C. S., Principles and applications of emulsion polymerization. Hoboken, New Jersey: John Wiley & Sons, Inc.; 2008. p. 54–91.
59. He, G., Pan, Q.*, Rempel, G.L.*, Synthesis of Poly(methyl methacrylate) Nanosize Particles by Differential Microemulsion Polymerization, *Macromol. Rapid Commun.,* 24, 585-588 (2003).
60. He, G., Pan, Synthesis of Polystyrene and Polystyrene/Poly(methyl methacrylate) Nanoparticles, *Macromol. Rapid Commun.,* 25, 1545-1548 (2004).
61. Nomura M., Minamino Y. and Fujita K., The role of chain transfer agents in the emulsion polymerization of styrene, *J. Polym. Sci., Polym. Chem., Ed.*20, 1261-1270 (1982).
62. Smith W. V., Regulator Theory in Emulsion Polymerization.[1] I. Chain Transfer of Low Molecular Weight Mercaptans in Emulsion and Oil-Phase, *J. Am. Chem. Soc*., 68, 2064 (1946).
63. Kolthoff I. M. and Harris W. E., Mercaptans as promoters and modifiers in emulsion copolymerization of butadiene and styrene using potassium persulfate as catalyst. II. Mercaptans as modifiers, J. *Polym. Sci*., 2, 41 (1947).
64. Harada M. et al., *J. Chem. Eng. Jpn*., 4 (1), 54 (1971).
65. Menger F. M. and Keiper J. S., Gemini Surfactants, *Angew. Chem., Int. Ed. Engl.*, 39, 1906-1920 (2000).
66. Bakshi M. S., Sharma P. and Banipal T. S., Lamellar Phase Supported Synthesis of Colloidal Gold Nanoparticles, Nanoclusters, and Nanowires, *Materials Letters*, 61 (28), 5004 -5009 (2007).
67. Zana R. and Talmon Y., Dependence of aggregate morphology on structure of dimeric surfactants, *Nature*, 362, 228-230 (1993).
68. Chern C. S., Tang H. J. Microemulsion polymerization kinetics and mechanisms. *J. Appl. Polym. Sci.,* 97, 2005–13 (2005).

69. Ryan J. Larsen and Charles F. Zukoski, Synthesis of Nonspherical Colloidal Particles with Anisotropic Properties, *Physical Review* E83, 051504 (2011).
70. D. Ben-Amotz and D. R. Herschbach, Estimation of effective diameters for molecular fluid, *J. Phys. Chem.*, 94, 1038(1990).
71. P. Agarwal H. Qi, and Archer L. H., *Nano. Lett.*, 10, 111 (2010).
72. Khoee S. and Sorkhi M., Microstructure Analysis of Brominated Styrene–Butadiene Rubber, *Polym. Eng. & Sci*., 47, 87 -94 (2007).

Appendix A: Raw Data

SBR Sample	Surfactant Adopted	Amt. of Surfactant (g)	BD (ml/g)	ST (ml/g)	KPS (g)	n-DDM (g)	DI Water (g)	Temp (°C)	Particle Size (nm)
7	GS	1.210	7.8/5	7.0/6.4	0.070	0.00	162	75	28
8	SDS	1.210	7.8/5	7.0/6.4	0.070	0.00	162	75	172
9	SDS	2.410	7.8/5	7.0/6.4	0.070	0.00	64	75	23
10	GS	0.610	7.8/5	7.0/6.4	0.070	0.00	64	75	45
11	SDS	0.610	7.8/5	7.0/6.4	0.070	0.00	64	75	51
12	SDS	1.210	7.8/5	7.0/6.4	0.070	0.00	94	75	64
13	SDS	1.410	7.8/5	7.0/6.4	0.070	0.00	94	75	59
14	GS	1.317	3.9/2.5	3.5/3.2	0.035	0.00	81	80	36
15	GS	0.664	3.9/2.5	3.5/3.2	0.035	0.00	32.33	75	42
16	GS	1.317	3.9/2.5	3.5/3.2	0.035	0.00	32.33	75	32
17	GS	1.535	3.9/2.5	3.5/3.2	0.040	0.00	47.1	80	26
18	GS	0.664	3.9/2.5	3.5/3.2	0.035	0.02	32.33	75	17
19	GS	0.664	3.9/2.5	3.5/3.2	0.035	0.02	32.33	75	34
20	GS	0.664	3.9/2.5	3.5/3.2	0.035	0.02	32.33	75	35
21	GS	0.664	3.9/2.5	3.5/3.2	0.035	0.02	32.33	75	28
22	GS	0.664	3.9/2.5	3.5/3.2	0.035	0.02	32.33	75	28
23	GS	0.664	3.9/2.5	0/0	0.035	0.11	32.33	75	-
24	GS	0.664	3.9/2.5	3.5/3.2	0.035	0.10	32.33	75	27
25	SDS	0.305	3.9/2.5	3.5/3.2	0.035	0.10	32.33	75	34
26	SDS	0.305	12.7/8.1	2.8/2.5	0.035	0.10	32.33	75	60
27	GS	0.664	12.7/8.1	2.8/2.5	0.035	0.09	32.33	75	29
28	SDS	0.305	12.7/8.1	2.8/2.5	0.035	0.00	32.33	75	96
29	GS	0.664	12.7/8.1	2.8/2.5	0.035	0.00	32.33	75	33
30	GS	0.664	12.7/8.1	2.8/2.5	0.035	0.10	32.33	75	35
31	SDS	0.305	12.7/8.1	2.8/2.5	0.035	0.02	32.33	75	83
32	GS	0.664	12.7/8.1	2.8/2.5	0.035	0.02	32.33	75	20
33	GS	0.664	7.0/4.4	1.54/1.38	0.035	0.02	64	75	22
34	GS	0.332	7.5/4.9	0.6/0.54	0.035	0.02	32.33	75	33
35	GS	0.664	12.7/8.1	2.8/2.5	0.035	0.02	32.33	75	18
36	GS	0.520	12.7/8.1	2.8/2.5	0.035	0.02	32.33	75	37
37	GS	0.664	12.7/8.1	2.8/2.5	0.035	0.02	32.33	75	20
38	GS	0.664	12.7/8.1	2.8/2.5	0.035	0.02	32.33	75	24
39	GS	0.664	12.7/8.1	1.4/1.3	0.035	0.02	32.33	75	23
40	GS	0.664	12.7/8.1	0/0	0.035	0.02	32.33	75	12
41	GS	0.664	12.7/8.1	0.7/0.63	0.035	0.02	32.33	75	14
42	GS	0.664	0/0	12.7/12.1	0.035	0.02	32.3	75	28
43	GS	0.664	12.7/8.1	2.8/2.5	0.035	0.02	42.3	75	49
44	GS	0.664	12.7/8.1	2.8/2.5	0.035	0.02	52.3	75	32
45	GS	0.664	12.7/8.1	2.8/2.5	0.035	0.02	62.3	75	40

SBR Sample	Surfactant Adopted	Amt. of Surfactant (g)	BD (ml/g)	ST (ml/g)	KPS (g)	n-DDM (g)	DI Water (g)	Temp (°C)	Particle Size (nm)
46	GS	0.664	12.7/8.1	2.8/2.5	0.035	0.02	72.3	75	42
47	GS	0.774	12.7/8.1	2.8/2.5	0.035	0.02	32.33	75	25
48	GS	0.874	12.7/8.1	2.8/2.5	0.035	0.02	32.33	75	28
49	GS	0.974	12.7/8.1	2.8/2.5	0.035	0.02	32.33	75	27
50	GS	1.074	12.7/8.1	2.8/2.5	0.035	0.02	32.33	75	32
51	GS	0.664	12.7/8.1	2.8/2.5	0.035	0.02	32.33	75	198
52	GS	0.664	12.7/8.1	2.8/2.5	0.035	0.02	32.33	75	44
53	GS	0.664	12.7/8.1	2.8/2.5	0.035	0.02	32.33	75	49
54	GS	0.664	12.7/8.1	2.8/2.5	0.035	0.02	32.33	65	28
55	GS	0.664	12.7/8.1	2.8/2.5	0.035	0.02	32.33	70	25
56	GS	0.664	12.7/8.1	2.8/2.5	0.035	0.02	32.33	75	22
57	GS	0.664	12.7/8.1	2.8/2.5	0.035	0.02	32.33	80	23
58	GS	0.664	12.7/8.1	2.8/2.5	0.035	0.02	32.33	85	19
59	SDS	0.305	12.7/8.1	2.8/2.5	0.030	0.02	32.3	50	42
60	SDS	0.305	12.7/8.1	2.8/2.5	0.035	0.02	32.3	50	42
61	SDS	0.305	12.7/8.1	2.8/2.5	0.040	0.02	32.3	50	44
62	SDS	0.305	12.7/8.1	2.8/2.5	0.045	0.02	32.3	50	40
63	SDS	0.305	12.7/8.1	2.8/2.5	0.050	0.02	32.3	50	42
64	SDS	0.305	12.7/8.1	2.8/2.5	0.055	0.02	32.3	50	86
65	GS	0.664	12.7/8.1	2.8/2.5	0.035	0.02	32.3	75	18
66	GS	0.664	12.7/8.1	2.8/2.5	0.035	0.02	32.3	75	34
67	Sodium Oleate	0.322	12.7/8.1	2.8/2.5	0.035	0.00	32.3	75	12
68	Sodium Oleate	0.322	12.7/8.1	2.8/2.5	0.035	0.02	32.3	75	14
69	Sodium Oleate	0.322	12.7/8.1	2.8/2.5	0.035	0.20	32.3	75	33
70	Sodium Oleate	0.322	12.7/8.1	2.8/2.5	0.035	0.04	32.3	75	37
71	Sodium Oleate	0.322	12.7/8.1	2.8/2.5	0.035	0.02	32.3	55	38
72	GS	0.664	12.7/8.1	2.8/2.5	0.035	0.02	32.3	55	83
73	SDS	0.305	12.7/8.1	2.8/2.5	0.035	0.02	32.3	55	53
74	SDS	0.305	12.7/8.1	2.8/2.5	0.035	0.02	32.3	55	50
75	Sodium Oleate	0.322	12.7/8.1	2.8/2.5	0.035	0.02	32.3	40	89
76	GS	0.664	12.7/8.1	2.8/2.5	0.035	0.02	32.3	40	91
77	Sodium Oleate	0.322	12.7/8.1	2.8/2.5	0.035	0.00	32.3	40	23
78	Sodium Oleate	0.322	12.7/8.1	2.8/2.5	0.035	0.02	32.3	40	105
79	Sodium Oleate	0.322	12.7/8.1	2.8/2.5	0.035	0.09	19.5	50	45
80	Sodium Oleate	0.322	12.7/8.1	2.8/2.5	0.035	0.02	32.3	35	490
81	Sodium Oleate	0.322	12.7/8.1	2.8/2.5	0.035	0.02	32.3	25	678
82	Sodium Oleate	0.322	12.7/8.1	2.8/2.5	0.035	0.02	32.3	40	135
83	Sodium Oleate	0.322	12.7/8.1	2.8/2.5	0.035	0.02	19.5	50	65
84	Sodium Oleate	0.322	12.7/8.1	2.8/2.5	0.035	0.02	32.3	50	34
85	SDS	0.305	12.7/8.1	0.45/0.4	0.035	0.02	32.3	50	12
86	SDS	0.305	12.7/8.1	0.45/0.5	0.035	0.02	32.3	50	-

SBR Sample	Surfactant Adopted	Amt. of Surfactant (g)	BD (ml/g)	ST (ml/g)	KPS (g)	n-DDM (g)	DI Water (g)	Temp (°C)	Particle Size (nm)
87	SDS	0.305	12.7/8.1	0.45/0.6	0.035	0.02	32.3	50	-
88	SDS	0.466	12.7/8.1	2.8/2.5	0.035	0.02	32.3	50	23
89	SDS	0.931	12.7/8.2	2.8/2.6	0.035	1.02	32.3	50	23
90	SDS	1.397	12.7/8.3	2.8/2.7	2.035	2.02	32.3	50	23
91	SDS	0.305	12.7/8.1	2.8/2.5	0.035	0.02	32.3	45	65
92	SDS	0.305	12.7/8.1	2.8/2.5	0.035	0.02	32.3	50	56
93	SDS	0.305	12.7/8.1	2.8/2.5	0.035	0.02	32.3	55	48
94	SDS	0.305	12.7/8.1	2.8/2.5	0.035	0.02	32.3	60	43
95	SDS	0.305	12.7/8.1	2.8/2.5	0.035	0.02	32.3	65	44
96	SDS	0.305	12.7/8.1	2.8/2.5	0.035	0.02	32.3	70	36
97	SDS	0.305	12.7/8.1	2.8/2.5	0.035	0.02	32.3	45	82
98	SDS	0.305	12.7/8.1	2.8/2.5	0.035	0.02	32.3	50	48
99	SDS	0.305	12.7/8.1	2.8/2.5	0.035	0.02	32.3	55	45
100	SDS	0.305	12.7/8.1	2.8/2.5	0.035	0.02	32.3	60	45
101	SDS	0.305	12.7/8.1	2.8/2.5	0.035	0.02	32.3	65	49
102	SDS	0.305	12.7/8.1	2.8/2.5	0.035	0.02	32.3	70	40
103	SDS	0.305	12.7/8.1	2.8/2.5	0.035	0.02	32.3	50	168
104	SDS	0.305	12.7/8.1	2.8/2.5	0.035	0.02	32.3	50	155
105	SDS	0.305	12.7/8.1	2.8/2.5	0.035	0.02	32.3	60	123
106	SDS	0.305	12.7/8.1	2.8/2.5	0.035	0.02	32.3	75	92
107	SDS	0.373	12.7/8.1	2.8/2.5	0.035	0.02	32.3	50	51
108	SDS	0.373	12.7/8.1	2.8/2.5	0.035	0.02	32.3	50	43
109	SDS	0.373	12.7/8.1	2.8/2.5	0.035	0.02	32.3	50	34
110	SDS	0.373	12.7/8.1	2.8/2.5	0.035	0.02	32.3	50	98
111	SDS	0.373	12.7/8.1	2.8/2.5	0.035	0.02	32.3	50	36
112	SDS	0.373	12.7/8.1	2.8/2.5	0.035	0.02	32.3	50	72
113	SDS	0.373	12.7/8.1	2.8/2.5	0.035	0.02	32.3	50	34
114	SDS	0.466	12.7/8.1	2.8/2.5	0.035	0.02	32.3	50	48
115	SDS	0.466	12.7/8.1	2.8/2.5	0.035	0.02	32.3	50	44
116	SDS	0.466	12.7/8.1	2.8/2.5	0.035	0.02	32.3	50	35
117	SDS	0.466	12.7/8.1	2.8/2.5	0.035	0.02	32.3	50	-
118	SDS	0.466	12.7/8.1	2.8/2.5	0.035	0.02	32.3	50	76
119	SDS	0.466	12.7/8.1	2.8/2.5	0.035	0.02	32.3	50	32
120	SDS	0.466	12.7/8.1	2.8/2.5	0.035	0.02	32.3	50	33
121	SDS	0.466	12.7/8.1	2.8/2.5	0.035	0.02	32.3	50	123
122	Na Oleate	0.322	13	3	0.035	0.09	32.3	50	45
123	Na Oleate	0.322	12.2	3	0.035	0.02	32.3	50	129
124	Na Oleate	0.322	12	3	0.035	0	32.3	50	16
125	Na Oleate	0.322	11.5	3	0.035	0.09	32.3	75	-
126	Na Oleate	0.322	12	3	0.035	0.02	32.3	50	167

SBR Sample	Surfactant Adopted	Amt. of Surfactant (g)	BD (ml/g)	ST (ml/g)	KPS (g)	n-DDM (g)	DI Water (g)	Temp (°C)	Particle Size (nm)
127	Na Oleate	0.322	12	3	0.035	0.02	32.3	50	223
128	Na Oleate	0.322	12	3	0.035	0.02	32.3	50	34
129	Na Oleate	0.322	12	3	0.035	0.19	32.3	50	64
130	Na Oleate	0.322	12	3	0.035	0.19	32.3	50	54
131	Na Oleate	0.322	12	3	0.035	0.02	32.3	50	32
132	Na Oleate	0.322	12	3	0.035	0.09	32.3	50	29
133	Na Oleate	0.322	12	3	0.035	0.09	32.3	50	39
134	Na Oleate	0.322	12	3	0.035	0.02	32.3	50	189
135	Na Oleate	0.322	12	3	0.035	0.37	32.3	50	47
136	Na Oleate	0.322	12	3	0.035	0.37	32.3	50	52
137	Na Oleate	0.322	12	3	0.035	0	32.3	50	17
138	Na Oleate	0.322	12	3	0.035	0	32.3	50	17
139	Na Oleate	0.322	12	3	0.035	0	32.3	50	14
140	Na Oleate	0.322	12	3	0.035	0.02	32.3	50	41
141	Na Oleate	0.322	12	3	0.035	0.02	32.3	50	46
142	Na Oleate	0.322	12	3	0.035	0.02	32.3	50	56
143	Na Oleate	0.322	12	3	0.035	0.02	32.3	50	66

Appendix B: ^{1}H NMR Spectra

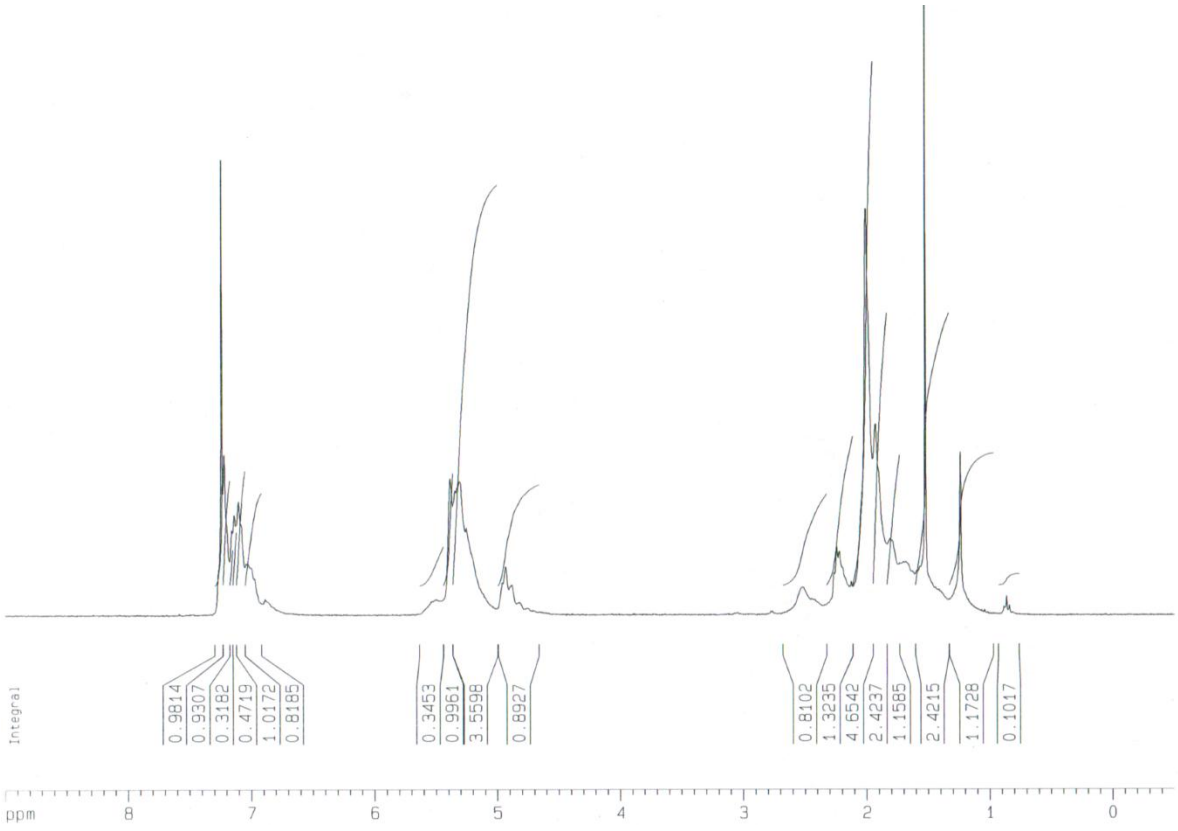

Spectrum – sample 127

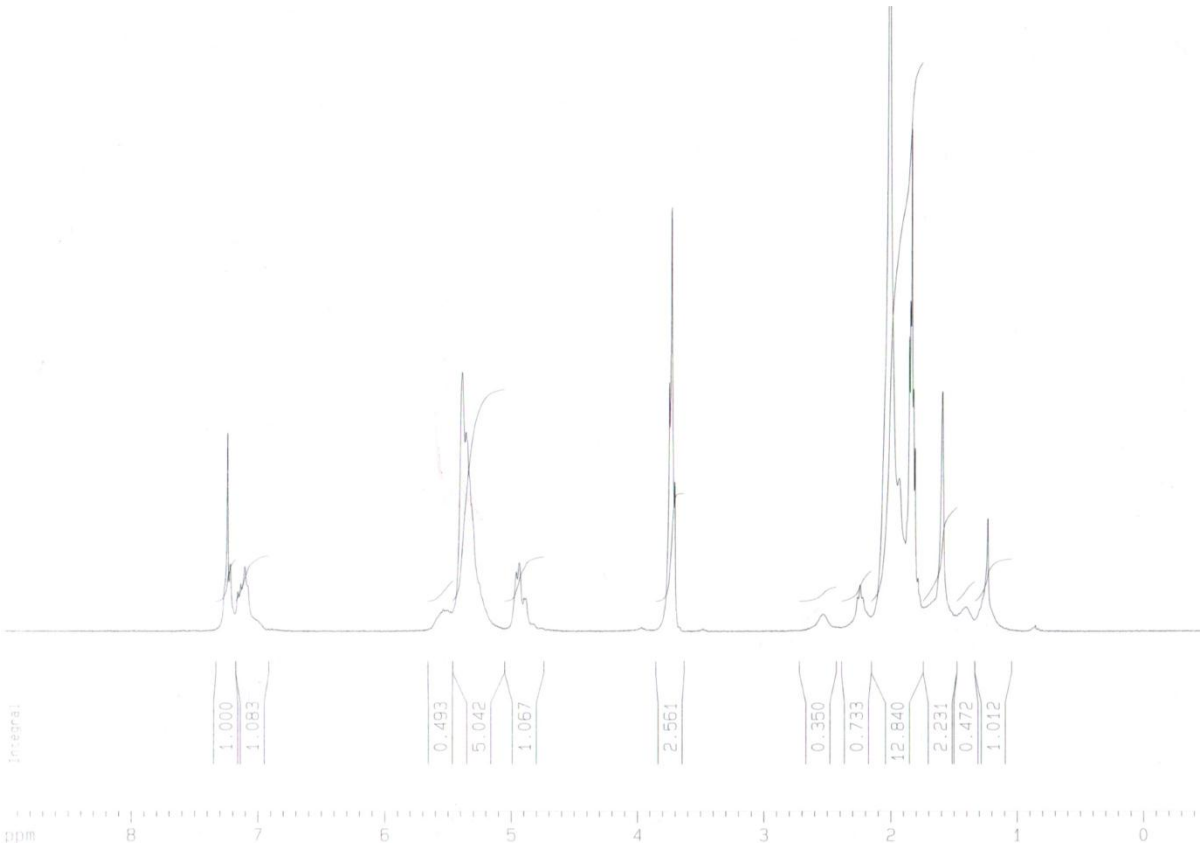

Spectrum – sample 123

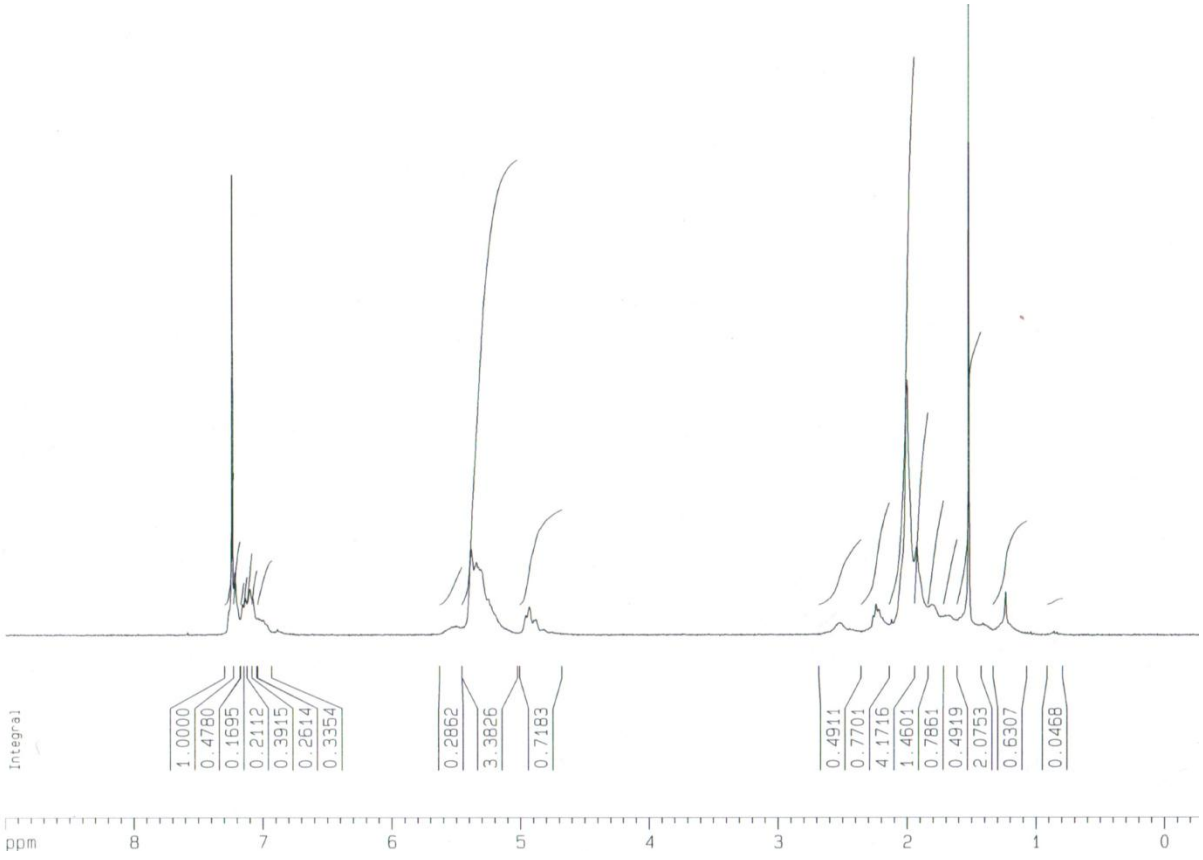

Spectrum – sample 140

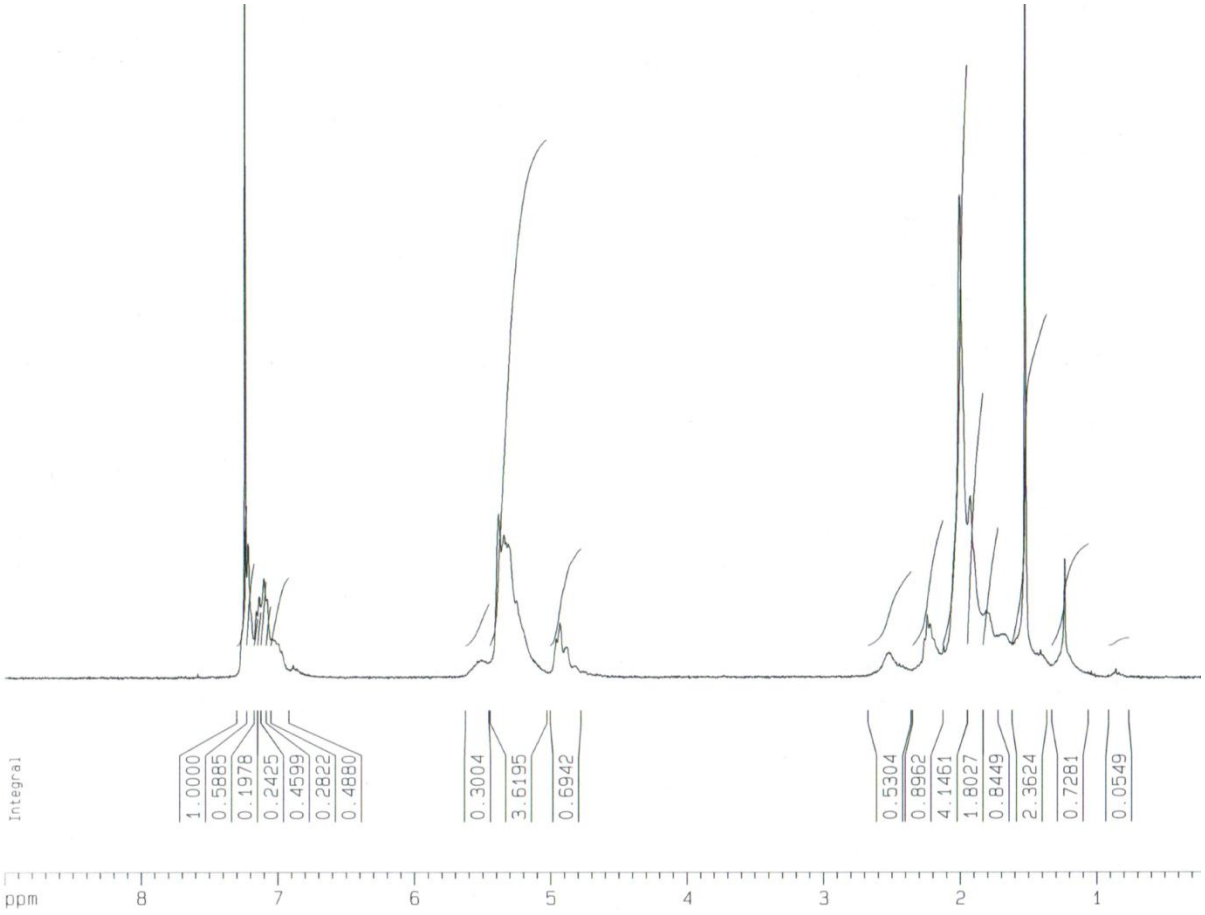

Spectrum – sample 143